Cobalt oxide catalysts for wet lean methane combustion

by

Somaye Nasr

A thesis submitted in partial fulfillment of the requirements for the degree of

Doctor of Philosophy

Chemical Engineering

Department of Chemical and Materials Engineering

University of Alberta

Abstract

Over the past several decades, there have been environmental concerns over anthropogenic emissions of methane, highlighting the need to minimize methane emissions. Natural gas has been employed as one of the alternatives for gasoline combustion engines. Methane is the main constituent of natural gas. Due to the high stability of methane molecules, its complete oxidation is not possible in a combustion engine. One way to minimize methane emissions from combustion engine exhaust would be using a catalytic converter. Increasing interest in natural gas (NG) fueled vehicle has increased the demand for research on a suitable catalyst. Flameless catalytic methane combustion has been investigated extensively as a means of reducing pollutant emissions and enhancing combustion efficiency. The main benefit of this method is the relatively low reaction temperature and low production of NO_x. This technology enables industry to employ a safer and cleaner approach for energy production. It is well established that palladium and platinum are efficient methane combustion catalysts. Unfortunately, the high price of these precious metals restricts their practical applications. The goal of our research is to identify an optimal catalyst that partially substitutes noble metals with mixed transitional oxides, while minimally reducing the catalyst activity and significantly reducing the material's cost. To achieve this goal, the research focused on using non-PGM transition metals as a promoter and as a support for Pd catalysts used for lean methane combustion reaction under wet conditions. Cobalt was chosen because of its low oxygen bonding energy and its relatively high activity in oxygen and methane activation among 3d elements. At first, reaction kinetics of methane combustion was investigated on Co_3O_4 and Pd/Co_3O_4 (0.27 wt.% Pd) catalysts for a fuel-lean feed. Significant cobalt oxide contribution to the activity of the bimetallic catalyst was observed,

especially at higher water concentrations and lower temperatures (up to 70 %). The Co_3O_4 contribution was not only in performing the methane combustion itself but also in supplying surface oxygen rather than in affecting the activation energy. The kinetic evidence shows that the observed behaviour of Pd/Co_3O_4 catalyst is the effect of strong metal-support interactions (SMSI).

To shed light on the chemical states of Pd and Co in bimetallic catalysts an *in-situ* X-ray absorption spectroscopy (XAS) study can also be a viable investigation. The Co_3O_4 and Pd/Co_3O_4 catalysts were analyzed for Pd and Co speciation during wet lean methane combustion at temperature ranges below 450 °C by means of *in situ* X-ray absorption spectroscopy. The contributions from metallic Pd, PdO and Pd $(OH)_2$ and metallic Co, Co (II), and Co(III) oxides were quantified as a function of temperature. It is concluded that Pd/CoO_x system the formation of methane combustion inactive Pd $(OH)_2$ seems to be suppressed as compared to the Al_2O_3 system. The results revealed that Pd activates and supplies oxygen to Co-O suprafacial active sites, and therefore, enhances the Co-catalyzed methane combustion performance. As the cobalt oxide surface is more resistant to water poisoning than PdO, the reaction order with respect to water is affected in a positive way, as Co sites contribute to methane combustion because of Pd feeding activated oxygen to them. It is concluded that CoO_x does not affect the degree of hydroxylation of the Pd surface.

After Pd and Co speciation, the next goal was to design a practical catalyst that is relatively cheap while exhibiting high activity under wet condition. To do so it was hypothesized that the use of ceria oxide in the cobalt oxide system would enhance the low dispersion of cobalt, hence improving the catalyst activity. Ceria was chosen due to its high oxygen storage capacity and

wide use in converter formulations. The Co_3O_4/CeO_2 catalyst demonstrated the same performance after 100 hours on stream, suggesting that the ceria stabilized the Co_3O_4 nanoparticles against sintering. In addition, due to the large Co_3O_4 crystals the metal-support interactions are improbable. Cobalt deposition did not impact the activation energy comparing to the bulk catalyst but did increase the catalyst active sites.

Overall, the cobalt and the interaction with Pd in the Pd/Co_3O_4 catalyst was studied and the results showed enhancement in the catalyst activity by supplying oxygen to the Co-O active sites. Presence of water vapor deactivates the Co_3O_4/CeO_2 catalyst, but the results revealed the reversible impact. Collectively, this study deepens our knowledge of cobalt role in catalyst system employed for lean methane combustion specifically under wet environment.

Preface

Chapter 1 as introduction contains the literature review related to the present research study.

Chapter 2 of the thesis contains the methodology used for conducting the experiments and the calculations related to quantification of the reaction products, flow regime, and heat and mass transfer limitations.

Chapter 3 of the thesis has been published as "Kinetic modeling of Co_3O_4 and Pd/Co_3O_4-catalyzed wet lean methane combustion" Somaye Nasr, Natalia Semagina, Robert E. Hayes. The paper is reprinted with the permission of co-authors. The reaction setup for methane oxidation was originally designed and built by Dr. Long Wu and Dr. Robert E. Hayes. The lab view program to communicate with the reaction setup was written by Les Dean. The ICP analysis was performed by Guangcheng Chen at the Earth and Atmospheric Sciences Department of University of Alberta. XRD was performed by Katie Nikolas at the Earth and Atmospheric Sciences Department of University of Alberta. Dr. Jing Shen collected the TEM images. The author performed all the syntheses, catalytic reactions, analyses, and other characterizations. Dr. Robert E. Hayes prepared the final plots and addressed the comments of the reviewers. Manuscript draft preparation and writing were conducted by the author under the supervision and final approval of Dr. Robert E. Hayes and Dr. Natalia Semagina.

A version of Chapter 4 of the thesis was published in the Catalysis Science & Technology journal as "Strong metal-support interactions in Pd/Co_3O_4 catalyst in wet methane combustion: *in situ* X-ray absorption study" William Barrett, Somaye Nasr, Jing Shen, Yongfeng Hu, Robert E. Hayes, Robert W.J. Scott, and Natalia Semagina. The paper is reprinted by the permission of co-authors. The reaction setup for methane oxidation was originally designed and built by Dr. Long Wu and Dr. Robert E. Hayes. The lab view program to communicate with the reaction setup was written by Les Dean. The NAA analysis was performed by Maxxam Analytics, Ontario. Dr. Jing Shen synthesized the nano palladium. The author performed all the syntheses, catalytic reactions, analyses, and other characterizations. Dr. Shihong Xu acquired the XPS spectra at nanoFAB, University of Alberta, the XPS data analyses was performed by Somaye Nasr. H_2-TPR was performed by Dr. Jing Shen. The *in situ* XAS was performed by William

Barrett under the supervision of Dr. Robert W.J. Scott at the Canadian Light Source, Saskatoon. Manuscript draft preparation and writing were conducted by the authors William Barrett and Somaye Nasr under the supervision of Dr. Robert W.J. Scott and Dr. Natalia Semagina. Dr. Natalia Semagina performed the final manuscript writing and she addressed all the comments of the reviewers. The work is conducted under the supervision and final approval of Dr. Natalia Semagina, Robert W.J. Scott and Dr. Robert E. Hayes.

Chapter 5 of the thesis has been submitted to the Canadian Journal of Chemical Engineering as "Remarkable stability of kinetic parameters of Co_3O_4/CeO_2 catalyzed methane combustion" Somaye Nasr, Robert E. Hayes, Natalia Semagina. The reaction setup for methane oxidation was originally designed and built by Dr. Long Wu and Dr. Robert E. Hayes. The lab view program to communicate with the reaction setup was written by Les Dean. The NAA analysis was performed by Maxxam Analytics, Ontario. XRD was performed by Katie Nikolas at the Earth and Atmospheric Sciences of University of Alberta. TEM-EDX mapping were performed by Dr. Shihong Xu at the University of Alberta Nanofabrication and Characterization Facility (nanoFAB). Manuscript draft preparation and writing were conducted by Somaye Nasr under the supervision of Dr. Natalia Semagina and Dr. Robert E. Hayes. Dr. Natalia Semagina performed the final manuscript editing and she addressed all the comments of the reviewers.

Dr. Natalia Semagina, my supervisor, provided discussions and feedback on experimental results, and comments and revisions for all writing work including the present thesis. Dr. Robert E. Hayes, my co-supervisor, and Dr. Robert W. J. Scott provided discussions and feedback on methane oxidation and kinetics data analyses and XAS analysis, respectively. The rest of the research work such as the literature review, catalyst synthesis, some of the catalyst characterizations, the catalytic reaction experiments, data collection and analysis, and interpretation of the experimental results were all conducted by Somaye Nasr in the Department of Chemical and Materials Engineering at the University of Alberta.

The research project of the present thesis is funded by the Natural Sciences and Engineering Research Council of Canada (NSERC).

This thesis is dedicated to my husband, Soheil, who has been a constant source of support and encouragement during the challenges of graduate school and life. This work also is dedicated to my parents, Fateme and Reza, who have always loved me unconditionally and whose good examples have taught me to work hard for the things I aspire to achieve. This work also is dedicated to my lovely daughter, Sonya, who is my inspiration in life.

Acknowledgments

The completion of this dissertation would not have been possible without the help and guidance of several individuals who I would like to take the opportunity to thank.

I gratefully acknowledge the financial support of the Natural Sciences and Engineering Research Council of Canada (NSERC).

First and foremost, I would like to extend my sincere gratitude to Dr. Natalia Semagina who gave me the opportunity to work under her supervision. I could not have imagined a better advisor and mentor for my Ph.D. study. She provided encouragement, insight, and mentorship that were crucial to the direction and completion of this thesis.

My sincere thanks also go to my co-supervisor, Dr. Robert Hayes, for his valuable feedback and constant support. His extensive knowledge in the combustion field was the backbone of this research. His continuous support, suggestions, technical advice were instrumental to this study.

The XAS analysis part of this study would not have been possible without the collaboration of Dr. Robert Scott from the University of Saskatchewan and I truly appreciate the time, knowledge, and skills Dr. Robert Scott added to this research. I also would like to thank Dr. Yongfeng Hu from the Canadian Light Source for facilitating the beamline. I am particularly indebted to William Barret for his help with the XAS experiments, and positive teamwork through our joint research collaboration.

I would also like to thank my committee members, Dr. Vinay Prasad, Dr. Neda Nazemifard, Dr. Charles Xu, Dr. Jing Liu for serving as my committee members and for their time, helpful feedbacks, and valuable questions.

I would like to express my gratitude to the University staff who provided their assistance and expertise in completion of this study, Dr. Shihong Xu, Dr. Anqiang He (NanoFab), Herb Green (CME machine shop), Kate Nichols (Department of Earth and Atmospheric Sciences), Lilly Laser (graduate administrative assistant).

I would like to recognize Dr. Jing Shen for her invaluable assistance in the lab and friendship during my study. I also wish to show my gratitude to fellow lab mate Amir Roohi for his assistance in the lab.

I am indebted to my lovely friend Fereshteh who provided me with endless encouragement, companionship, and positivity through my toughest moments. My lovely friends Pantea, Leila have always been there for me whenever I needed them. Very special thanks to my friend, Michael Sewanaku for his help with proof reading.

A very special thanks to my family back home. Words cannot express how grateful I am to my parents (Fateme and Reza) and sisters, Elham, Elaheh and Najmeh, for supporting me throughout this study regardless of how difficult this endeavor was on them.

I would also like to thank to my husband, Soheil whose love, patience and help through hardships have been priceless throughout my PhD studies. To my beloved bundle of joy, Sonya, my daughter. I am very thankful you entered my life during my studies and brought me so much love, happiness, and inspiration.

Somaye Nasr

June 2020

Table of Contents

List of Tables

List of Figures

Nomenclature

C_M	Methane concentration (mol/m^3)
C_{WP}	Weisz-Prater criterion
D_{AB}	Bulk diffusivity (m^2/s)
D_{eff}	Effective diffusivity (m^2/s)
D_K	Knudsen diffusivity (m^2/s)
D_p	Particle diameter (m)
d_{pore}	Catalyst pore diameter(m)
D_{pore}	Diffusivity in a pore (m^2/s)
E	Activation energy (kJ/mol)
F_{Mo}	Initial methane molar flow rate (mol/s)
h	Heat transfer coefficient ($kJ/(m^2 \cdot s \cdot K)$
k	Reaction rate constant
k_c	Mass transfer coefficient(m/s)
k_{eff}	Effective thermal conductivity (W/m.K)
k_t	Thermal conductivity (W/m.K)
M	Molecular mass (kg/mol)
n	Reaction order
Nu	Nusselt number
P	Pressure (Pa)
Pr	Prandtl number
R	Particle radius (m)
Re	Reynolds number
R_{gas}	Universal gas constant (J/mol K)
$-r_M$	Reaction rate (mol/kg_{cat} s)
S	Catalyst surface area (m^2/g)
Sc	Schmidt number
Sh	Sherwood number
T	Temperature (K)
U	Free-stream velocity (m/s)

W	Catalyst weight (kg)
X_{CH_4}	Fractional methane conversion
$-\Delta H_{ads}$	Enthalpy of adsorption
$-\Delta H_{rx}$	Heat of reaction (kJ/mol)
ΔT_{max}	Maximum internal temperature rise (K)
μ	Dynamic viscosity (Pa.s)
τ	Tortuosity
υ_i	Diffusion volume (m^3)
ϕ_p	Particle porosity
β	Prater number
ρ	Density (kg/m^3)

Abbreviations

A/F	Air to Fuel ratio
BET	Brunauer-Emmett-Teller
CNG	Compressed Natural Gas
DFT	Density Functional Theory
DR-FTIR	Diffuse Reflectance-Fourier Transform Infrared (DR-FTIR) spectroscopy
EDX	Energy-dispersive X-ray spectroscopy
EG	Ethylene Glycol
ER	Eley-Rideal
FID	Flame Ionization
GC	Gas Chromatography
GHG	Greenhouse Gas
GWP	Global Warming Potential
LH	Langmuir-Hinshelwood
LNG	Liquefied Natural Gas
MvK	Mars-van-Krevelen
NGV	Natural Gas Vehicle
OMA	Ordered Mesoporous Alumina
PGM	Pt-group metals
SSA	Specific Surface area
TCD	Thermal Conductivity
XAS	X-ray absorption spectroscopy
XPS	X-ray photoelectron spectroscopy

1 Introduction

1.1 Natural Gas Vehicles

Stringent environmental regulations and standards create a steady demand for improvement of combustion engines to minimize pollutant emissions. Natural gas (NG) driven combustion engines are a good alternative to gasoline/diesel engines in achieving this objective, due to their lower greenhouse gas (GHG) emissions, the high abundance of natural gas, and low NO_x and SO_x emissions produced during combustion. NG vehicles use compressed natural gas (CNG) or liquefied natural gas (LNG). Natural gas, composed primarily of methane (CH_4), produces the highest amount of energy per CO_2 molecule of any fossil fuel, due to its low C/H ratio[1, 2]. However, methane that passes through the system, without being oxidized, contributes to GHG emissions. Even though methane is the most carbon-efficient fossil fuel and is toxicologically inert, it has a high potency as a greenhouse gas due to its high global warming potential (GWP). Over a hundred-year period, methane's GWP is 28-36 times higher than that of CO_2 and 86 times higher than CO_2 over 20 years. As a result, methane emission controls were implemented in Canada in 2016 to mitigate CH_4 emissions from both natural and anthropogenic sources.

Methane is the least reactive hydrocarbon molecule [3] A practical solution to counteract its low reactivity is to use a catalytic converter, which constitutes the heart of an exhaust gas abatement system. This has drawn the attention of many research groups over the past few decades. Exhaust gases pass through a catalytic converter to ensure complete combustion. Complete oxidation of CH_4, using a catalytic converter, poses a significant challenge, due to low CH_4 concentrations (about 1000 ppmv), low exhaust gas temperatures (below 550 ºC), water vapor (10 vol, the presence of NO_x or SO_x, and strong C-H bonding (energy bond of 415 $kJmol^{-1}$).

Methane combustion can be achieved in one of two ways: conventional thermal combustion and catalytic combustion. The former requires high temperatures (up to 1600 °C) and the presence of a flame. Conventional flame combustion occurs only within specific air/fuel ratios and often produces pollutants. Compared to conventional thermal combustion, the heterogeneous catalysts

allow greater control of combustion products over a wide range of air/fuel ratios. The air/fuel mixture must pass through the catalyst at a temperature that is sufficiently high to allow total oxidation to occur. With emerging catalyst technology, the required oxidation temperature is lowered compared to the conventional combustor, which means less pollutant would be released from the exhaust.

Catalytic combustion is flameless with a smaller unit than conventional fireboxes. Most importantly, a low combustion temperature substantially reduces the emission of NO_x and CO [4]. NO_x is highly persistent in the atmosphere; it is therefore considered as one of the significant greenhouse gases [5]. Methane is a promising fuel alternative. Catalytic combustion of methane has been used in a variety of industrial applications (i.e. in catalytic heaters, boilers, and gas turbines to produce energy or elimination of pollutant from the vehicle exhaust and industrial clean-up units). Catalytic methane combustion encourages complete methane oxidation to occur under fuel- lean burn condition and at relatively low temperatures (300-500ºC).

The exhaust is a complex mixture including compounds in forms of gaseous, liquid and solid aerosols. Several factors have an impact on the composition of the mixture including fuel, engine type and operating conditions (e.g. air-fuel ratio and temperature), and the emission control devices used. Air-fuel ratio (A/F) is the mass flowrates ratio of air to fuel in a combustion engine. The engine can operate under lean, stoichiometry or rich conditions. Depending on the condition the A/F will have different values. A/F ratio for gasoline engines under stoichiometric condition is 14.7 parts of air to one part of fuel on a mass basis [5,6]. A/F ratios higher than stoichiometry, supply an excess amount of oxygen, which leads to complete combustion and a lower amount of CO and NO_x in the combustion products. Conversely, a lower A/F ratio than the stoichiometry condition corresponds to a higher CO concentration and hydrocarbon in the exhaust.

A catalytic converter is located inside the exhaust pipe, between the engine and muffler. The exhaust gases (CO_x, NO_x, hydrocarbons) pass through the catalytic converter before being discharged to the atmosphere. The function of the catalytic converter is to convert the non-CO_2 components into CO_2, water and N_2, thereby reducing harmful emissions (Figure 1.1). The catalytic converter is the main component of the exhaust emission control system. The limitation

on the catalytic converter size imposes having a highly active catalyst at relatively lower temperatures. Another challenge facing the catalytic abatement of methane is the presence of water vapor (10-15%) which is well known to cause catalyst deactivation. The primary research objective is to find a highly active yet stable catalyst, which can operate under wet conditions preferably with minimal cost.

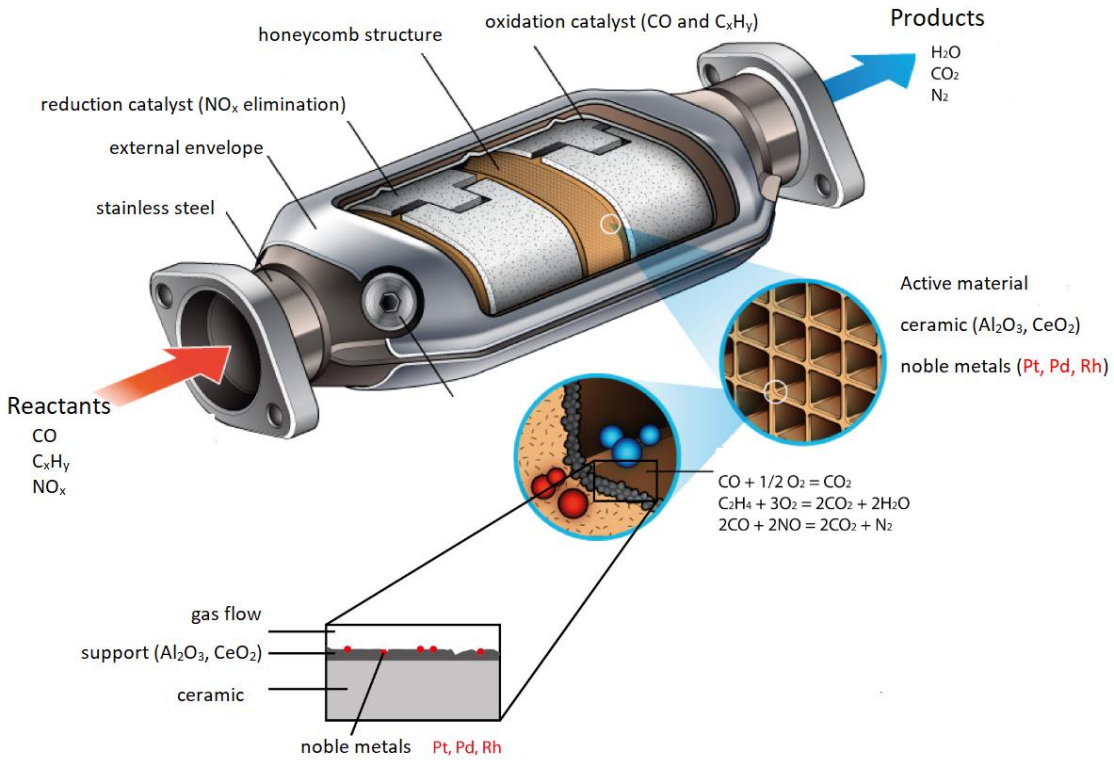

Figure 1.1 . Schematic of catalytic converter. Adapted with permission from [7].

In a catalytic converter, the core is usually a porous ceramic or metallic monolith that has a honeycomb structure. The monolith structure consisting of many parallel channels acts as an inert substrate coating with a washcoat and active catalyst. Low surface area can be overcome by utilizing high surface area support systems such as monoliths [5]. A monolith can be prepared either by layer-layer deposition or a dipping method. In the deposition method, a layer of washcoat is first deposited on the substrate and the catalysts are then deposited on the washcoat. In the dipping method, the monolith is dipped into a slurry, which contains washcoat components and an active catalyst [8]. Note that excess washcoat that has deposited on the

substrate is typically removed using high-pressure air. After the deposition, the monolith undergoes calcination to obtain the finished catalyst. The monolith's geometrical characteristics such as brick cell per square inch has a significant impact on light-off behavior and pressure drop of the converter. The washcoat acts as a carrier to provide high surface area upon which the catalyst can be deposited. The washcoat material is selected to increase the roughness and irregularity of the surface. The washcoat must be stable and retain its surface area at high temperatures. Other metal oxides (i.e. ceria or zirconia) may be added to the washcoat to increase stability and oxygen storage capacity of the catalyst.

A higher level of emissions is produced during the early part of an engine's operational cycle (especially during a cold start), mainly owing to the engine being substantially colder than its steady-state operating temperature. Light off temperature corresponds to the temperature at which 50% conversion occurs. Therefore, the light off temperature of a catalyst is one of the main variables used to assess its efficiency. One way to improve a catalytic converter's performance is to lower the light off temperature as low as possible to minimize cold start emissions.

As mentioned earlier, methane is a potent GHG gas and has been the focus for many research groups. To decrease the CH_4 emissions from mobile or stationary sources two main approaches have been taken:

1. Optimization of the fuel oxidation process by modifying the engine or the fuel.

2. Lowering the exhaust gas emissions to the atmosphere by using a suitable catalytic converter.

This study focuses on the former approach, aiming to develop a catalyst to be used for NG combustion engines with the aim of promoting the total oxidation of methane at lower temperatures. This would enable adherence of the increasingly stringent regulations regarding exhaust emissions.

1.2 Methane Combustion Reaction

Methane is known as the least reactive alkane with a strong C-H bond (bond strength of 104 $kJmol^{-1}$) [9]; its combustion has been extensively studied. At low CH_4/O_2 ratios, complete combustion of methane produces carbon dioxide and water (R1). At a relatively high CH_4 inlet concentrations, partial oxidation of methane could lead to CO and H_2 formation (R2); this is applied for syngas production. CO production can be prevented through low reaction temperature and increasing the air-to-CH_4 ratio.

$$CH_4(g) + 2O_2(g) \rightarrow CO_2(g) + 2H_2O(g) \quad (\Delta H_r^\circ = -802\ kJmol^{-1}\ \text{methane at } 25°C) \quad (R1)$$

$$CH_4(g) + \frac{1}{2}O_2(g) \rightarrow CO(g) + 2H_2(g) \quad (\Delta H_r^\circ = -36\ kJmol^{-1}\ \text{methane at at } 25°C) \quad (R2)$$

Methane combustion is a highly exothermic reaction (R1). Many researchers have studied complete methane combustion at low temperatures, which will also prevent toxic NO_x and CO formation. High temperatures promote partial oxidation and therefore produce CO. In addition, the temperature of exhaust gases from lean burn NGVs is low, in the range of 300 – 500ºC. Complete combustion of hydrocarbons favors lean operating conditions (conditions with abundant oxygen) which are also the conditions of real exhaust gases from lean burn NG fueled engines.

1.3 Catalytic methane combustion

In catalytic combustion, reaction occurs on the catalyst surface. Lean-burn NGV exhaust has specific conditions that should be considered in designing a catalyst suitable for the following operating condition [10]:

- low temperatures (typically less than 500–550 ºC),
- low methane concentration (500–1000 ppm),
- large amounts of water vapor (10–15%) and CO_2 (15%),
- large excess of oxygen,

- presence of SO_x (about 1 ppm) and NO_x.

The catalytic oxidation of methane can be performed over Pt-group metals (PGM) and a number of other transition metal oxides. These catalysts can be either supported or unsupported. Supported catalysts are usually preferred because of efficient utilization of the metal and much higher stability (i.e. deactivation due to sintering or poisoning). A supported catalyst has metal present as small particles on the support surface, meaning a large fraction of catalytic metal is at the surface. The catalyst may be supported on the variety of materials including pellets, honeycomb monoliths, parallel plates and so on [5]. The support may also have oxygen storage capability and plays a role in the oxidation reactions by providing oxygen. In general, an ideal catalyst for the catalytic combustion of NG should have high activity at low temperatures, a relatively low ignition temperature, high thermal stability, resistance to poisoning (i.e. due to wet conditions and/or the presence of sulfur compounds), low toxicological impact, and a reasonable price. Unfortunately, no such catalyst encompassing all these characteristics has been discovered yet. Nevertheless, these criteria are used to quantify the performance of the catalysts and choose the appropriate catalyst for specific applications.

Pd-based catalysts are the most efficient for methane combustion and have been the focus of many studies over the last two decades. Despite their widespread use, there are some disadvantages such as their poor stability for methane combustion, catalyst sintering at higher temperatures, and large hysteresis effects because of PdO reduction to Pd at high temperatures [1]. Even though Pd based catalysts are recognized for their high initial activity in catalytic oxidation reaction, the rapid decline in catalyst activity, leads to difficulty in fuel ignition [11,12].

Pt-based catalysts have different characteristics compared to Pd-based catalysts [13]. Their relatively low activity for lean methane oxidation reaction has been noted by several authors. One example would be Gélin et al. [14] who studied the influence of water and sulfur on Pd and Pt-based catalysts. Their results showed that Pd is more resistant than Pt to hydrothermal aging. However, better resistance of Pt/Al_2O_3 to sulfur poisoning also have been identified. This makes Pt a good candidate for use as the promoter in bimetal catalysts. Platinum has been utilized as a suitable promoter to palladium through the stabilization of PdO [15]. Persson et al. suggested

that the better methane dissociation of Pd-Pt compared to monometallic catalysts is responsible for their higher activity. The high sensitivity of Pd-based catalysts to water and sulfur poisoning limits their application in NGV exhaust abatement [12]. The exposure to water and sulfur-containing compounds causes catalyst activity loss, which can be significant and irreversible [16,17].

1.4 The redox mechanism over PdO

The redox behavior of palladium and the dynamic nature of the active sites during the methane oxidation reaction are still a matter of debate and no clear consensus has been reached regarding the mechanisms involved. G.Groppi[18] conducted a study using Pd catalyst supported on La_2O_3 stabilized alumina to clarify palladium redox behavior. The authors concluded the active sites can switch between metallic Pd and PdO depending on the reaction temperature. The work suggested PdO is much more active than Pd at a moderate temperature range, while at higher temperatures (above 700 ºC) PdO decomposes to metallic Pd.

In a study by Fujin et al. [19] Pd catalyst supported on La-modified $Al_2O_3$with and without doping CeO_2-ZrO_2 were tested to explore the active site during methane oxidation reaction under a A/F ratio close to stoichiometric conditions. The results confirmed both Pd and PdO act as the active sites under much richer conditions, while under lean conditions; PdO plays an important role in methane oxidation. In a recent study by Bychkov et al. [20] variation of Pd oxidation state and the corresponding impact on Pd catalytic activity was investigated by means of *in situ* thermogravimetry. Catalytic activity was found to increase as Pd^0 became oxidized to $PdO_{0.3}$. Under methane rich condition the metallic state Pd is active [21] where the metal surface remains substantially free of chemisorbed oxygen and thus is available for C–H bond activation in methane molecules [20].

As discussed earlier much research has focused on assessing whether metallic Pd or PdO is the active site during methane combustion reactions. Understanding the reaction mechanism and pathways helps in designing/improving a catalyst. In the scientific literature, several mechanisms have been proposed for methane combustion reaction over Pd and Pt-based catalysts including the Langmuir-Hinshelwood (LH) [22,23,24], Eley-Rideal (ER)[22,25],and Mars-van-Krevelen

(MvK)[24,26-28]. However, the most frequently used mechanism for the oxidation of organic compounds over noble metals as well as over many metal oxides has been via MvK mechanism.

The transformation of the oxide phase to the metallic phase (PdO ⇌ Pd) is a reversible reaction, which plays an important part in the combustion reaction. This phase transformation affects the structure, morphology, chemical state, and surface energy of the active metal [11]. Many research studies reported that metallic Pd is significantly less active than oxide phase (PdO) for methane combustion reaction and the redox mechanism changes in the course of the PdO ⇌ Pd transformation [12,16,17]. The different reaction for methane oxidation observed for the oxide and the metallic phase, implies a different reaction mechanism. Zhu et al. [29] argued that the reaction mechanism on the reduced metallic Pd phase is different from the palladium oxide (PdO) phase. The reaction on the Pd phase and the PdO phase can be interpreted by the LH and MvK mechanisms respectively [29]. The catalyst pretreatment, time on history, and operating conditions used during the reaction impact the PdO species distribution [30].

Fujimoto et al. [13] proposed a mechanism (see Scheme 1 and 2) with elementary steps similar to the MvK reduction-oxidation pathways (the asterisks stand for oxygen vacancies on PdO surfaces). In this mechanism, methane molecule adsorbs on palladium oxide surface via interaction with oxygen vacancy sites. This results in an adsorbed OH and CH_3 (step 2). Later, the adjacent surface PdO sites sequentially abstract H atoms to form OH groups on the catalyst surface (step 3). In this mechanism, the hydrogen abstraction is believed to be the rate-determining step. During the $C-H$ bond activation steps, surface OH groups formed on the catalyst surface regenerate new oxygen vacancies (Scheme 1 and 2) [13]. The higher CH_4^* and O* species, the higher the reaction rate. Negative first-order dependence of the reaction rate to water indicates the water inhibition effect (hydroxyl radical blocks reaction sites, manifesting itself in -1 order to water). Fujimoto et al. believed that there is a pseudo-equilibrium adsorption-desorption of water ($2OH^* \rightleftharpoons H_2O + O^* + *$). Increasing the H_2O concentration will cause the reaction to favor greater hydroxyl concentrations, leading to the reduction of surface vacancies (*), and consequently inhibiting the reaction rate. At higher temperatures, the forward reaction is favored, resulting in the formation of active sites. The mentioned examples indicate that the inhibition effect of water is reversible.

$$r = k(CH_4)^1(O_2)^0(H_2O)^{-1} \quad (1\text{-}1)$$

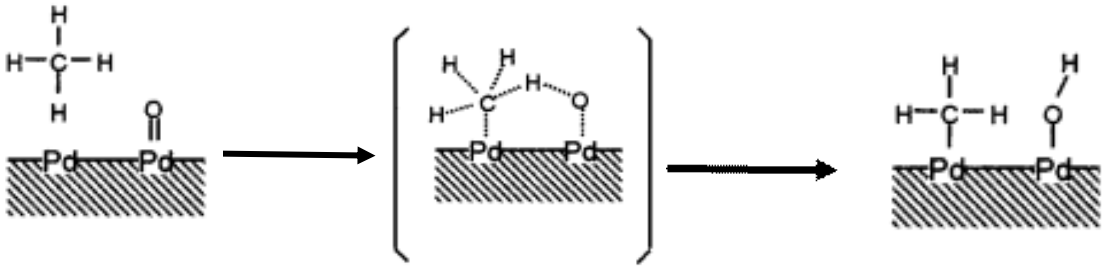

Step1. CH_4 and Pd interaction Step2. C-H bond activation Step3. PdOH formation

Scheme 1. 1 Mechanism of CH_4 dissociation on Pd/PdO site pair. Reprinted from [13] with permission from Elsevier copyright 1998.

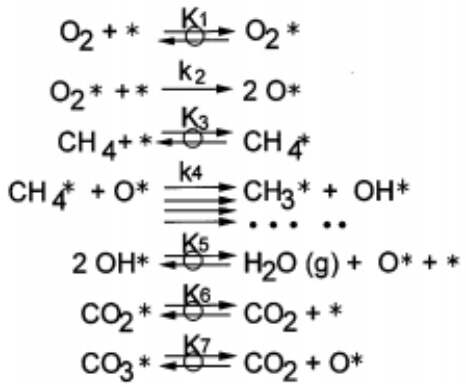

Scheme 1.2. Reaction mechanism of methane combustion on Pd, where * are unsaturated metal atoms from scheme 1.1. Reprinted from [13] with permission from Elsevier copyright 1998.

The catalyst ability in generation of oxygen vacancies is critical; therefore, the direct impact of $Pd-O$ bond strength on the catalyst activity has been identified. In this mechanism, the authors claimed smaller PdO holds stronger $Pd-O$ bonds and less surface vacancies concentration (a lesser concentration of surface vacancies), which negatively affects the methane combustion reaction. This hypothesis explains low activity of non-crystalline PdO and metallic Pd [9].

In the MvK redox mechanism, oxygen from the solid oxide phase is used in the oxidation reaction, followed by the metal reoxidation by gas-phase O_2[31]. The Pd/support interface has a direct impact on the overall catalytic activity [32,33]; consequently, it affects the quantity of active catalytic sites, particle size, and catalyst surface area. The strong influence of the catalyst support on the palladium species (PdO →Pd) decomposition and transformation, and consequently the overall catalyst activity has been suggested by Farrauto et al. [34].

Recently, Stotz et al. [11] studied methane combustion with a Pd/Al_2O_3 catalyst under quasi-auto thermal operating conditions with metallic Pd being the predominant phase. Using the in-situ sampling technique, they showed that methane activation occurs through three different paths which involve different site-pairs [11] including (1) Pd – Pd, (2) Pd–O, and (3) O–O with Pd–O. The authors [35] concluded that PdO deactivation occurs for a combination of effects such as sintering, structural, morphological particle shape change because of water presence either in the feed mixture or external source. They studied the impact of pressure on the light-off curves and the obtained result showed increasing pressure had no effect on the dry cases. Contrarily, under wet condition (12%) higher conversion was observed at higher pressure (4bar) compared to 1 bar. These findings suggest that changes related to the deactivation are more pronounced at higher pressure under wet condition, and that the catalyst exhibits more stability under dry conditions [35].

Stotz et. al [35] conducted a detail reaction path analysis for the dry and wet (12vol. % H_2O) feed to study which paths are preferred. The preferential reaction path was evaluated through identifying the maximum contribution for each species by density functional theory (DFT) data for PdO (1 0 1). The detailed study revealed the surface intermediate species and path preferences have strong dependence on the temperature and position [35]. Based on the reaction path preferences catalytic cycles were proposed by Stotz et. al (Figure 1.2) for wet and dry conditions according to a MvK mechanism with vacancy regeneration over PdO along the (1 0 1) plane. Hydroxide formation and reversible H_2O/OH adsorption on Pd sites result in site blocking therefore, causes water inhibition. Under wet condition due to larger amount of water present in the gas phase, H_2O covers almost all free Pd sites which leads to a shift (100K) in the light-off temperature [35]. Water adsorption on$(*)_{Pd(cus)}$ sites may interrupt transfer of oxygen

from the support to $(*)_{Pd(cus)}$ sites, leading to a reduced availability of $(*)O_{(cus)}$-$(*)_{Pd(cus)}$ site pairs[35].

1.5 Catalyst deactivation

The major concern in the operations of heterogeneous catalysts is catalyst deactivation, the loss of catalyst activity with time-on-stream, needs to be addressed. Deactivation can occur by either physical or chemical causes is an inevitable phenomenon causing elimination or blockage of catalyst active centers. Understanding underlying physical and chemical processes allows developing deactivation-resistant catalysts with a slower deactivation rate.

Catalyst deactivation happens by several mechanisms including sintering, phase transformation, fouling/coking, and poisoning. It has to be noted that the loss of active elements can cause deactivation, erosion, attrition, and volatilization [36]. Catalyst poisoning arises from chemisorption of species that are present in the feed and/or a product or by-product of the reaction. Because chemisorption is strong, the active sites typically become permanently blocked (irreversible blocking). In some cases, the chemisorbed species might slowly desorb (i.e. reversible poisoning) [5].

The Pd-based catalyst deactivation has been the focus of many scholars over the past few decades; several factors have been introduced in the literature as the main causes of the Pd catalysts deactivations e.g. $Pd(OH)_2$ formation[21,37,38], water induced sintering[39,40] and thermal sintering[41]. As discussed earlier, Pd based are the most active catalyst for fuel-lean methane combustion. However, a significant barrier to its application is its susceptibility to water. Burch et al.[42] showed that water inhibition was substantial below temperatures of ~450 °C. Ciuparu et al.[43] demonstrated that the reaction order to water varies with temperature (from -1 at 300 °C to 0 at 500 °C). To understand the water inhibitory effect, monitoring the surface hydroxyls is crucial. Water, a reaction product and a component of the exhaust stream, may impede the exchange of oxygen between PdO and support [31], which depends on the reaction temperature and the type of the support.

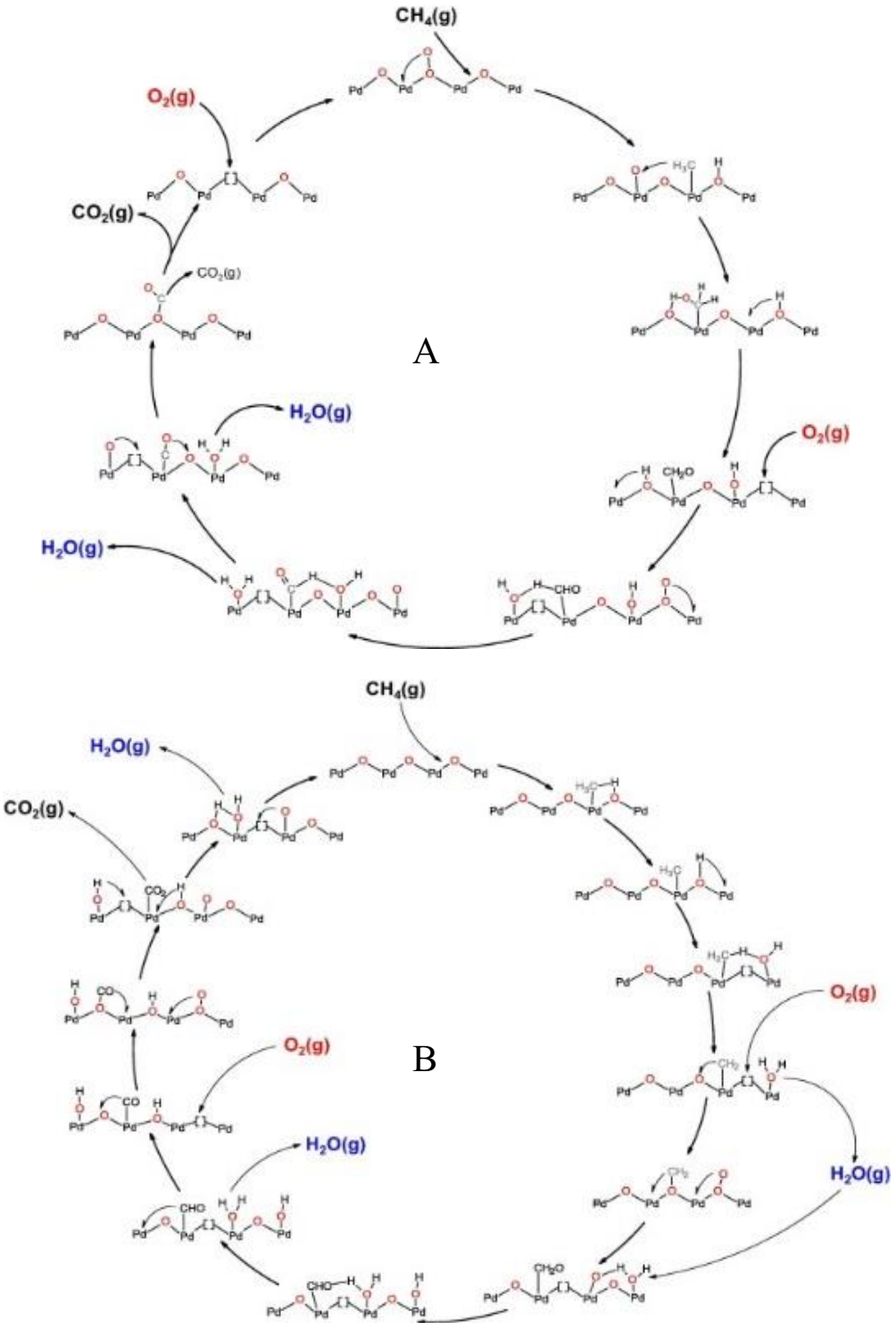

Figure 1.2 Catalytic cycle of the preferential reaction path following a Mars-van-Krevelen redox mechanism for methane oxidation over PdO(1 0 1) as found at (A) dry feed (200–400 °C) and (B) wet feed (12% H_2O, 300-550 °C). Reprinted from [35] with permission from Elsevier copyright 2019.

Methane combustion mechanisms for temperatures below 450 ^{o}C need to include these exchange step. Catalytic deactivation is caused by the OH buildup on the surface caused by external water source or reaction itself [44]. This buildup hinders the migration of oxygen between the support and the PdO/Pd phase, inhibiting them from participating in the oxidation reaction [45]. Although direct impact of water poisoning on the catalyst deactivation have been identified, the search for an appropriate mechanism for the catalyst deactivation is an ongoing research objective.

Ciuparu et al. [43] proposed that OH groups that are formed from the dissociation of C–H bonds bind stronger compared to hydroxyl groups resulting from water molecules. Consequently, the authors believe that the studies on external water adsorption may produce incorrect results [46]. Ciuparu et al. [9] investigated the fuel-lean methane combustion reaction using alumina-supported Pd catalyst at 350 °C specifically focusing on the production of surface hydroxyls using diffuse reflectance-Fourier transform infrared (DR-FTIR) spectroscopy. The authors identified three well-defined bands, which were associated with the terminal (3732 cm^{-1}), bridged (3699 cm^{-1}) and multi-bound (3549 cm^{-1}) OH groups on the catalyst surface. The surface hydroxyl group binding energy decreases as OH_{III}> OH_{II}> OH_{I}. According to Ciuparu et al.[47] the dehydroxylation from catalyst surface at low to moderate temperatures occurs in sequential steps (OH_{III} (multibound)⇌ OH_{II} (bridged) ⇌ OH_{I} (terminal) ⇌ $H_2O_{(g)}$), among which the terminal OH recombine to H_2O molecules, which finally will desorb to the gas phase. It has been found that the rate-determining step of the surface dehydroxylation.

The nature of the support is critical in the water inhibition effect. The catalyst resistance to water inhibition effect is proportional to the support oxygen mobility. Ciuparu et al. [47] studied supports with different oxygen surface mobilities, comparing Pd catalysts deposited on alumina, zirconia and $Ce_{0.1}Zr_{0.9}O_2$. The authors concluded that the supports with higher oxygen surface mobility ($Ce_{0.1}Zr_{0.9}O_2$) provided higher water resistance. The surface hydroxyl removal rate increases in the order of $Al_2O_3 < ZrO_2 < Ce_{0.1}Zr_{0.9}O_2$.

Stotz et al. studied the impact of water on Pd/Al_2O_3 catalyst for methane combustion (at different water concentrations (0, 6, 12 vol.%) at 1 and 4 bar). They observed that the catalytic activity of the light-off (first heating curve) and the subsequent light out (fist cooling off) under dry

condition was closely overlaid. While under wet condition (6 and 12 vol.% water), the catalyst activity curves showed visible conversion hysteresis between ignition and extinction branches [35]. Obtained results showed that increasing the amount of water in the feed resulted in a decreasing trend in the slope of the light-off curves. The authors suggested that the observed hysteresis is due to deactivation of the catalyst during the light-off period [35]. Under fuel-lean operation, the water inhibition effect over PdO is pronounced at lower temperatures (T < 500 °C) [35]. Their investigation into the impact of elevated pressure on the ignition and extinction curve also indicated that higher pressures may facilitate enhanced water adsorption and interactions with PdO particle surface and/or support as compared to the wet low-pressure case or at even dry conditions.

1.6 Promoters to active Pd and to the support

One of the important ways to enhance the efficiency of the catalyst active phase is the addition of promoters (activators) to the catalyst. Promoters improve the catalyst active phases via increasing the thermal, hydrothermal, and/or chemical stability against sintering and decomposition, increasing the reaction rates and the selectivity of the catalytic reaction [49].

Noble metals are appealing because of their good stability and high activity, particularly when alloyed [15]. Enhanced performance of bimetallic catalysts via support impregnation with two metal precursors in catalytic combustion have been investigated in numerous studies. One of the important characteristics of a bimetallic catalyst is the effect of water on its activity. The addition of another Pt-group metal was shown to stabilize Pd [15,50]. It has been reported that bimetallic Pt–Pd catalysts demonstrate better catalytic activity under wet conditions compared to monometallic catalysts [15,51]. The active phase in Pd-based catalysts differs from Pt-based catalysts. Pd transforms to PdO at temperatures below 800 ^{o}C in air; however, PtO_2, which is very unstable, can hardly be generated at temperatures below 600 ^{o}C. Because PdO has greater stability in comparison with PtO_2, PdO is generally known as the active phase, while metallic Pt is present in Pt-based catalysts. The PdO activity is higher than that of Pt in fuel-lean conditions. Although the activity of PdPt bimetallic catalyst is also damaged in presence of the water in the feed, because of the interaction between Pt and Pd and their synergistic effects, the activation

loss is less severe can be recovered when the water is removed[52]. In the presence of 10% water, the activity of the 1:1 Pd-Pt catalyst was about four times higher than that of monometallic Pd [52]. It was suggested that in the lack of oxygen, caused by the presence of water, the PdO-catalyzed methane activation shifts to the Pt-catalyzed process [21].

The primary focus of this research is investigating different catalyst support and their impact on the catalyst performance. A catalyst with sustained activity and stability is still needed [53]. Different promoters to the catalyst support have been used (lanthanum oxide, calcium oxide, magnesium oxide, nickel oxide, cerium oxide, yttrium oxide, etc.). Promoters increase the efficiency of the active phase by supplying the required oxygen [49]. Using cobalt oxide as the promoter is of main interest of this research. Having a very weak metal-oxygen bond makes it a potential oxygen provider to noble metal (Pd), as will be shown below.

As discussed earlier, palladium oxide is the most widely used catalyst in catalytic methane oxidation reaction, but because of its high cost and susceptibility to water, alternative transition metals have been explored to identify catalysts with higher thermal stability and lower precious metal requirements. The oxygen mobility in the system seems to be of high importance. By exchanging oxygen with Pd/PdO, the support can partake in the oxidation reaction [54].

There are three sources of oxygen available for methane combustion under fuel lean environment: gas-phase O_2, O from PdO and from the support. It is hypothesized by Ciuparo et al. that high oxygen mobility supports play a significant role in reoxidation while moderating water inhibition at the metal/oxide interface [9].

To determine the origin of oxygen partaking in the methane oxidation reaction, Ciuparo et al. [46] used $^{18}O_2$ as the trackable oxygen supply for catalytic methane combustion. At the beginning of reaction, oxygen from the support was found to be present in the products. The authors suggested that metal oxide support contributes to the oxidation by providing O to PdO at the interface of these components. This phenomenon confirms the key role of metal oxide support in the catalytic combustion [9]. Having several oxidation states enables the transition metals to go through a redox cycle with lattice oxygen being consumed or replenished [55]. In this study, we proposed using an earth-abundant promotor with high oxygen surface capacity for

Pd-based catalyst. Cobalt has low $Co - O$ bond energy (368 kJ/mol) is a very good candidate to be used as promoter.

1.7 The redox mechanism over cobalt

Recently cobalt has attracted a lot of attention for methane combustion reaction owing to its inherent multi-valence state (Co^{2+} and Co^{3+}). It was reported as a catalyst itself, as a minute-amount promoter to platinum group metals (PGM) [56-58] and as a support for PGM [58]. Cobalt provides oxygen species in the lattice with a high mobility [24] and it can activate methane and oxygen. Co_3O_4 has different coordination of the constituent ions, both in the bulk and at the surface which enables its catalytic behavior [60].

In a recent study by Zasada et al. [24] participation of adsorbed and lattice oxygen in catalytic combustion of methane (1%) on cobalt spinel (Co_3O_4 nanocubes) was investigated in the presence or in the absence of oxygen. By using molecular modeling (DFT+U calculations) along with catalytic isotopic experiments, the authors identified three distinct temperature/conversion stages of the methane oxidation reaction. In the lower temperature (stoichiometric) region (300 °C < T < 450 °C), the suprafacial (L-H) pathway, in association with adsorbed oxygen species, dominates. Within the middle temperature range (450 °C < T < 650°C, X_{CH_4} < 80%), dioxygen reoccupies the oxygen vacancies produced upon CO_2 and H_2O's release, the underlying mechanism can be well described by the means of both suprafacial (L-H) and intrafacial (MvK). At the higher temperature region (T > 650 °C, X_{CH_4} > 80%), the catalyst is mainly reduced, and the methane oxidation reaction proceeds primarily according to the MvK mechanism due to the gradual involvement of lattice oxygen. Methane combustion on Co_3O_4 occurs via a Langmuir-Hinshelwood mechanism involving suprafacial highly active tetrahedral cobalt oxo-centres at temperatures below 450 °C, with an increased contribution from less active intrafacial lattice oxygen (Mars-van Krevelen mechanism) at higher temperatures [24]. Molecular modelling showed that the suprafacial $Co\text{-}O_{ads}$ species are more active compared to the intrafacial $Co\text{-}O_{surf}$ surface sites in the CH_4 combustion reaction, with ΔE_a=0.83 eV and 1.11 eV respectively [24].

Zasada et. al [61] conducted a theoretical study of water adsorption on cobalt spinel nanocrystals using plane-wave periodic DFT calculations together with statistical thermodynamics. They considered the three most stable surface planes (100, 110, and 111) of Co_3O_4 nanograins exposed to water. The authors used an atomistic thermodynamic modeling approch in which the gas phase acts as a reservoir in equilibrium with the solid surface and the adsorbed molecules. By using multisite Langmuir equation, free enthalpies of water adsorption for the surface planes (G_i) was equated into changes in the surface coverage with temperature and partial pressure[61]. Then, the total surface coverage Θ_{total} is expressed as a sum of water species adsorbed on different sites, expressed in equation form as following:

$$\Theta_{total} = \sum_{i=1} x_i \frac{\beta_i^n}{1+\sum_{i=1} \beta_i{}^n} \quad (1\text{-}2)$$

The above expression describes adsorption on the i^{th} site, with H_2O molecule only binding to the site if the sites with a lower index number that are already occupied (multisite Langmuir) [61]. In the equation $x_i=N_i/N$ is the ratio of N_i sites per total number of possible adsorption sites(N), $\beta^n = K_1 . K_2 . \ldots . K_n$ is the cumulative adsorption equilibrium constant. K_i values denote the adsorption equilibrium constant between the subsequent surface phases that differ in the number of H_2O admolecules:

$$K_i = \exp\left(-\frac{\Delta G_i - \Delta G_{i+1}}{RT}\right) \quad (1\text{-}3)$$

in which G denotes the free enthalpy of a surface. To epitomize water adsorption in a concise way, two-dimensional Θ(p,T) diagrams of water sorption on the planes of Co_3O_4 are shown in Figure 1.3[60]. As it can be seen the (100) surface panel showed less water adsorption in compares to the (111) and (110) planes, 5 H_2O molecule in full coverage state(Θ=1) and bare surface around 160°C and 10 Pa.

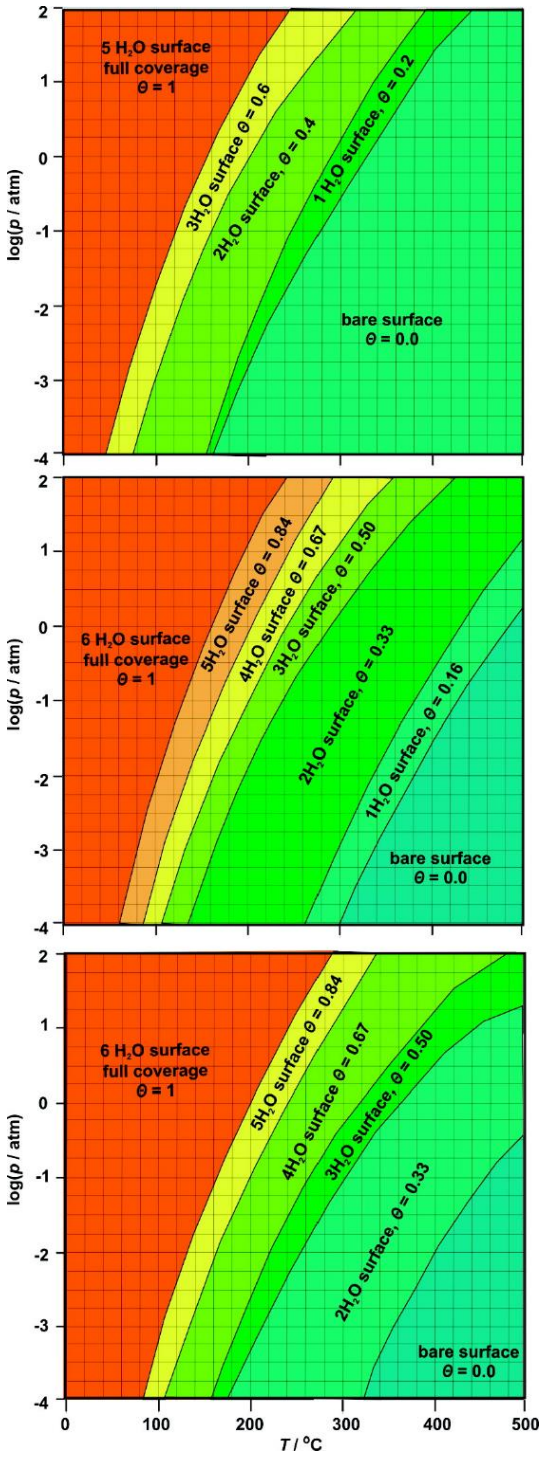

Figure 1.3 Two-dimensional diagrams of water coverage as a function of temperature and partial pressure of water for (a, top panel) (100), (b, middle panel) (110), and (c, bottom panel) (111) planes of cobalt spinel. Reprinted from [61] with permission from American Chemical Society copyright 2010.

1.8 Thermodynamics of Co/CoO and Pd/PdO

The palladium can be completely oxidized (in dry condition) in temperature range of 200-600 ºC, according to the reaction (R3):

$$Pd + 1/2\,O_2 \rightleftharpoons PdO \quad \Delta H^{\circ}_{298} = -119\ \text{kJmol}^{-1}\ Pd \qquad \text{(R3)}$$

Regardless of the temperature, the partial pressure of oxygen will attempt to remain in equilibrium with the metal and metal oxide. There is a unique partial pressure (called the decomposition pressure) at any temperature, which can be obtained from Equation (1-5) [5]. At oxygen partial pressures below the equilibrium value, the oxide will be reduced to Pd metal. Conversely, at partial pressures above the equilibrium value, oxidation of the metal takes place. Figure 1.4 represents the plot of the equilibrium O_2 pressure for $Pd \rightleftharpoons PdO$ transformation.

$$\Delta G^{\circ}_{R} = -RT\ \text{Ln}\ K_{eq} \qquad \text{(1-4)}$$

In which ($K_{eq} = \frac{1}{P_{O_2}^{0.5}}$). By substitution for Gibs free energy of the R3 we obtain [5].

$$p_{O_2}^{0.5}(\,1\ \text{atm})^{-0.5} = \exp\left(-\frac{11273}{T(K)} - 2.89\log(T) + 18.57\right) \qquad \text{(1-5)}$$

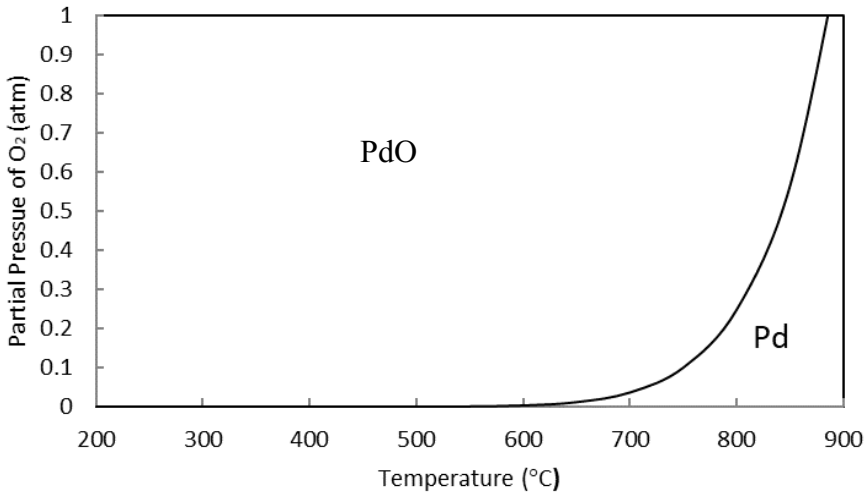

Figure 1.4 Equilibrium O_2 pressure for Pd⇌ PdO transformation

Kubaschewski and Alcock[62] presented an expression for ΔG_R° for the reaction R4 and R5:

$$Co_3O_4 \rightleftharpoons 3CoO + {}^1/_2\, O_2 \quad \text{(R4)}$$

$$PO_2^{0.5}(1\ atm^{-0.5}) = \exp\left(\frac{-22043.28}{T} + 17.816\right) \quad \text{(1-6)}$$

$$2CoO \rightleftharpoons Co + O_2 \quad \text{(R5)}$$

$$PO_2(1\ atm) = \exp\left(\frac{-56259.49}{T} + 17.009\right) \quad \text{(1-7)}$$

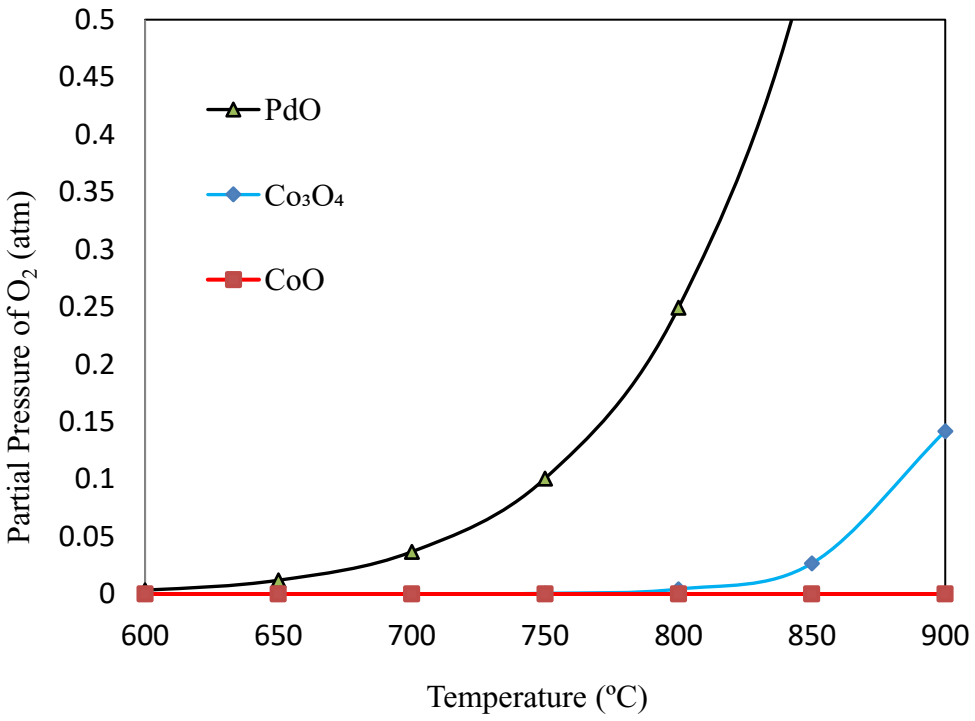

Figure 1.5 Equilibrium oxygen pressure for R3,R4 and R5 phase transformation calculated using expressions presented in [62].

Equilibrium oxygen partial pressure is calculated using equations (1-5 to 1-7) and the results are presented in Figure 1.5. This plot shows the cobalt potential to retain oxygen at lower partial

pressures than Pd. Therefore, it may be a useful oxygen donor under wet conditions, when surface lacks oxygen and PdO becomes reduced, but not CoO_X.

1.9 Literature review of Co use in methane combustion

Cobalt oxide has been reported in five different oxidation states in literature [CoO_2, Co_2O_3, CoO (OH), Co_3O_4 and CoO][63]. Cobalt oxide has been used in several industrial sectors, including CoO(OH) in electrodes of rechargeable alkaline batteries [64], CoO in carbon monoxide gas sensors[65] and as a magnetic material [66], Co_3O_4 as catalyst for the abatement of methane[67] and carbon monoxide abatement [68]. Due to their instability, cobalt oxides with oxidation states greater than three are not typically used in industry. Conversely, stable cobalt oxides such as Co_3O_4 and CoO are widely used by industry [63].

Among oxides of 3d elements, Co_3O_4 exhibits the fastest oxygen binding with the lowest heat, which unfavourable effect is counterbalanced by the high number of oxygen activation sites [69]. For example, the rate of oxygen exchange between molecular oxygen and Co_3O_4 at 300 °C is three orders of magnitude higher than that on Al_2O_3 [70]. Pd / Co_3O_4 catalysts were reported in several studies of methane combustion. Table 1-1 provides a rough comparison between reported catalysts, which exploit cobalt as promoter, support, and active metal. The effect of steam injection on catalyst performance has not been investigated thoroughly and is one of the aims of this study. Bare Co_3O_4 shows some catalytic activity (Table 1-1). Analysis of the listed catalysts that tested under wet conditions shows that PdCo/La-Al_2O_3 and $NiCo_2O_4$ show similar T_{100} under wet condition and the effect of Pd is remarkable in improving catalyst activity.

Lin et al. [59] synthesized Pd/Co-OMA-y via sol-gel approach. Ordered mesoporous alumina (OMA) has a well-defined pore structure which results in higher surface area therefore, more active sites for methane combustion reaction. Results showed that 0.5wt.% Pd/ Co-OMA-6 wt.% has higher content of Co^{2+}. The authors believed the variation of microstructure between Pd and Co has an impact on the surface oxygen, surface acidity/basicity, reducibility and after all the kinetics of the reaction [59].

In another recent study authors investigated the impact of using different precursors in Co_3O_4 synthesis on physiochemical properties/activity of catalyst [71]. They used cobalt acetate, cobalt nitrate, cobalt chloride, and cobalt sulfate. It was found that the Co_3O_4-Ac catalyst had relatively smaller surface area while higher stability and catalyst activity under wet and dry condition. The higher activity of this catalyst was manifested by its higher surface adsorbed oxygen and Co^{2+} concentration which was confirmed by XPS and Raman spectra [71].

Setiawan et al. [72] evaluated the activity and hydrothermal stability Co_3O_4, Fe_2O_3, as well as loaded with Au for oxidation of lean air-methane fuels. They showed that incorporating cobalt oxide in the catalyst improve the catalyst activity (i.e. T_{90} of Fe_2O_3 is about 510°C while T_{90} for Co_3O_4 is 440°C). In addition, the T_{90} of Co_3O_4 is about 50 °C lower than that of Au/Co_3O_4. According to Setiawan et al. [72] Co_3O_4 and Au/Co_3O_4 catalysts demonstrated exceptional hydrothermal stability. Additionally, the oxidation state of Co_3O_4 was observed to be reversible after stability tests. Andoni et al. [73] compared Co_3O_4 -based catalysts, comparison was among bulk, Al_2O_3-suppported and Ce-doped and they reported that the alumina-supported catalysts (10–40%wt. Co), often caused formation of $CoAl_2O_4$ which further impedes participation of cobalt species in the redox cycle therefore, it showed the least activity. They concluded that the activity of the bulk catalyst is controlled by an increased $Co^{3+/}Co^{2+}$ molar ratio, inferring the active role of the surface lattice oxygen in the reaction. The addition of 10% wt. of cerium to the Co_3O_4 lattice, resulted in a catalyst which exhibited higher stability under both dry and wet conditions owing to an improvement in the lattice oxygen mobility [73] In another study[74] they investigated the amount of ceria(5-30 %wt.) needed for optimal catalytic behavior of the above-mentioned catalyst (30% wt. Co/x-Ce-Al_2O_3) under both dry and wet environment. They concluded that all Co/xCe-Al showed better activity "irrespectively the ceria loading "with T_{50} values in the 480-540 °C. The best behavior was reported for Co/20Ce-Al catalyst [74]. The catalyst was tested under prolonged reaction time 150h under dry condition. The authors reported that wet environment affected the catalyst performance in a partially reversible manner [74].

Ercolino et al. [75] studied Pd/Co_3O_4 catalysts with palladium loading 0.5–5wt. %, they attributed the improved catalytic activity to the efficient PdO phase dispersion. The authors suggested that cobalt oxide aids in OH species removal from PdO liberating active sites for

methane adsorption. In addition, cobalt spinel supplies O to the PdO phase, assisting in active sites regeneration [75]. The metal-support interaction between Co_3O_4 and palladium oxide nanocrystals varies with the cobalt spinel morphology [76] and has been postulated that because of this interaction CoO(OH) is one of the main surface species [67]. Consequently, cobalt spinel may serves as a reservoir for OH groups from $Pd(OH)_2$[75]. Thus, proximity of the cobalt oxide to PdO improves the regeneration of active sites. The regeneration is achieved through the accommodation of hydroxyl molecules and by supplying the oxide in catalyst material (lattice oxygen). The authors stated XPS measurements indicate the increase of Co^{2+} surface concentration caused improved oxygen supply, resulting from the increase in the oxygen vacancies concentration, and thus higher oxygen mobility in the Co_3O_4 subsurface layer [75].

Hoflund et al. [67] performed the surface characterization on Pd/Co_3O_4 as highly active catalyst for methane combustion reaction. The authors reported palladium oxide (II) (PdO) is the prevalent state of palladium. Hydrogen formed because of methane dissociation participates in the formation of hydroxyl species on cobalt oxide surface. Recombination of hydroxyls liberates water and the oxide phase [67]. The oxidation-reduction cycle between Co^{2+} and Co^{3+} plays a critical role for the catalytic behavior of cobalt in methane oxidation reaction. Cobalt oxide stabilizes the palladium in its oxidized form and acts as the oxygen storage [77]. Hoflund et al. [78] investigated the impact of different oxide supports (ZrO_2, SnO_2, Co_3O_4, CeO_2, Al_2O_3, TiO_2, MnO_2 and Mn_3O_4) over Pd-based catalysts in methane combustion. They found that T_{100} is achieved at 320, 330, 330, 340, 372, 372, 450 and 460˚C, respectively. The oxide supports demonstrated high activity in the order $Co_3O_4 > MnO_2 > TiO_2 > ZrO_2$.

Wang et al. suggested that facile Co^{2+} -to- Co^{3+} transformation and the abundance of surface $Co^{3+}$is the primary causes for the enhanced catalytic behavior of Co_3O_4/γ-Al_2O_3 catalyst in CH_4 oxidation reaction [84]. Jodłowski et al. studied Co_3O_4 catalyst doped with CeO_2 and PdO and the structural analysis of the catalysts was performed by Raman and XPS spectroscopies. The obtained results revealed that cobalt spinel is the active form of cobalt and oxidized form of palladium (PdO) form is present [85].The comparison between PdCo/La-Al_2O_3 and Pd/La-Al_2O_3 was done by Long et al. [57] the results indicated that in the presence of steam, as temperature increased, activity of Pd/La-Al_2O_3 increased more slowly than that of PdCo/La-Al_2O_3. While at T> 404˚C, the catalytic activity order changed to PdCo/La-Al_2O_3>Pd/LaAl_2O_3>Pd/Co/La-Al_2O_3

[57]. It was noted that adding Co to the catalyst enhanced the catalytic activity for methane conversion, while, it decreased the water poisoning effect for palladium-based catalysts, that are susceptible to water. The authors concluded that the preparation method plays an important role in enhancing the catalyst performance. They concluded PdCo/La-Al_2O_3, prepared by co-impregnation method, showed higher resistance to water poisoning. The competition between water and methane molecules on the active sites caused formation of $Pd(OH)_2$, that effectively blocked methane molecules access to the active palladium oxide phase surface. Since the co-impregnated catalyst by Pd and Co showed better water-resistance than Pd/La-Al_2O_3 therefore, authors postulated that Co_3O_4 might be more active to react with water than PdO [57].

Tang et al. [63] conducted TG-MS analysis to study the transformation of CoO(OH) → Co_3O_4 → CoO indicates two weight losses at 280 ˚C for Co_3O_4 (equation R6) and 850 °C for CoO (equation R7), implying different cobalt oxide structures (Figure 1.6)

$$12CoO(OH) \rightarrow 4Co_3O_4 + O_2 + 6H_2O \quad \text{(R6)}$$

$$2Co_3O_4 \rightarrow 6CoO + O_2 \quad \text{(R7)}$$

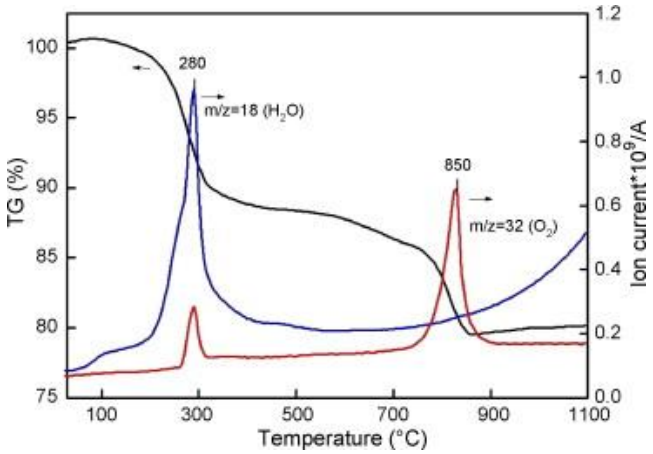

Figure 1.6 Thermogravimetric analysis of the outlet gases from the decomposition of CoO(OH) by TG-MS H_2O (blue) and O_2 (red). Reprinted from [62] with permission from Elsevier copyright 2008.

Table 1-1 Summary of different catalysts containing CoO_x in the application of catalytic lean methane combustion under various operating conditions.

#	**Catalyst Type,** **Pd content (wt.%)** **SSA (m^2 g^{-1})**	**Reaction conditions:** **Reactive mix (vol.%)** **Flow rate (NL min^{-1})** **GHSV (h^{-1}) or** **WHSV (NL h^{-1} g^{-1})** **Time on stream (h)**	**Wet/Dry**	**T_{50} (°C)** **Activity window (°C)**	**T_{100} (°C)**	**Reference** **Year**
1	Pd/Co-OMA-6 wt.% OMA: ordered mesoporous alumina	CH_4 (1 vol.%), O_2 (10 vol.%) N_2 (balance gas) 30000 mL/g h 50h on stream	Wet	400 340 - 450	450	[59] 2020
2	Co_3O_4-Ac* *Acetate BET = 15.4 m^2/g	0.5% CH_4, 8.0% O_2 N_2 (balance gas)	Wet/Dry	318		[71] 2020
3	Co/20Ce-Al BET= 93 m^2/g	1% CH_4, 10% O_2 N_2 (balance gas) 60000 h^{-1} 150 h on stream	Wet/Dry	480	>575	[74] 2020
4	Pd–$NiCo_2O_4/SiO_2$ BET = 156.54 m^2/g	1.0% CH_4 in air into the 40 ml/min WHSV = 30000 ml g^{-1} h^{-1}	Dry	~300	378	[58] 2017
	Pd–Co_3O_4/SiO_2 BET = 156.76 m^2/g				420	
	$NiCo_2O_4/SiO_2$ BET = 168.22 m^2/g				455	
	Co_3O_4/SiO_2 BET = 176.48 m^2/g				525	

Table 1-1 continued

#	**Catalyst Type,** **Pd content (wt.%)** **SSA (m^2 g^{-1})**	**Reaction conditions:** **Reactive mix (vol.%)** **Flow rate (NL min^{-1})** **GHSV (h^{-1}) or** **WHSV (NL h^{-1} g^{-1})** **Time on stream (h)**	**Wet/Dry**	**T_{50} (°C)** **Activity window (°C)**	**T_{100} (°C)**	**Reference Year**
5	Co_3O_4 nanosheets Co_3O_4-EG(10)	1.6% CH_4, 7.0% O_2, N_2 (balance gas) GHSV = 15000 mL/(gh) 13h on stream	Dry	T_{10} = ~260	T_{90} = ~385	[54] 2017
6	ZrO_2(2)-Co_3O_4 BET = 41 m^2/g	0.5% CH_4, 8% O_2 N_2 (balance gas) Gas feed = 40 ml·min^{-1}	Dry		Highest activity with T_{90} = ~335 T_{90} over ZrO_2(10)-Co_3O_4= 425	[79] 2017
7	Pd/Co_3O_4 over an alumina Al_2O_3 monolith, 3 wt.%	0.5% or 1% CH_4 WHSV = 30 and 60 $NLh^{-1}gcat^{-1}$	Dry		lower than 400	[80] 2017
8	3 wt.% Pd/CoFe	2.0 % CH_4	Dry	(250–550)	T_{50}= 483	[81] 2017
9	1% Pd/Co_3O_4 BET = 6 m^2 g^{-1}	0.5% CH_4, 2% O_2 N_2 (balance gas) 0.1 NL min^{-1} 12000 h^{-1}	Dry	390 (320–460)		[82] 2016

Table 1-1 continued

#	**Catalyst Type,** **Pd content (wt.%)** **SSA (m^2 g^{-1})**	**Reaction conditions:** **Reactive mix (vol.%)** **Flow rate (NL min^{-1})** **GHSV (h^{-1}) or** **WHSV (NL h^{-1} g^{-1})** **Time on stream (h)**	**Wet/Dry**	**T_{50} (°C)** **Activity window (°C)**	**T_{100} (°C)**	**Reference Year**
10	2.2% Au/Co_3O_4 BET=33 m^2/g	0.6% CH_4 in air GHSV = 100000 h^{-1} 6000 ppm CH_4 3% H_2O 24h on stream	Wet	380 (275–550)	500 for Co_3O_4	[68] 2015
11	3% (Pd + Co)/Al_2O_3 Pd:Co = 1:1	0.4% CH_4, 10% O_2, N_2 (balance gas) 0.1 L min^{-1} 300 h^{-1}		425 (300–550)		[56] 2015
12	$NiCo_2O_4$	10% CH_4, 99.99% O_2 Ar (balance gas) GHSV =24000 ml $g^{-1}h^{-1}$ CH_4 0.2%, O_2 5%, CO_2 15%, H_2O 10% 48 h on stream	Dry Wet	230 240	350 450	[83] 2015

Table 1-1 continued

#	**Catalyst Type,** **Pd content (wt.%)** **SSA (m^2 g^{-1})**	**Reaction conditions:** **Reactive mix (vol.%)** **Flow rate (NL min^{-1})** **GHSV (h^{-1}) or** **WHSV (NL h^{-1} g^{-1})** **Time on stream (h)**	**Wet/Dry**	**T_{50} (°C)** **Activity window (°C)**	**T_{100} (°C)**	**Reference Year**
13	Co_3O_4/γ-Al_2O_3 BET = 131 m2/g	0.2 % CH_4, 10 % O_2 GHSV = 36000 mL/h g	Dry	300	550	[84] 2015
14	Co_3O_4 catalyst doped with CeO_2 and PdO	4000 ppm CH_4, 10% O_2 He (balance gas) Gas flow 200 cm^3/min 10 days on stream	Dry			[85] 2014
15	Porous Co_3O_4 nanorods BET = 170.2 m^2/g	2% CH_4, 98% Air GHSV = 48000 h^{-1}	Dry	420	T_{90} = 515	[86] 2011
16	PdCo/La-Al_2O_3 1.25 wt.% Pd, 2 wt.%Co, BET = 132 m^2/g	630 ppm CH_4, 0.4 % CO, 5 % O_2, 12 % CO_2 N_2 (balance gas) GHSV = 34000 h^{-1}	Dry Wet 10%		410 450	[57] 2010

Table 1-1 continued

#	**Catalyst Type,** **Pd content (wt.%)** **SSA (m^2 g^{-1})**	**Reaction conditions:** **Reactive mix (vol.%)** **Flow rate (NL min^{-1})** **GHSV (h^{-1}) or** **WHSV (NL h^{-1} g^{-1})** **Time on stream (h)**	**Wet/Dry**	**T_{50} (°C)** **Activity window (°C)**	**T_{100} (°C)**	**Reference Year**
17	$La_{0.1}Ce_{0.4}Co_{1.5}O_{3\pm\delta}$	2% CH_4 in He (balance gas) GHSV = 55500 h^{-1}	Dry	390	550	[87] 2008
18	10% Pd/Co_3O_4 BET = 20 m^2/g	1.2% CH_4, 12% O_2, 0.033 L min^{-1} 6 days on stream	Dry	240 (170–280)	300	[67] 2006
19	10 wt.% Co_3O_4/ZrO_2	CH_4 (1 vol.%), Air (99 vol.%) GHSV = 40000 h^{-1}	Dry	650 (550-750)	>700	[88] 2001
20	Pd/Co_3O_4 5 wt.% BET = 14.7 m^2/g	1.2% CH_4, 12% O_2 80 mL/min	Dry	260 (5%)	310 (5%)	[78] 1999
	10 wt.% BET = 20.1 m^2/g			246 (10%)	300(10%)	

1.10 Hypothesis and research objective

Among the transition metal oxides, cobalt oxide is a promising promoter or even an alternative catalyst for Pd-catalyzed methane combustion because of its ability to activate methane, its oxygen storage capacity, and its potential effect on the extent of H_2O inhibition. Recently, it has attracted significant attention in the field, as shown in Table 1-1, but the reported catalytic tests were mostly performed with dry feed and a narrow set of conditions. Due to its relatively low $Co-O$ bond energy (368 kJ/mol), the oxide may provide beneficial effects during wet methane combustion. This thesis aims to verify this hypothesis and understand the role of Co in the wet catalytic combustion reaction. From a practical point of view, we aim to develop an active Pd-Co or Co-only catalyst with stable performance in methane combustion.

As follows from the above literature review, only a few studies have been done involving cobalt oxide under wet environment and there is a knowledge gap regarding methane combustion kinetics. To shed light on the contribution of Co_3O_4, in this study the kinetic study of methane combustion on Pd/Co_3O_4 and Co_3O_4 under fuel lean condition are performed in temperature range (250-550°C) in presence of 5 and 10% water.

To investigate the Pd and Co speciation in cobalt oxide and Pd/CoO_x catalysts during lean methane combustion in wet feeds at temperatures below 450° C, *in situ* X-ray absorption spectroscopy (XAS) are performed. Obtaining the distribution of Pd and Co species, including their hydroxides, as a function of reaction temperature will help understanding the underlying mechanism of methane combustion using cobalt oxide.

The thesis also attempts to improve the mass-based activity of Co_3O_4 by its deposition on the CeO_2 support. Testing cobalt catalyst supported on ceria oxide alongside with kinetics would provide more information about the Co-Ce system. The material represents a viable alternative to Pt-group metal catalysts from the viewpoint of the catalyst price, abundance, and water tolerance.

1.11 Research plan and thesis outline

The focus of this study is to evaluate monometallic cobalt catalysts and the effect of a cobalt oxide as a support on Pd catalysts in wet methane combustion. Cobalt will be added as a component to the support (CeO_2). The reduction of PdO under the reaction conditions could be hindered by incorporating metal oxides with high oxygen capacity, such as cobalt oxide. As highlighted in the previous paragraphs, various parameters such as preparation method, metal loading, precursors, support, and pretreatments can greatly affect properties of metal-oxide catalysts including the morphology, dispersion, and specific surface area. These parameters have direct impact on the activity and performance of the catalysts. Based on this fact, a series of catalysts with different Pd and Co loadings evaluated to study catalysts with different particle sizes and different oxygen storage capacities. These catalysts will be characterized and tested for methane combustion.

We also addressed Co-Ce formulation, with the goal of minimizing noble metals needed in the catalyst formulation. The hypothesis is that if Co provides oxygen to Pd, which is active in oxygen-deficient feeds, will be needed in lower quantities. If this hypothesis is proven to be true, this would result in lower catalyst costs. To achieve the thesis objective, a catalyst was synthesized and tested for the combustion application alongside with kinetics studies to ensure the understanding of the main reaction, which would help in catalyst design.

In Chapter 1, a brief introduction of methane emission control from the NGV and utilizing catalytical combustion approach was addressed. Redox mechanism, water poisoning effect on methane combustion, thermodynamic of the system and a brief literature review on using cobalt in catalytic methane combustion.

In chapter 2, a brief information on experimental set up and procedures presented. The method for identification/quantification of the reaction products was discussed. Later the equations and criteria used to verify kinetic regime (heat and mass transfer), plug flow behavior were presented.

In chapter 3, a kinetic study of lean methane combustion on Pd/Co_3O_4 and Co_3O_4 catalysts presented. Experiments were conducted at varying different methane and water concentration. The results have been correlated with first order corresponding to the methane concertation.

In chapter 4, has driven significant effort toward fundamental studies of lean methane combustion using Pd/Co_3O_4 and Co_3O_4 by means of *in situ* X-ray absorption spectroscopy. The analysis shed light on the metal support interactions in Pd/Co system to elucidate the relationship between the performance and its physico chemical properties of catalyst. To investigate the Pd and Co speciation in cobalt oxide and Pd/CoO_x catalysts during lean methane combustion in wet feeds, *in situ* X-ray absorption spectroscopy (XAS) were performed. It was suggested that Pd has a double role: as a promoter for Co-catalyzed methane combustion and as an active catalyst itself.

In chapter 5, with the acquired knowledge on cobalt system through previous chapters, a new support (CeO_2) was employed to improve the catalyst activity and present as a practical catalyst with lower cost. Cobalt deposition on ceria produced a sintering-resistant catalyst for lean wet methane combustion.

Chapter 6 contains the conclusions of this research and recommendation for further this study was addressed.

1.12 References

1. Strobel, R., Grunwaldt, J.-D., Camenzind, A., Pratsinis, S.E., Baiker, A.: Flame-made alumina supported Pd-Pt nanoparticles: Structural properties and catalytic behavior in methane combustion. Catal. Letters. 104, 9–16 (2005). doi:10.1007/s10562-005-7429-y

2. Abbasi, R., Wu, L., Wanke, S.E., Hayes, R.E.: Kinetics of methane combustion over Pt and Pt-Pd catalysts. Chem. Eng. Res. Des. 90, 1930–1942 (2012). doi:10.1016/j.cherd.2012.03.003

3. Liu, B., Checkel, M.D., Hayes, R.E.: Experimental study of a reverse flow catalytic converter for a dual fuel engine. Can. J. Chem. Eng. 79, 491–506 (2001). doi:10.1002/cjce.5450790405

4. Cargnello, M., Delgado Jan, J.J., Hernndez Garrido, J.C., Bakhmutsky, K., Montini, T., Calvino Gmez, J.J., Gorte, R.J., Fornasiero, P.: Exceptional activity for methane combustion over modular Pd@CeO_2 subunits on functionalized Al_2O_3. Science, 337(6095), 713–717 (2012). doi:10.1126/science.1222887

5. Hayes, R.E., Kolaczkowski, S.T.: Introduction to catalytic combustion. Gordon and Breach, Australia (1997)

6. Taylor, K.C.: Automobile Catalytic Converters BT - Catalysis: Science and Technology Volume 5. Presented at the (1984)

7. Impacts des normes antipollution sur la demande mondiale en platinoïdes : cas du platine, du palladium et du rhodium | Minéralinfo, http://www.mineralinfo.fr/ecomine/impacts-normes-antipollution-demande-mondiale-en-platinoides-cas-platine-palladium-rhodium

8. Irandoust, S., Andersson, B.: Monolithic Catalysts for Nonautomobile Applications. Catal. Rev. 30, 341–392 (1988). doi:10.1080/01614948808080809

9. Ciuparu, D., Lyubovsky, M.R., Altman, E., Pfefferle, L.D., Datye, A.: Catalytic combustion of methane over palladium-based catalysts. Catal. Rev. - Sci. Eng. 44, 593–649 (2002). doi:10.1081/CR-120015482

10. Gélin, P., Primet, M.: Complete oxidation of methane at low temperature over noble metal based catalysts: a review, (2002)

11. Stotz, H., Maier, L., Deutschmann, O.: Methane Oxidation over Palladium: On the Mechanism in Fuel-Rich Mixtures at High Temperatures. Top. Catal. 60, 83–109 (2017). doi:10.1007/s11244-016-0717-5

12. Chin, Y.-H., Buda, C., Neurock, M., Iglesia, E.: Consequences of metal-oxide interconversion for C-H bond activation during CH_4 reactions on Pd catalysts. J. Am. Chem. Soc. 135, 15425–15442 (2013). doi:10.1021/ja405004m

13. Fujimoto, K.-I., Ribeiro, F.H., Avalos-Borja, M., Iglesia, E.: Structure and reactivity of

PdOx/ZrO_2 catalysts for methane oxidation at low temperatures. J. Catal. 179, 431–442 (1998). doi:10.1006/jcat.1998.2178

14. Gélin, P., Urfels, L., Primet, M., Tena, E.: Complete oxidation of methane at low temperature over Pt and Pd catalysts for the abatement of lean-burn natural gas fuelled vehicles emissions: influence of water and sulphur containing compounds. Catal. Today. 83, 45–57 (2003). doi:10.1016/S0920-5861(03)00215-3

15. Nassiri, H., Lee, K.-E., Hu, Y., Hayes, R.E., Scott, R.W.J., Semagina, N.: Platinum Inhibits Low-Temperature Dry Lean Methane Combustion through Palladium Reduction in Pd-Pt/Al_2O_3: An In Situ X-ray Absorption Study. ChemPhysChem. 18, 238–244 (2017). doi:10.1002/cphc.201600993

16. Zhu, G., Han, J., Zemlyanov, D.Y., Ribeiro, F.H.: The turnover rate for the catalytic combustion of methane over palladium is not sensitive to the structure of the catalyst. J. Am. Chem. Soc. 126, 9896–9897 (2004). doi:10.1021/ja049406s

17. Au-Yeung, J., Chen, K., Bell, A.T., Iglesia, E.: Isotopic studies of methane oxidation pathways on PdO catalysts. J. Catal. 188, 132–139 (1999). doi:10.1006/jcat.1999.2643

18. Groppi, G., Cristiani, C., Lietti, L., Forzatti, P.: Study of PdO/Pd transformation over alumina supported catalysts for natural gas combustion. Stud. Surf. Sci. Catal. 130, 3801–3806 (2000). doi:10.1016/S0167-2991(00)80615-1

19. Huang, F., Chen, J., Hu, W., Li, G., Wu, Y., Yuan, S., Zhong, L., Chen, Y.: Pd or PdO: Catalytic active site of methane oxidation operated close to stoichiometric air-to-fuel for natural gas vehicles. Appl. Catal. B Environ. 219, 73–81 (2017). doi:10.1016/j.apcatb.2017.07.037

20. Bychkov, V.Y., Tulenin, Y.P., Slinko, M.M., Khudorozhkov, A.K., Bukhtiyarov, V.I., Sokolov, S., Korchak, V.N.: Self-oscillations during methane oxidation over Pd/Al_2O_3: Variations of Pd oxidation state and their effect on Pd catalytic activity. Appl. Catal. A Gen. 522, 40–44 (2016). doi:10.1016/J.APCATA.2016.04.024

21. Nassiri, H., Lee, K.-E., Hu, Y., Hayes, R.E., Scott, R.W.J., Semagina, N.: Water shifts PdO-

catalyzed lean methane combustion to Pt-catalyzed rich combustion in PdPt catalysts: In situ X-ray absorption spectroscopy. J. Catal. 352, 649–656 (2017). doi:10.1016/j.jcat.2017.06.008

22. Qi, W., Ran, J., Wang, R., Du, X., Shi, J., Niu, J., Zhang, P., Ran, M.: Kinetic consequences of methane combustion on Pd, Pt and Pd-Pt catalysts. RSC Adv. 6, 109834–109845 (2016). doi:10.1039/c6ra21150j

23. Pitchai, R., Klier, K.: Partial Oxidation of Methane. Catal. Rev. 28, 13–88 (1986). doi:10.1080/03602458608068085

24. Zasada, F., Janas, J., Piskorz, W., Gorczyńska, M., Sojka, Z.: Total Oxidation of Lean Methane over Cobalt Spinel Nanocubes Controlled by the Self-Adjusted Redox State of the Catalyst: Experimental and Theoretical Account for Interplay between the Langmuir-Hinshelwood and Mars-Van Krevelen Mechanisms. ACS Catal. 7, 2853–2867 (2017). doi:10.1021/acscatal.6b03139

25. Seimanides, S., Stoukides, M.: Catalytic oxidation of methane on polycrystalline palladium supported on stabilized zirconia. J. Catal. 98, 540–549 (1986). doi:10.1016/0021-9517(86)90342-8

26. Fujimoto, K.-I., Ribeiro, F.H., Bell, A.T., Iglesia, E.: Reaction pathways and structural requirements in the catalytic oxidation of methane at low temperatures. In: ACS Division of Petroleum Chemistry, Inc. Preprints. pp. 110–113 (1996)

27. Garbowski, E., Feumi-Jantou, C., Mouaddib, N., Primet, M.: Catalytic combustion of methane over palladium supported on alumina catalysts: Evidence for reconstruction of particles. Appl. Catal. A, Gen. 109, 277–291 (1994). doi:10.1016/0926-860X(94)80124-X

28. Bahlawane, N.: Kinetics of methane combustion over CVD-made cobalt oxide catalysts. Appl. Catal. B Environ. 67, 168–176 (2006). doi:10.1016/j.apcatb.2006.03.024

29. Zhu, G., Han, J., Zemlyanov, D.Y., Ribeiro, F.H.: Temperature dependence of the kinetics for the complete oxidation of methane on palladium and palladium oxide. J. Phys. Chem. B. 109, 2331–2337 (2005). doi:10.1021/jp0488665

30. Colussi, S., Trovarelli, A., Vesselli, E., Baraldi, A., Comelli, G., Groppi, G., Llorca, J.: Structure and morphology of Pd/Al_2O_3 and $Pd/CeO_2/Al_2O_3$ combustion catalysts in Pd-PdO transformation hysteresis. Appl. Catal. A Gen. 390, 1–10 (2010). doi:10.1016/j.apcata.2010.09.033

31. Schwartz, W.R., Pfefferle, L.D.: Combustion of methane over palladium-based catalysts: Support interactions. J. Phys. Chem. C. 116, 8571–8578 (2012). doi:10.1021/jp2119668

32. Müller, C.A., Maciejewski, M., Koeppel, R.A., Baiker, A.: Combustion of methane over palladium/zirconia derived from a glassy Pd-Zr alloy: Effect of Pd particle size on catalytic behavior. J. Catal. 166, 36–43 (1997). doi:10.1006/jcat.1997.1501

33. Müller, C.A., Maciejewski, M., Koeppel, R.A., Baiker, A.: Combustion of methane over palladium/zirconia: Effect of Pd-particle size and role of lattice oxygen. Catal. Today. 47, 245–252 (1999). doi:10.1016/S0920-5861(98)00305-8

34. Farrauto, R.J., Lampert, J.K., Hobson, M.C., Waterman, E.M.: Thermal decomposition and reformation of PdO catalysts; support effects. Appl. Catal. B, Environ. 6, 263–270 (1995). doi:10.1016/0926-3373(95)00015-1

35. Stotz, H., Maier, L., Boubnov, A., Gremminger, A.T., Grunwaldt, J.-D., Deutschmann, O.: Surface reaction kinetics of methane oxidation over PdO. J. Catal. 370, 152–175 (2019). doi:10.1016/J.JCAT.2018.12.007

36. Forzatti, P., Lietti, L.: Catalyst deactivation. Catal. Today. 52, 165–181 (1999). doi:10.1016/S0920-5861(99)00074-7

37. Cullis, C.F., Nevell, T.G., Trimm, D.L.: Role of the catalyst support in the oxidation of methane over palladium. J. Chem. Soc. Faraday Trans. 1 Phys. Chem. Condens. Phases. 68, 1406–1412 (1972). doi:10.1039/F19726801406

38. Burch, R.: Low NO_x options in catalytic combustion and emission control. Elsevier (1997)

39. Escandón, L.S., Niño, D., Díaz, E., Ordóñez, S., Díez, F. V: Effect of hydrothermal ageing

on the performance of Ce-promoted PdO/ZrO_2 for methane combustion. Catal. Commun. 9, 2291–2296 (2008). doi:10.1016/j.catcom.2008.05.026

40. Xu, Q., Kharas, K.C., Croley, B.J., Datye, A.K.: The Sintering of Supported Pd Automotive Catalysts. ChemCatChem. 3, 1004–1014 (2011). doi:10.1002/cctc.201000392

41. Arai, H., Machida, M.: Recent progress in high-temperature catalytic combustion. Catal. Today. 10, 81–94 (1991). doi:10.1016/0920-5861(91)80076-L

42. Burch, R., Crittle, D.J., Hayes, M.J.: C-H bond activation in hydrocarbon oxidation on heterogeneous catalysts. Catal. Today. 47, 229–234 (1999). doi:10.1016/S0920-5861(98)00303-4

43. Ciuparu, D., Altman, E., Pfefferle, L.: Contributions of lattice oxygen in methane combustion over PdO-based catalysts. J. Catal. 203, 64–74 (2001). doi:10.1006/jcat.2001.3331

44. Gholami, R., Alyani, M., Smith, K.J.: Deactivation of Pd catalysts by water during low temperature methane oxidation relevant to natural gas vehicle converters. Catalysts. 5, 561–594 (2015). doi:10.3390/catal5020561

45. Schwartz, W.R., Ciuparu, D., Pfefferle, L.D.: Combustion of methane over palladium-based catalysts: Catalytic deactivation and role of the support. J. Phys. Chem. C. 116, 8587–8593 (2012). doi:10.1021/jp212236e

46. Ciuparu, D., Bozon-Verduraz, F., Pfefferle, L.: Oxygen exchange between palladium and oxide supports in combustion catalysts. J. Phys. Chem. B. 106, 3434–3442 (2002). doi:10.1021/jp013577r

47. Ciuparu, D., Perkins, E., Pfefferle, L.: In situ DR-FTIR investigation of surface hydroxyls on γ-Al_2O_3 supported PdO catalysts during methane combustion. Appl. Catal. A Gen. 263, 145–153 (2004). doi:10.1016/j.apcata.2003.12.006

48. Willis, J.J., Goodman, E.D., Wu, L., Riscoe, A.R., Martins, P., Tassone, C.J., Cargnello, M.: Systematic Identification of Promoters for Methane Oxidation Catalysts Using Size- and

Composition-Controlled Pd-Based Bimetallic Nanocrystals. J. Am. Chem. Soc. 139, 11989–11997 (2017). doi:10.1021/jacs.7b06260

49. Rassoul, M., Gaillard, F., Garbowski, E., Primet, M.: Synthesis and Characterisation of Bimetallic Pd–Rh/Alumina Combustion Catalysts, (2001)

50. Watanabe, T., Kawashima, K., Tagawa, Y., Tashiro, K., Anoda, H., Ichioka, K., Sumiya, S., Zhang, G.: New DOC for light duty diesel DPF system. SAE Tech. Pap. (2007). doi:10.4271/2007-01-1920

51. Persson, K., Pfefferle, L.D., Schwartz, W., Ersson, A., Jrs, S.G.: Stability of palladium-based catalysts during catalytic combustion of methane: The influence of water. Appl. Catal. B Environ. 74, 242–250 (2007). doi:10.1016/j.apcatb.2007.02.015

52. Yeh, T.-F., Bi, J.-L., Lee, H.-G., Chu, K.-S., Wang, C.-B.: Phase transformation and catalytic activity of hexaaluminates upon high temperature pretreatment. J. Alloys Compd. 425, 353–356 (2006). doi:10.1016/j.jallcom.2006.01.055

53. Wang, F., Zhang, L., Xu, L., Deng, Z., Shi, W.: Low temperature CO oxidation and CH_4 combustion over Co_3O_4 nanosheets. (2017). https://doi.org/10.1016/j.fuel.2017.04.140

54. Chen, J., Arandiyan, H., Gao, X., Li, J.: Recent Advances in Catalysts for Methane Combustion. Catal. Surv. from Asia. 19, 140–171 (2015). doi:10.1007/s10563-015-9191-5

55. Satsuma, A., Tojo, T., Okuda, K., Yamamoto, Y., Arai, S., Oyama, J.: Effect of preparation method of Co-promoted Pd/alumina for methane combustion. Catal. Today. 242, 308–314 (2015). doi:10.1016/j.cattod.2014.05.046

56. Long, E., Zhang, X., Li, Y., Liu, Z., Wang, Y., Gong, M., Chen, Y.: Effect of cobalt oxide on performance of Pd catalysts for lean-burn natural gas vehicles in the presence and absence of water vapor. J. Nat. Gas Chem. 19, 134–138 (2010). doi:10.1016/S1003-9953(09)60044-X

57. Huang, Q., Li, W., Lin, Q., Zheng, X., Pan, H., Pi, D., Shao, C., Hu, C., Zhang, H.: Catalytic performance of Pd–$NiCo_2O_4/SiO_2$ in lean methane combustion at low temperature. J. Energy

Inst. 91, 733–742 (2018). doi:https://doi.org/10.1016/j.joei.2017.05.008

58. Lin, J., Chen, Y., Liu, X., Chen, X., Zheng, Y., Huang, F., Xiao, Y., Zheng, Y., Jiang, L.: Microstructural property regulation and performance in methane combustion reaction of ordered mesoporous alumina supported palladium-cobalt bimetallic catalysts. Appl. Catal. B Environ. 263, (2020). doi:10.1016/j.apcatb.2019.118269

59. Zasada, F., Gryboś, J., Budiyanto, E., Janas, J., Sojka, Z.: Oxygen species stabilized on the cobalt spinel nano-octahedra at various reaction conditions and their role in catalytic CO and CH_4 oxidation, N_2O decomposition and oxygen isotopic exchange. J. Catal. 371, 224–235 (2019). doi:10.1016/J.JCAT.2019.02.010

60. Zasada, F., Piskorz, W., Cristol, S., Paul, J.-F., Kotarba, A., Sojka, Z.: Periodic Density Functional Theory and Atomistic Thermodynamic Studies of Cobalt Spinel Nanocrystals in Wet Environment: Molecular Interpretation of Water Adsorption Equilibria. J. Phys. Chem. C. 114, 22245–22253 (2010). doi:10.1021/jp109264b

61. Kubaschewski, O., Alcock, C.B.: Metallurgical thermochemistry. Oxford ; New York : Pergamon Press, c1979; 5th ed., rev. and enl (1979)

62. Tang, C.-W., Wang, C.-B., Chien, S.-H.: Characterization of cobalt oxides studied by FT-IR, Raman, TPR and TG-MS, (2008). https://doi.org///doi.org/10.1016/j.tca.2008.04.015

63. Lichtenberg, F., Kleinsorgen, K.: Stability enhancement of the CoOOH conductive network of nickel hydroxide electrodes. J. Power Sources. 62, 207–211 (1996). doi:10.1016/S0378-7753(96)02431-7

64. Wu, R.-J., Wu, J.-G., Tsai, T.-K., Yeh, C.-T.: Use of cobalt oxide CoOOH in a carbon monoxide sensor operating at low temperatures, (2006). https://doi.org///doi.org/10.1016/j.snb.2006.01.053

65. Makhlouf, S.A.: Magnetic properties of Co_3O_4 nanoparticles. J. Magn. Magn. Mater. 246, 184–190 (2002). doi:10.1016/S0304-8853(02)00050-1

66. Hoflund, G.B., Li, Z.: Surface characterization study of a Pd/Co_3O_4 methane oxidation catalyst. Appl. Surf. Sci. 253, 2830–2834 (2006). doi:10.1016/j.apsusc.2006.05.115

67. Lin, H.-K., Chiu, H.-C., Tsai, H.-C., Chien, S.-H., Wang, C.-B.: Synthesis, characterization and catalytic oxidation of carbon monoxide overcobalt oxide. Catal. Letters. 88, 169–174 (2003). doi:1024013822986

68. Sokolovskii, V.D.: Principles of Oxidative Catalysis on Solid Oxides. Catal. Rev. 32, 1–49 (1990). doi:10.1080/01614949009349939

69. Boreskov, G.K., Muzykantov, V.S.: Investigation of Oxide-Type Oxidation Catalysts By Reactions of Oxygen Isotopic Exchange. Ann. N. Y. Acad. Sci. 213, 137–170 (1973). doi:10.1111/j.1749-6632.1973.tb51065.x

70. Zheng, Y., Yu, Y., Zhou, H., Huang, W., Pu, Z.: Combustion of lean methane over Co_3O_4 catalysts prepared with different cobalt precursors. RSC Adv. 10, 4490–4498 (2020). doi:10.1039/C9RA09544F

71. Setiawan, A., Kennedy, E.M., Dlugogorski, B.Z., Adesina, A.A., Stockenhuber, M.: The stability of Co_3O_4, Fe_2O_3, Au/Co_3O_4 and Au/Fe_2O_3 catalysts in the catalytic combustion of lean methane mixtures in the presence of water, (2015). https://doi.org///doi.org/10.1016/j.cattod.2014.11.031

72. Choya, A., de Rivas, B., González-Velasco, J.R., Gutiérrez-Ortiz, J.I., López-Fonseca, R.: Oxidation of residual methane from VNG vehicles over Co_3O_4-based catalysts: Comparison among bulk, Al_2O_3-supported and Ce-doped catalysts. Appl. Catal. B Environ. 237, 844–854 (2018). doi:10.1016/J.APCATB.2018.06.050

73. Choya, A., de Rivas, B., González-Velasco, J.R., Gutiérrez-Ortiz, J.I., López-Fonseca, R.: Oxidation of lean methane over cobalt catalysts supported on ceria/alumina. Appl. Catal. A Gen. 591, (2020). doi:10.1016/j.apcata.2019.117381

74. Ercolino, G., Stelmachowski, P., Grzybek, G., Kotarba, A., Specchia, S.: Optimization of Pd catalysts supported on Co_3O_4 for low-temperature lean combustion of residual methane. Appl.

Catal. B Environ. 206, 712–725 (2017)

75. Hu, L., Peng, Q., Li, Y.: Low-temperature CH_4 Catalytic Combustion over Pd Catalyst Supported on Co3O4 Nanocrystals with Well-Defined Crystal Planes. ChemCatChem. 3, 868–874 (2011). doi:10.1002/cctc.201000407

76. Stefanov, P., Todorova, S., Naydenov, A., Tzaneva, B., Kolev, H., Atanasova, G., Stoyanova, D., Karakirova, Y., Aleksieva, K.: On the development of active and stable Pd-Co/γ-Al_2O_3 catalyst for complete oxidation of methane. Chem. Eng. J. 266, 329–338 (2015). doi:10.1016/j.cej.2014.12.099

77. Li, Z., Hoflund, G.B.: Catalytic oxidation of methane over Pd/Co_3O_4. React. Kinet. Catal. Lett. 66, 367–374 (1999)

78. Pu, Z., Liu, Y., Zhou, H., Huang, W., Zheng, Y., Li, X.: Catalytic combustion of lean methane at low temperature over ZrO_2-modified Co_3O_4 catalysts, (2017)

79. Ercolino, G., Karimi, S., Stelmachowski, P., Specchia, S.: Catalytic combustion of residual methane on alumina monoliths and open cell foams coated with Pd/Co_3O_4, (2017)

80. Ercolino, G., Stelmachowski, P., Kotarba, A., Specchia, S.: Reactivity of Mixed IronCobalt Spinels in the Lean Methane Combustion. Top. Catal. 60, 1370–1379 (2017). doi:10.1007/s11244-017-0826-9

81. Ercolino, G., Grodzka, A., Grzybek, G., Stelmachowski, P., Specchia, S., Kotarba, A.: The Effect of the Preparation Method of Pd-Doped Cobalt Spinel on the Catalytic Activity in Methane Oxidation Under Lean Fuel Conditions. Top. Catal. 60, 333–341 (2017). doi:10.1007/s11244-016-0620-0

82. Tao, F.F., Shan, J.-J., Nguyen, L., Wang, Z., Zhang, S., Zhang, L., Wu, Z., Huang, W., Zeng, S., Hu, P.: Understanding complete oxidation of methane on spinel oxides at a molecular level. Nat. Commun. 6, (2015). doi:10.1038/ncomms8798

83. Wang, Q., Peng, Y., Fu, J., Kyzas, G.Z., Billah, S.M.R., An, S.: Synthesis, characterization,

and catalytic evaluation of Co_3O_4/γ-Al_2O_3 as methane combustion catalysts: Significance of Co species and the redox cycle. Appl. Catal. B Environ. 168–169, 42–50 (2015). doi:10.1016/j.apcatb.2014.12.016

84. Jodłowski, P.J., Jędrzejczyk, R.J., Rogulska, A., Wach, A., Kuśtrowski, P., Sitarz, M., Łojewski, T., Kołodziej, A., Łojewska, J.: Spectroscopic characterization of Co_3O_4 catalyst doped with CeO_2 and PdO for methane catalytic combustion, (2014)

85. Teng, F., Chen, M., Li, G., Teng, Y., Xu, T., Hang, Y., Yao, W., Santhanagopalan, S., Meng, D.D., Zhu, Y.: High combustion activity of CH4 and catalluminescence properties of CO oxidation over porous Co_3O_4 nanorods. Appl. Catal. B Environ. 110, 133–140 (2011). doi:10.1016/j.apcatb.2011.08.035

86. Machin, N.E., Karakaya, C., Celepci, A.: Catalytic combustion of methane on La-, Ce-, and Co-based mixed oxides. Energy and Fuels. 22, 2166–2171 (2008). doi:10.1021/ef8000983

87. Xiao, T., Ji, S., Wang, H., Coleman, K.S., Green, M.L.H.: Methane combustion over supported cobalt catalysts. 175, 111–123 (2001). https://doi.org/10.1016/S1381-1169(01)00205-9

2 Methodology

2.1 Experimental set up and reaction procedure

Methane combustion over various catalysts was conducted in a packed-bed reactor. The bench scale combustion set-up consisted of a reactor, furnace, thermocouples, temperature controller, flow meters, methane and water supplies (Figure 2.1). The micro-reactor included a 316 stainless steel inner tube of 3/8" diameter with an outer sleeve of 7/8" diameter to provide a reactor support also maintaining the isothermal reaction, constant temperature along the reactor wall (Figure 2.2). Thermocouples T1 and T2 were located in the inner tube, before and after the catalyst bed, respectively. The third thermocouple, T3, was placed in the outer sleeve. The exhaust gas composition analysis was performed by a gas chromatograph (GC). The exhaust is passed through a cold trap to remove water vapor then, the product composition was analyzed by an online Agilent HP-7890A. The GC was equipped with two detectors: thermal conductivity (TCD) and flame ionization (FID). Methane and air flow rates were controlled by flow meters in separate lines. The gases were mixed before entering the reactor. For wet combustion environment, water was added to the reactor by a peristaltic pump, prior to injection to reactor the water was vaporized by using the heating tape. The LabVIEW software that records both the experimental conditions and results in Excel sheets.

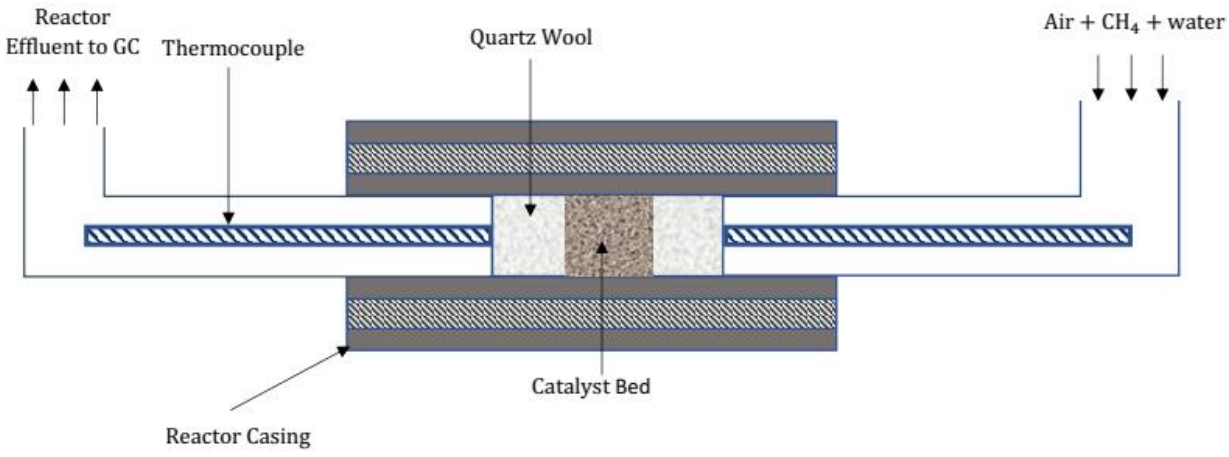

Figure 2.1 Schematic of the reactor system.

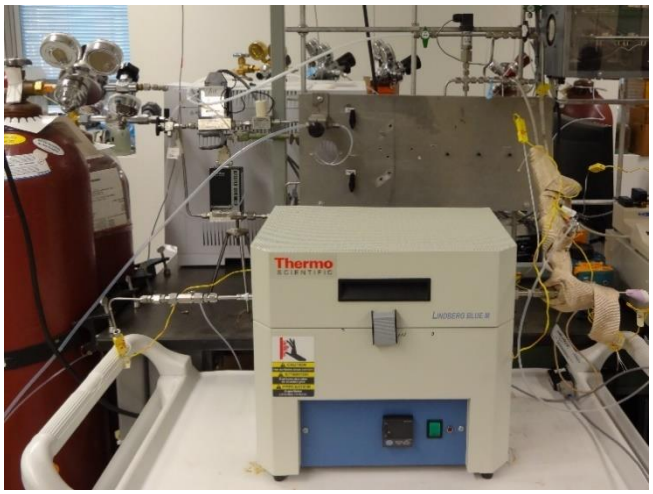

Figure 2.2 Methane combustion set up.

The combustion ignition-extinction (I-E) (200°C – 550°C – 200°C) tests were performed in three stages to help in evaluating the catalyst stability. The first I-E test was conducted under dry condition and for the second I-E test, which started right after the first round; steam was injected to study the combustion under wet condition. As expected, water injection significantly suppressed methane conversion. After the second stage of I-E, the hydrothermal ageing was performed for 40h to record the catalyst time-on-stream history. The temperature range for hydrothermal ageing was around (550 °C – a lower T); the lower T was chosen based on the previous ignition-extinction test (wet condition). It is the temperature that gives ~40-60% methane conversion. The final step was the third I-E test under wet condition. This thorough experimental procedure was used to identify the catalyst stability and the reaction kinetics.

2.2 Kinetic data analysis

Methane conversion was calculated based on the following formula (Eq. 2-1) in which $C_{m,inlet}$ and $C_{m,outlet}$ denote methane inlet and outlet concentration, respectively.

$$CH_4 \text{ conversion } \left(X_{CH_4}\ \%\right) = \frac{C_{CH_4,inlet} - C_{CH_4,outlet}}{C_{CH_4,inlet}} \quad (2\text{-}1)$$

The rate constants were calculated using a plug flow reactor model and first order kinetics. The mole balance is thus written as:

$$-\frac{dF_{CH_4}}{dw} = kCH_4 \quad (2\text{-}2)$$

Where w is the catalyst mass. Converting the molar flow rate to volumetric flow rate, and introducing the fractional conversion gives:

$$+Q\ C_{CH_{4,0}} \frac{dX_{CH_4}}{dw} = kC_{CH_{4,0}}(1 - X_{CH_4}) \quad (2\text{-}3)$$

Integrating over the reactor length gives an expression for the rate constant as:

$$k = \frac{Q}{w} ln\left(\frac{1}{1-X_{CH_4}}\right) \quad (2\text{-}4)$$

where X_{CH_4} is the fractional methane conversion, w is the catalyst mass and Q is the volumetric flow rate adjusted for the reactor pressure and temperature (average of the readings of two internal thermocouples placed at each end of the catalyst bed).

2.3 Verification of kinetic regime and plug-flow reactor behavior

When using measured conversion data to determine kinetic parameters, it is important to ensure that the kinetic results are obtained in the absence of both internal and external heat and mass transfer effects. Overall, the three main steps in a heterogeneous catalytic reaction are:

(1) Diffusion from the bulk gas to the catalyst external surface.

(2) Diffusion of reactants into the catalyst if it is porous.

(3) Reaction on the active sites.

If intrinsic kinetics are desired, then the reaction rate must be measured under conditions where step (3) is the rate determining step. A standard methodology using classical correlations from literature was used to verify the absence of heat and mass transfer limitations. All the necessary steps and formulas for the empirical criteria used to verify the axial dispersion and absence of

heat and mass transfer limitations are specified in the below sections. The sample calculations were performed for 80% conversion at 700K for Pd/Co_3O_4 catalyst (0.6 g) and 5000 ppm CH_4(210 mL STP/min) with 5% H_2O.

2.3.1 Mass transfer limitation (MTL)

Table 2-1 Absence of MTL verification.

Formula	Parameters	Obtained value
Methane concentration at specific condition [mol/L] $C_M = C_{M_0}(1 - X_{CH_4})$	C_M, C_{M_0}: methane bulk, initial concentration (0.0304, 0.1522 mol/m^3) X_{CH_4}:methane conversion (0.8)	0.03
Reaction rate [mol/kg$_{cat}$ s]=$(-r_M) = kC_M$	k: rate constant (8.36 L/kg.s)	1.27E-03
Particle Reynolds number $(Re) = \frac{Ud_p}{\nu}$	U: free stream velocity (0.225 m/s) d_p: particle diameter (0.000177m) ν: kinematic viscosity (0.000066 m^2/s)	0.602
Fuller equation, estimated methane bulk diffusivity in air [m^2/s] [1,2]: $D_{AB} = \frac{1.013 \times 10^{-2} T^{1.75} \left(\frac{1}{M_{Air}} + \frac{1}{M_{CH_4}}\right)^{0.5}}{P\left[(\sum \upsilon_{Air})^{1/3} + (\sum \upsilon_{CH_4})^{1/3}\right]^2}$	T: temperature (700K) molecular mass (M_{Air}=29, M_{CH_4}=16 g/mol) P: pressure (101325 Pa) diffusion volume (υ_{Air}=20.1, υ_{CH_4}=24.42 m^3)	0.00016
Schmidt number [3]: $Sc = \frac{\nu}{D_{AB}}$		0.412
Fröessling correlation, Sherwood number [3,4]: $Sh = 2.0 + 0.6Re^{1/2}Sc^{1/3}$		2.346

Mass transfer coefficient [m/s][3]: $k_c = \frac{D_{AB}\,Sh}{d_p}$		2.123
Mears criterion for external diffusion [3,5]: $\frac{-r_M\,\rho_b R}{k_c C_M}$<0.15 If the condition is satisfied, then external MTL is not present.	ρ_b: bed density (3666 kg/m^3) R: particle radius (0.0000885m)	6.39E-03
Knudsen diffusivity[m^2/s] [1]: $D_K = \frac{d_{pore}}{3}\sqrt{\frac{8R_gT}{\Pi M}}$	d_{pore}: catalyst effective pore diameter (62.3nm) R_g: gas constant (8.314 J/mol K) T: temperature (700K) M: methane molecular mass (16 g/mol)	2.00E-05
Diffusivity in a pore[m^2/s] [1]: $D_{pore} = \left(\frac{1}{D_{AB}} + \frac{1}{D_K}\right)^{-1}$		1.78E-05
Particle porosity [1]: $\varphi_p = \frac{S\rho_c d_{pore}}{4}$	S: catalyst surface area (m^2/g) ρ_c: catalyst density(6110kg/m^3)	0.4[1]
Effective diffusivity [m^2/s][1]: $D_e = \frac{\phi_P D_{pore}}{\tau}$	τ: tortuosity (0.4) [1]	2.85E-06
Weisz-Prater criterion for internal MTL [3]: If CWP < 0.3 for a first-order reaction, then internal MTL is not present. $C_{wp} = \frac{-r_M\rho_c R^2}{D_e C_M}$		0.703

2.3.2 Flow regime

Plug-flow operation assumption and absence of axial dispersion were verified.

L_{bed} (bed length) = 0.0164 (m); d_p (particle diameter) = 0.000177 (m); $D_{reactor}$= 0.00925 (m)

Table 2-2 Plug flow and absence of axial dispersion verifications.

Criteria	Obtained value
To neglect axial dispersion [6]: $L_{bed}/d_p > 50$	92
To neglect wall effects [7]: $D_{reactor}/d_p > 10$	52.3

If the above criteria are met, the plug-flow operation can be assumed.

2.3.3 Heat transfer limitations (HTL)

Table 2-3 Absence of HTL verification.

Formula	Parameters	Obtained value
Prandtl number of Air @ 700K [3]		0.684
Nusselt number[3]: $\mathrm{Nu} = 2 + 0.6\mathrm{Re}^{1/2}\mathrm{Pr}^{1/3}$		2.41
Heat transfer coefficient kJ/(m^2·s·K) [3]: $h = \frac{k_{air}Nu}{d_p}$	k_{air}: air thermal conductivity (0.05236 W/m.K)	713
External temperature gradient criterion [3]: $\Delta T_{ext} = \left\lvert \frac{-r_M(-\Delta H_{rxn})\rho_{bed}RE_a}{hT^2R_g} \right\rvert$	$-\Delta H_{rxn}$: heat of reaction (-890 kJ/mol) E_a: activation energy (88.5 kJ/mol)	1.21E-05
Prater number [3]: $\beta = \frac{-\Delta H_{rxn}D_{eff}C_M}{k_{eff}T}$	k_{eff}: effective thermal conductivity (0.025 W/m.K)	0.00044
Maximum internal temperature rise [K]: $\Delta T_{max} = \beta T$		0.3084

2.4 References

[1] Hayes, R., Mmbaga, J. (2013). Introduction to Chemical Reactor Analysis, 2nd Ed., Boca Raton

[2] Fuller, Edward N, Paul D Schettler, and J Calvin. Giddings. 1966. New Method for Prediction of Binary Gas-Phase Diffusion Coefficients. *Industrial & Engineering Chemistry* 58 (5): 18–27. https://doi.org/10.1021/ie50677a007

[3] H.S. Fogler. (2005). Elements of chemical reaction engineering, 4th Ed., Prentice Hall.

[4] N. Frössling.(1938),Uber die Verdunstung fallender Tropfen. *Gerlands, Beitr.Geophys.,* 52, 170-178

[5] Mears, D E. 1971. Tests for Transport Limitations in Experimental Catalytic Reactors. *Industrial & Engineering Chemistry Process Design and Development* 10 (4): 541–47. https://doi.org/10.1021/i260040a020

[6] Le Page, J. F. (1987). Applied heterogeneous catalysis: design, manufacture, use of solid ctalysts. Paris: Technip

[7] Pérez-Ramírez, J, R J Berger, G Mul, F Kapteijn, and J A Moulijn. 2000. "Six-Flow Reactor Technology a Review on Fast Catalyst Screening and Kinetic Studies." *Catalysis Today* 60 (1): 93–109. https://doi.org/10.1016/S0920-5861(00)00321-7.

3 Kinetic modeling of Co_3O_4- and Pd/Co_3O_4-catalyzed wet lean methane combustion[1]

3.1 Introduction

Recently, cobalt oxide has attracted considerable attention in methane combustion not only as a catalyst itself but also as a promoter and a support or a support modifier for active Pd. Methane combustion on Co_3O_4 occurs via a Langmuir-Hinshelwood mechanism involving suprafacial highly active tetrahedral cobalt oxo-centres at temperatures below 450 °C, with an increased contribution from less active intrafacial lattice oxygen (Mars-van Krevelen mechanism) at higher temperatures. Among oxides of 3d elements, Co_3O_4 exhibits the fastest oxygen binding with the lowest heat, which unfavourable effect is counterbalanced by the high number of oxygen activation sites. For example, the rate of oxygen exchange between molecular oxygen and Co_3O_4 at 300 °C is three orders of magnitude higher than that on Al_2O_3. Such an ability of Co_3O_4 to activate and supply oxygen species makes it an especially valuable support for Pd-catalyzed methane combustion in the wet environment, as is typical for the exhaust of natural gas vehicles. The presence of water is known to impede oxygen exchange and mobility on oxide supports and thus inhibit methane combustion.

Only a few studies of methane combustion involving cobalt oxide used added water in the feed. A comprehensive kinetic study with steam addition was reported only for Co^{2+} (CoO)-promoted Pd/Al_2O_3 catalysts, which showed that only PdO catalyzed the reaction, with a negligible contribution from cobalt itself, most likely due to its low concentration on the support (1% and below. Herein, we report the kinetic study of Co_3O_4 and Pd/Co_3O_4 catalysts in fuel-lean methane combustion in the temperature range between 250 and 550 °C in the presence of 5 and 10 vol. % water in the feed and with CH_4 concentrations varied between 1,000 and 5,000 ppmv inclusive.

---

[1] Chapter 3 of the thesis has been published as "Kinetic modeling of Co_3O_4 and Pd/Co_3O_4-catalyzed wet lean methane combustion" Somaye Nasr, Natalia Semagina, Robert E. Hayes, Emission Control Science and Technology doi.org/10.1007/s40825-019-00143-0. Reprinted with permission from Springer Nature © 2019. The author performed all the syntheses, catalytic reactions, analyses, and other characterizations. Dr. Robert E. Hayes prepared the final plots and addressed the comments of the reviewers. Manuscript draft preparation and writing were conducted by the author under the supervision and final approval of Dr. Robert E. Hayes and Dr. Natalia Semagina.

3.2 Experimental

3.2.1 Catalyst synthesis and characterization

A hydrothermal cobalt oxide synthesis method was adopted from a previously published study by Teng et al. 0.003 mole $CoCl_2 \cdot 6H_2O$ (98%, Sigma-Aldrich), 0.018 mole urea (Sigma-Aldrich) was used as a precipitation agent and 11.66 g of 45 wt. % K60 polyvinylpyrrolidone solution (PVP, Sigma-Aldrich) were dissolved in 25 mL milli-Q water. PVP is water soluble and the acts as a steric stabilizer to prevent excessive growth of metal oxide nanoparticles. A clear pink solution was formed. The precipitation took place at 90 ºC for 24 h in a 50 mL Teflon-lined autoclave in a furnace. The suspension was centrifuged and washed with milli-Q water and ethanol trice. The powder was dried at 60 ºC overnight in a furnace, followed by calcination at 400 ºC for 3 h. Pd/Co_3O_4 catalyst was prepared via incipient wetness impregnation using $Pd(NO_3)_2 \cdot 2H_2O$ (Sigma-Aldrich). The Co_3O_4 and Pd/Co_3O_4 catalysts were calcined at 550 °C for 16 h as a conventional de-greening procedure prior to the methane combustion tests. Such catalysts are denoted as “fresh” or “calcined”. The catalysts after the hydrothermal ageing and methane combustion tests, as described in Section 3.1.2, are denoted as “spent”.

The final Pd loading was found as 0.27 wt. % by inductively-coupled plasma – mass spectrometry (ICP-MS) with the detection limits for Pd and Co being 0.01 and 0.03 ppm, respectively. The catalysts were analyzed by N_2 adsorption and desorption, X-ray diffraction (XRD), CO chemisorption and transmission electron microscopy (TEM). N_2 adsorption and desorption isotherms were measured at 77 K using Autosorb iQ analyzer. XRD profiles were obtained using Rigaku Ultima IV D/max-RB diffractometer with D/Tex Ultra detector with Fe Filter (K-beta filter). The step scans were taken over a 2q range of 5–90° with a step size of 0.02° and scan speed 2 °/min, continuous scan mode. Radiation source used was cobalt tube at 38 kV and 38 mA. Data interpretation is done using JADE 9.6 software with the 2019 ICDD Database PDF 4+, and 2018-1 ICSD databases. Scans were converted from Co radiation to Cu in Jade 9.6. CO chemisorption was performed in a Micromeritics AutoChem 2950 HP instrument. The Pd/Co_3O_4 catalyst was reduced in 5% H_2/He at 150 °C, followed by purging in He. The CO pulse chemisorption analysis was performed by dosing a 3% CO/He gas mixture at room temperature. TEM analyses were performed using a JEOL JEM-ARM200cF scanning/transmission electron

microscope operated at 200 kV accelerating voltage (nanoFAB Fabrication & Characterization Center at the University of Alberta).

3.2.2 Methane combustion tests

The catalytic tests were performed in a packed-bed reactor (PBR) of a 3/8" ID. The details of the experimental setup and the on-line gas chromatographic analysis of the products were described previously. No catalyst dilution was used. The catalyst powder size was measured to be less than 177 mm (80 mesh), 2/3 of the material being smaller than 125 mm (120 mesh). For the transport effect evaluation, the largest size of 177 mm was used. The catalyst bed (0.6 g) was fixed with quartz glass wool. The feed with 1000, 2000, 3000, 4000 or 5000 ppmv CH_4 was prepared by mixing dry air and 10% CH_4/N_2 (Praxair). The absolute reactor pressure was adjusted at 1.5±0.3 atm. Water was added by a peristaltic pump. A total gas flow of 210±5 mL_{STP}/min and 19.5 vol.% O_2 was used, which corresponded to a gas hourly space velocity (GHSV) of 21,000 LSTP/(kg_{cat}·h).

The calcined catalysts were hydrothermally aged *in situ* for 72 h in the feed with 4000 ppmv CH_4 and 10 vol. % H_2O by performing 0.5-h long cycles between 400 °C and 550 °C. The ignition curves were obtained by increasing temperature from 200 °C to 550 C in 25 °C increments at the rate of 10 °C/min with an 8-min. stabilization period at each temperature. After each ignition, the reactor was purged with air for 10 min, bringing the temperature to 200 °C, which was immediately followed by the next ignition test.

For each catalyst, the ignition curves for each methane and water concentration were measured trice, totaling 15 curves. For each set ("Trial, T"), five initial CH_4 concentrations were tested: 1000, 2000, 3000, 4000, and 5000 ppmv in a random order. For Co_3O_4 the following trial order was used: Trial 1 T1 5 vol. % H_2O; Trial 1 T1 10 vol. % H_2O; Trial 2 T2 10 vol. % H_2O; Trial 2 T2 5 vol. % H_2O; Trial 3 T3 10 vol. % H_2O; Trial 3 T3 5 vol. % H_2O. For Pd/Co_3O_4 the order was as follows: Trial 1 T1 5 vol. % H_2O; Trial 2 T2 5 vol. % H_2O; Trial 1 T1 10 vol. % H_2O; Trial 2 T2 10 vol. % H_2O; Trial 3 T3 5 vol. % H_2O; T3 10 vol. % H_2O.

3.3 Results and discussion

3.3.1 Characteristics of Co_3O_4 and Pd/Co_3O_4 catalysts

XRD profiles of the fresh catalysts confirmed that Co_3O_4 phase was formed during the catalyst synthesis (Figure 3.1). Neither fresh, not spent catalysts demonstrated features of CoO, Co, $Co(OH)_3$ or $Co(OH)_2$ according to the XRD databases. A 55-nm crystal size of Co_3O_4 in the spent Pd/Co_3O_4 catalysts was calculated using Scherrer equation with Scherrer constant of 1.333 [21]. The TEM analysis confirmed that the Co_3O_4 crystal size ranged from 20 to 70 nm with some inclusion of larger cylindrical particles of approximately 300 nm height (Figure 3.2). The Pd dispersion was measured by CO chemisorption as 13% (9 nm particle size) assuming 1:1 CO/Pd stoichiometry.

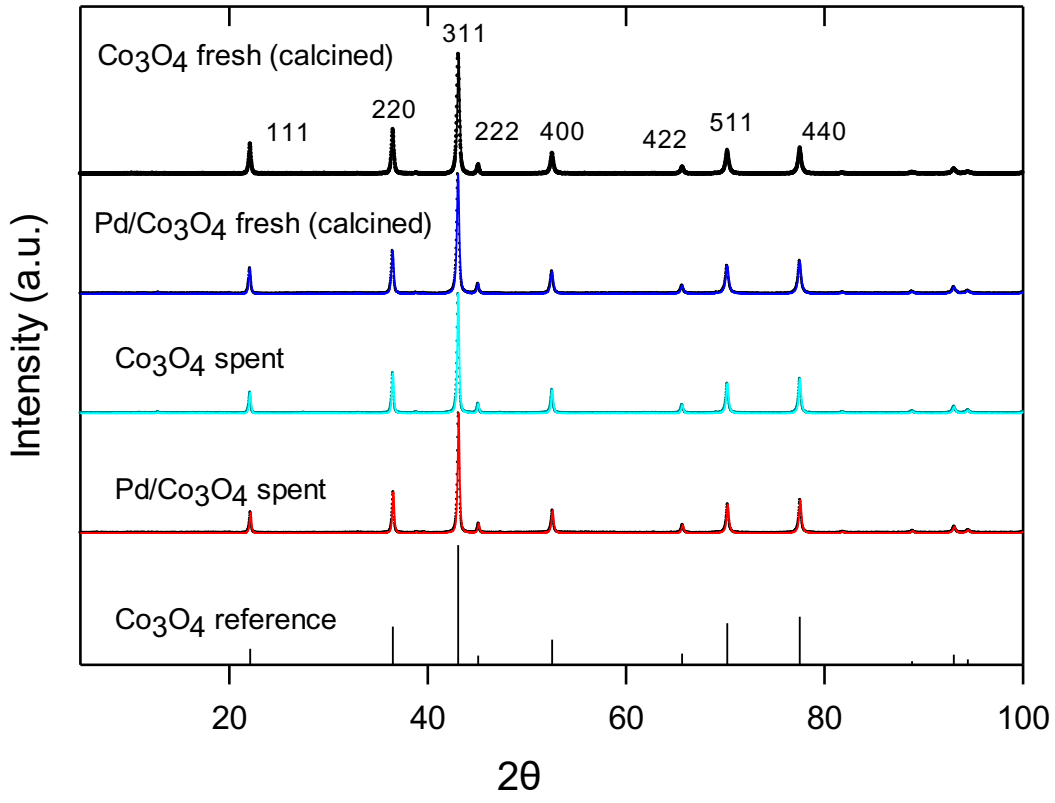

Figure 3.1 XRD profiles of the fresh and spent catalysts.

The BET surface areas were determined as 13, 7, 12, and 7 m^2/g for the fresh and spent Co_3O_4, and the fresh and spent Pd/Co_3O_4 catalysts, respectively. All C constants in the BET equations were between 53 and 73 confirming the validity of the method. Figure 3.3 shows a representative N_2 adsorption-desorption isotherm for the spent Pd/Co_3O_4 catalyst. All catalysts exhibited the Type II isotherms with a hysteresis loop type H3, which is characteristic of non-porous or macroporous adsorbents with aggregates of plate-like particles or macropore networks. The average 55-nm crystal size of the spent Pd/Co_3O_4 catalyst at bulk density of 6110 kg/m^3 translates into the external surface area of 17 m^2/g, which implies that the measured BET surface area is the external area only and the crystals are non-porous.

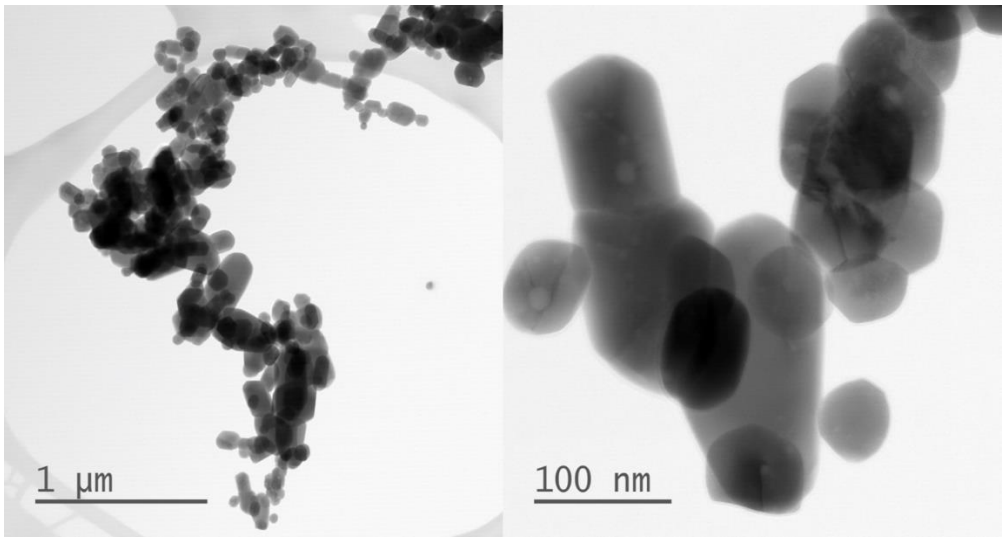

Figure 3.2 TEM images of the spent Co_3O_4 catalyst.

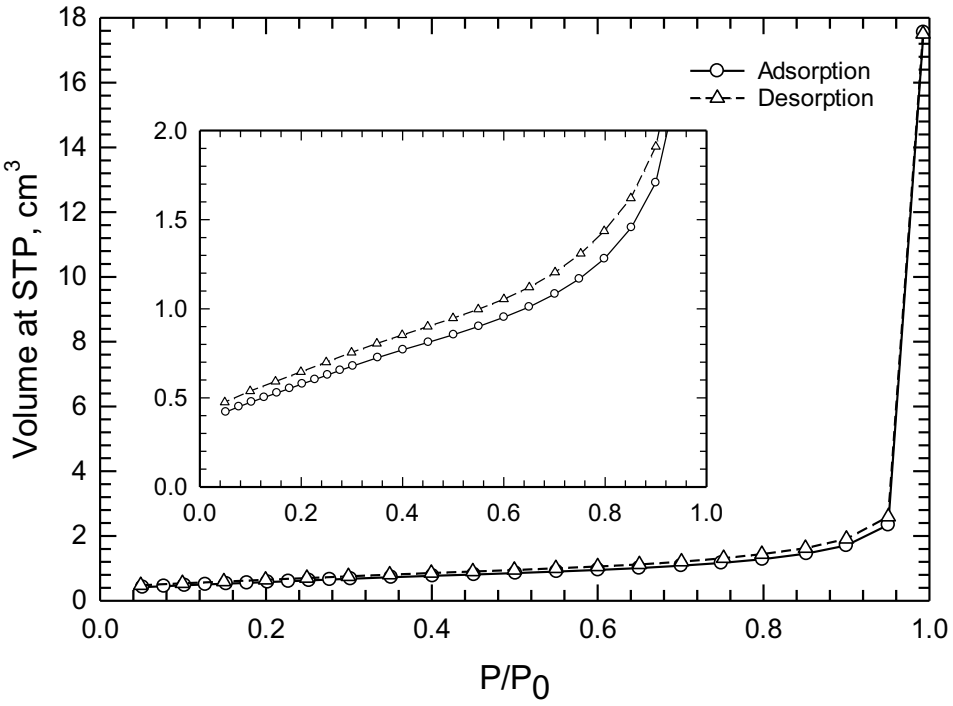

Figure 3.3 N_2 adsorption-desorption isotherms measured for the spent Pd/Co_3O_4 catalyst. The inset graph highlights the hysteresis observed at low adsorbed volume.

3.3.2 Vis-à-vis: methane combustion on Co_3O_4 and Pd/Co_3O_4 catalysts

Figure 3.4 compares the catalytic behaviour of Pd-doped and Pd-free Co_3O_4 in methane combustion with 5 and 10 % water addition. There is a significant contribution of the support to the Pd/Co_3O_4-catalyzed reaction. Remarkably, the Co_3O_4 activity is not affected by the water concentration and the Pd/Co_3O_4 catalyst is less susceptible to the water poisoning as compared to PdO and Pd/Al_2O_3, which typically demonstrate negative first order behaviour with respect to H_2O. The following sections quantify the observed kinetics.

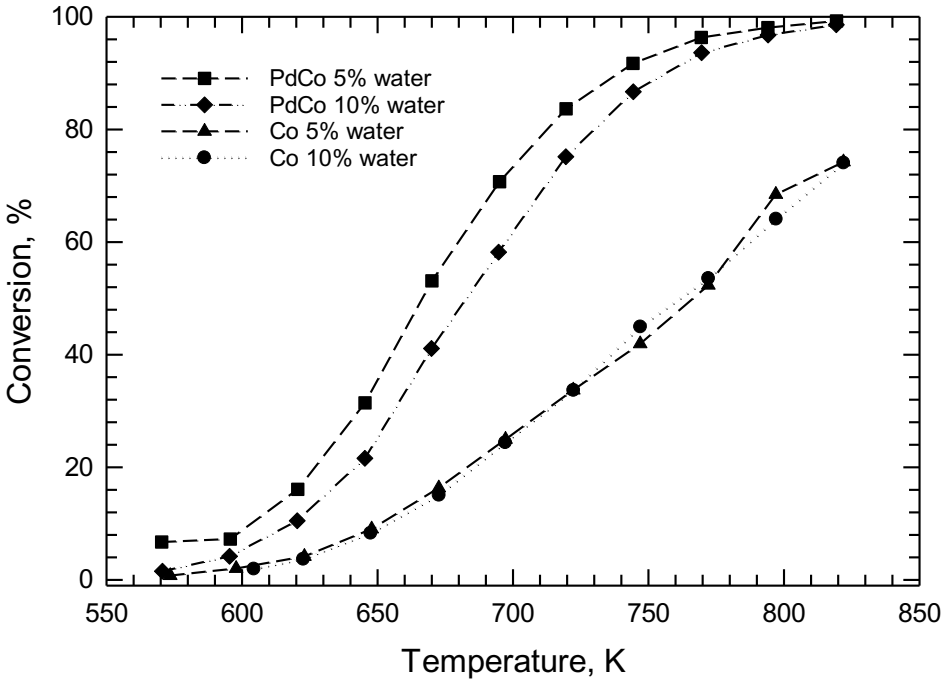

Figure 3.4 Ignition curves in catalytic methane combustion of the wet lean feed, 0.6 g catalyst (Co_3O_4 or Pd/Co_3O_4, 0.27 wt.% Pd), 210 mL_{STP}/min, 5000 ppm CH_4, 19.5 vol. % O_2, GHSV = 21,000 $L_{(STP)}/(kg_{cat} \cdot h)$. The data are for Trial 2 (T2).

3.3.3 Verification of isothermal kinetic regime and ideal PBR behavior

The verification was performed using appropriate dimensionless criteria. The most active catalyst at high temperature point was selected, which was Pd/Co_3O_4 catalyst tested with 5% water addition at 80% conversion of the feed with 5000 ppm methane. Methane diffusivity was calculated using Fuller's formula, air properties were used to estimate Sc, particle Re (with the largest particle diameter in the powder of 177 mm), and Pr numbers. Mass transfer and heat transfer coefficients were calculated from Sh and Nu numbers as found by Frössling correlation. The detailed formula for the calculations can be found in our earlier paper for other methane combustion catalysts [20]. The observed reaction rate and activation energy were determined from the modeling results described in the Section 3.3.5. Mears criteria for external mass and heat transfer were found as 10^{-2} and 10^{-5} confirming the absence of the external transport

limitations. The intraparticle intercrystalline limitations between non-porous 55-nm Co_3O_4 crystals in catalyst particles of up to 177 mm were estimated only for the macropores with effective diameter of 62 nm (based on the measured surface area of 7 m^2/g). The respective Weisz-Prater criterion for the kinetic regime was satisfied for the internal effectiveness factor of 0.94. The observed 1st order to methane is in line with the absence of internal mass transfer limitations. The Prater number predicts temperature rise by 0.3 K assuming 5% effective thermal conductivity of cobalt oxide [26]. The criteria for the ideal plug flow behavior were satisfied as well (reactor diameter / particle diameter >10; reactor Peclet number > 10 for Bodenstein number of 0.7 at low Reynolds numbers. Thus, the following sections describe the observed kinetics as intrinsic kinetics in an ideal isothermal PBR.

3.3.4 Kinetic tests and modeling results: cobalt oxide

Figure 3.5(a) shows the ignition curves for the experiments with 5 % H_2O in the feed. The data for the 10 % H_2O are shown in the Electronic Supplementary Material (Figure 3.8). For each trial (T), methane conversion was independent of its initial concentration, indicating 1st order behaviour with respect to CH_4. The rate constants were thus calculated from the ideal packed-bed reactor mole balance and a first-order rate law as shown in equation (3-1).

$$k = \frac{Q}{W} Ln\left(\frac{1}{1-X_A}\right) \qquad (3\text{-}1)$$

where X_A is the fractional methane conversion, W is the catalyst mass (0.6 g) and Q is the volumetric flow rate adjusted for the reactor pressure and temperature (average of the readings of two internal thermocouples placed at each end of the catalyst bed). For the kinetic analysis, only data from 10 to 90 % conversion were used (due to higher experimental error at higher and lower conversions). The 1st order model prediction is demonstrated for T2 at 5% water in Figure 3.5b (the ES Material contains similar Figure 3.9 and Figure 3.10for other trials and water concentration).

As seen from Figure 5.4, regardless of the 72 h long hydrothermal catalyst ageing prior to the reactions, the catalyst deactivated. The difference was less pronounced between trials T2 and T3 versus T1 (experimental order of 4, 6 and 1, respectively, out of six total trials). The BET surface

area, as measured by N_2 adsorption, decreased from the original 12 m^2/g (prior to hydrothermal ageing) to 7 m^2/g (after the kinetic experiments). Indeed, when the Arrhenius law parameters were calculated for each trial (Table 3.1), the activation energy remained nearly constant at 69 kJ/mol but the number of active sites decreased by almost one half.

As seen from Figure 3.4 and the Arrhenius law parameters in Table 3-1, the Co_3O_4 catalyst performance was insignificantly affected by the double increase in water concentration from 5 to 10 %. The combined modelling of the Arrhenius law parameters for the two water concentrations for Trial 2 is shown in Figure 5.4(c) (since these two experiments followed one another so the sintering effect is less pronounced), with the model parameters summarized in Table 3-1.

Thus, for the studied temperature and concentration ranges, the Co_3O_4 catalyst demonstrates a 1st order behaviour with respect to CH_4, is 0 order in H_2O and has an activation energy of 69 kJ/mol. Similar activation energies of 71-74 kJ/mol were reported for dry methane combustion on Co_3O_4. However, the catalyst progressively loses its active sites by sintering, as was observed earlier for the Co_3O_4-based catalyst in the wet feed. As was demonstrated by first-principles calculations, multiple sites are involved in methane activation on Co_3O_4 with a different affinity to water; (110) surface significantly outperforms the (100) surface. At 0.1 atm H_2O, the (100) surface is fully dehydroxylated above 280 °C, with only 33 % and 50 % surface hydroxylation of the (110) and (111) surfaces, respectively [28]. For the Pd catalysts, on the other hand, water is an accepted most abundant surface-dominating intermediate, which gives rise to negative first order to water. Due to the concurrent interplay of the Langmuir-Hinshelwood and Mars-van Krevelen mechanism in the studied temperature range, it is likely that cobalt oxide adjusts its redox state to the current thermodynamic conditions.

Table 3-1 Arrhenius law parameters for Co_3O_4 catalyst.

Water, vol. %	5			10			5 and 10
Trial	T1	T2	T3	T1	T2	T3	T2
Experimental order	1	4	6	2	3	5	3 and 4
Pre-exponential factor, L/(g·s)	543.32	389.96	310.38	426.84	462.34	214.58	410.18
Activation energy, J/mol	68092	68703	68811	68965	70387	67092	69324
Rate constant at 700 K, L/(kg·s)	4.51	2.91	2.27	3.05	2.58	2.11	2.75

3.3.5 Kinetic tests and modeling results: Pd/Co_3O_4

The ignition curves (Figure 3.8) demonstrate an outstanding stability of the Pd/Co_3O_4 catalyst at each water concentration, with no variations between trials as in the case of the Co-only catalyst above, although the surface area also decreased from 12 m^2/g (prior to hydrothermal ageing) to 7 m^2/g. All the 15 curves for each water concentration are nearly identical. Applying the 1^{st} order to CH_4, as per equation (3-1), Arrhenius law parameters were calculated for all trials and concentrations with 5 and 10 % water in the feed. Table 3-2 summarizes the results obtained. The parity plots for the experimental and predicted conversions can be found in the ES Material (Figure 3.11).Table 3-2 also contains the fitting results assuming an average activation energy between the experiments with 5 and 10% water; the modelled kinetic curves with this common observed activation energy of 90.7 kJ/mol are presented in Figure 3.6.

The order to water in the studied temperature range is -0.37 versus typically observed negative first order for PdO, Pd/Al_2O_3 and Pd/ZrO_2 catalysts [24]. The observed activation energy of 90.7 kJ/mol can be thus corrected for the heat of water adsorption on PdO as $E_{obs} = E_a - 0.37 \cdot \Delta H$. Assuming ΔH = -81.5 kJ/mol as reported for Pd/Al_2O_3 catalyst at similar conditions [30], the activation energy becomes E_a = 60.6 kJ/mol which is surprisingly exactly the same as was reported for the Pd/Al_2O_3 catalyst at similar reaction conditions (60.6 ± 11.5 kJ/mol [30]). Thus, it is unlikely that the presence of Co_3O_4 decreases the activation barrier for methane activation on Pd.

Table 3-2 Arrhenius law parameters for Pd/Co_3O_4 catalyst.

	5 % water, all trials	10 % water, all trials	5 % water, common E_a	10 % water, common E_a
Pre-exponential factor, L/(g·s)	33628	49598	46365	35972
Activation energy, J/mol	88501	92976	90738, (60583 if corrected for water)	
Rate constant k at 700 K, L/(kg·s)	8.36	5.72	7.85	6.09
% Contribution from Co_3O_4 to k at 700 K*	32%	48%	35%	45%

*Based on rate constant of 2.75 L/(kg·s) from Table 3-1

3.3.6 Modelling-based evidence of metal-support interactions in Pd/Co_3O_4 catalyst

As seen from the ignition curves (Figure 3.5) and the calculated kinetic parameters (Table 3-1 and Table 3-2), Co_3O_4 contributes significantly to the observed rate constant on the Pd/Co_3O_4 catalyst. For example, at 700 K, the contribution is 32 and 48 % at 5 and 10 % water in the feed, respectively; at 625 K and 10% water the contribution is as high as 70%. The water-corrected activation energy for Pd/Co_3O_4 catalyst is the same as for Pd/Al_2O_3 catalyst (60.6 kJ/mol) and is rather similar to the activation energy for Co_3O_4 is (69 kJ/mol). It is thus feasible that the improved performance of Pd/Co_3O_4 catalyst over Co_3O_4 is simply due to the Pd additive contribution, which would also explain the order to water being between 0 and -1.

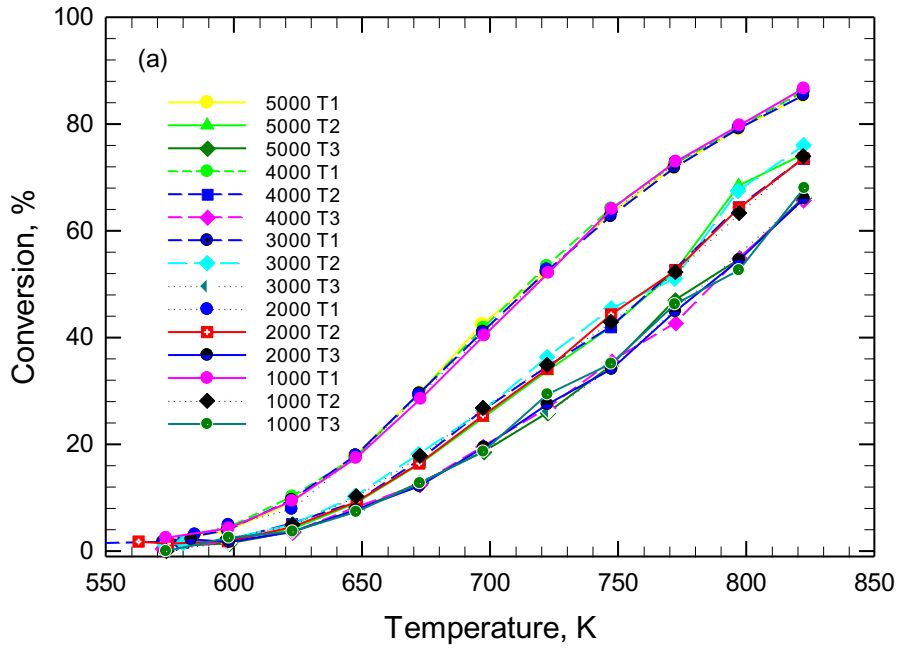
(a)
5000 T1
5000 T2
5000 T3
4000 T1
4000 T2
4000 T3
3000 T1
3000 T2
3000 T3
2000 T1
2000 T2
2000 T3
1000 T1
1000 T2
1000 T3
Conversion, %
Temperature, K
0
20
40
60
80
100
550
600
650
700
750
800
850

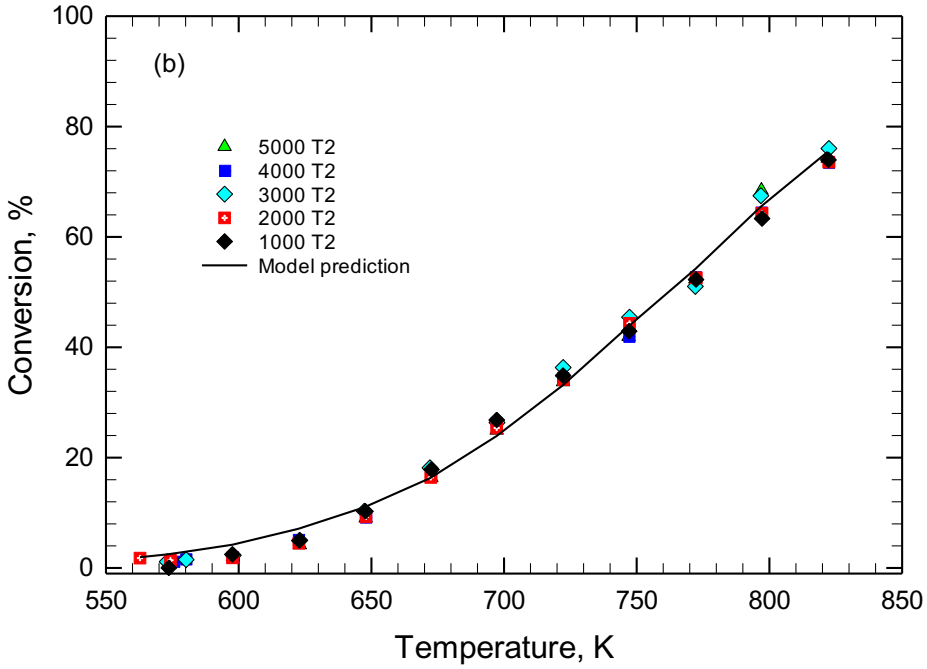
(b)
5000 T2
4000 T2
3000 T2
2000 T2
1000 T2
Model prediction
Conversion, %
Temperature, K
0
20
40
60
80
100
550
600
650
700
750
800
850

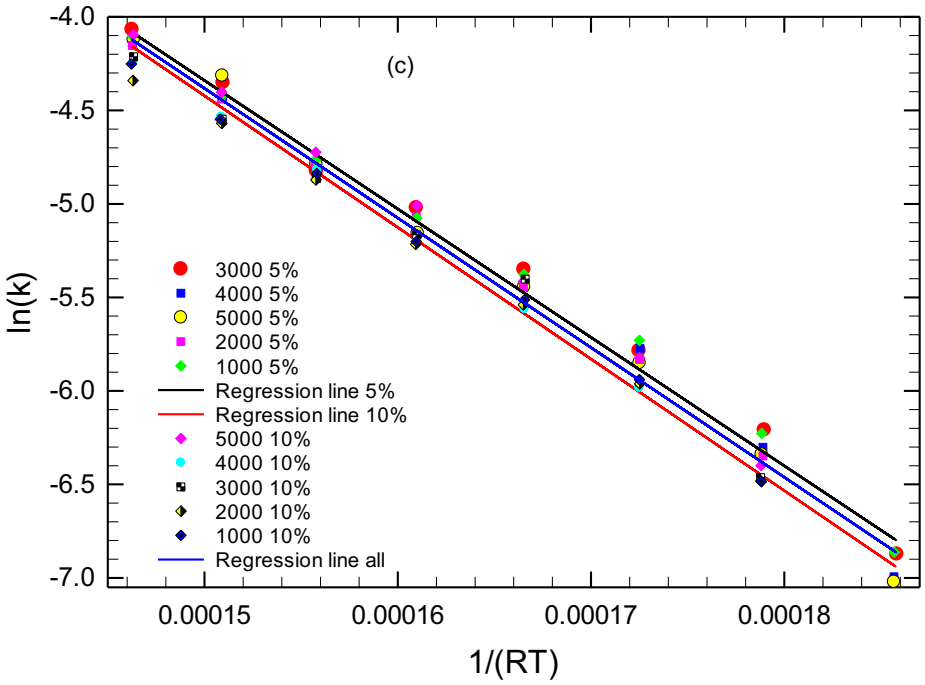

Figure 3.5 Co_3O_4 catalyst performance: (a) ignition curves for Co_3O_4 catalyst for three trials (T1-T3) at different CH_4 concentrations (ppmv), 5 vol. % H_2O, 0.6 g, 210 mL_{STP}/min, 19.5 vol. % O_2, GHSV = 21,000 $L_{(STP)}/(kg_{cat} \cdot h)$; (b) model prediction (first order to CH_4) for T2 with 5 % water; (c) Arrhenius plot for trial 2 data with 5 and 10 % water

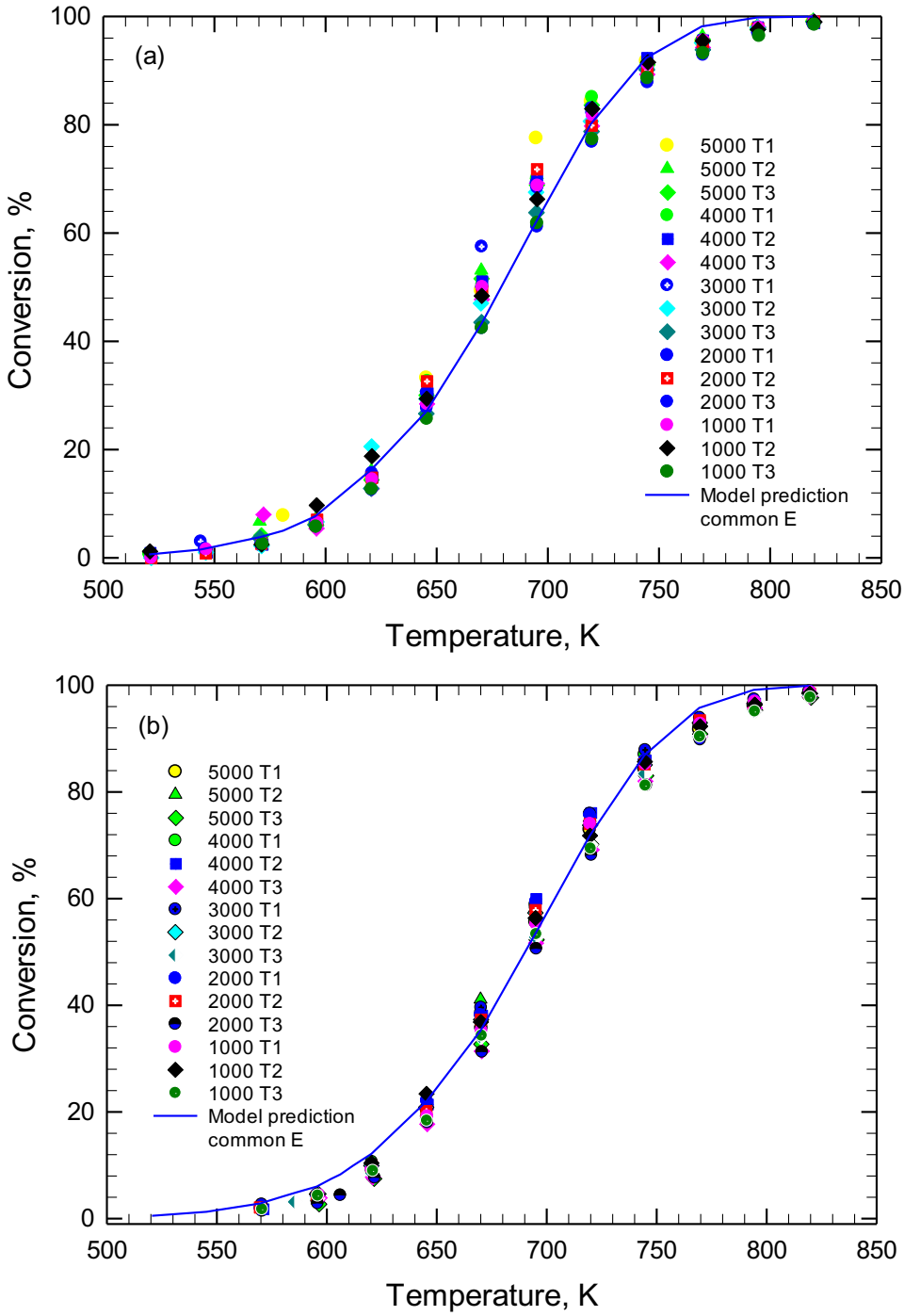

Figure 3.6 Ignition curves for Pd/Co_3O_4 (Pd 0.27 wt. %) catalyst for three trials (T1-T3) at different CH_4 concentrations (ppmv) at (a) 5 vol. % H_2O (a) and (b) 10 vol. % H_2O in the feed. Reaction conditions are the same as for the Co_3O_4 catalyst (Fig. 2). The model is based on the parameters in Table 3-2 with a common activation energy of 90.7 kJ/mol.

We tested this hypothesis assuming that the reaction rate is the sum of the rates of Co and Pd counterparts. For the Pd counterpart a negative first order to water is widely accepted. Let R_{PdCo} be the rate on the Pd/Co_3O_4, k_1 – rate constant on Co_3O_4, k_2 – rate constant on Pd only, k* - water-dependent apparent rate constant on Pd/Co_3O_4 as found above in Table 3-2:

$$R_{\mathrm{PdCo}} = k_1 C_{\mathrm{CH_4}} + k_2 \frac{C_{\mathrm{CH_4}}}{C_{\mathrm{H_2O}}} = \left(k_1 + k_2 \frac{1}{C_{\mathrm{H_2O}}} \right) C_{\mathrm{CH_4}} = k^* C_{\mathrm{CH_4}} \qquad (3\text{-}2)$$

$$k_2 = \left(k^* - k_1 \right) C_{\mathrm{H_2O}} \qquad (3\text{-}3)$$

Figure 3.7 shows the Arrhenius plot for the thus computed Pd-only rate constants k_2 at 5 and 10 % water in the feed. The non-compliance of the obtained plot with the expected linear correlations rejects the hypothesis of the additive contribution of Pd and Co_3O_4 to Pd/Co_3O_4 performance and provides kinetic evidence of the strong-metal support interactions. Equation (3-3) can be linearized by introducing an order to water. This order for the Pd counterpart shifts from -1 to -0.5 with the temperature increase from 625 K to 823 K.

Given similar water-corrected activation energies for Pd/Co_3O_4 catalyst and Pd/Al_2O_3 catalyst, but higher water tolerance of the former, it appears that the Co_3O_4 contribution is not only in performing the methane combustion itself but also in providing surface oxygen rather than in decreasing the activation energy. Lack of oxygen is a known limiting factor under wet methane combustion conditions. We currently investigate the reason of the improved water tolerance of Pd/Co_3O_4 catalyst as compared to other Pd catalysts. Reported studies of palladium-cobalt catalysts in dry and wet conditions suggest that cobalt oxide helps to stabilize Pd in oxidized state [1] and serve as a reservoir of oxygen species, as well as it removes poisonous hydroxyls from $Pd(OH)_2$[16]. The Pd addition, in turn, facilitates the formation of reduced cobalt oxide thus providing vacancies for enhanced oxygen activation.

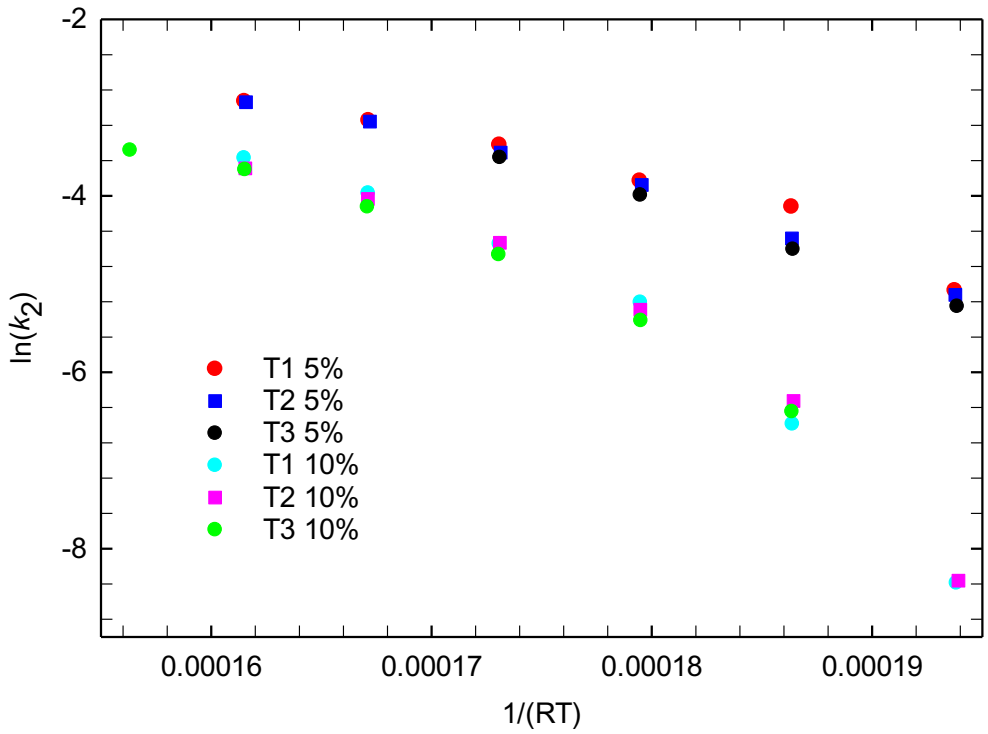

Figure 3.7 . Verification of additive Pd and Co_3O_4 contribution hypothesis by computing rate constants for Pd component only. The non-linearity rejects the hypothesis and suggests strong metal-support interactions.

3.4 Conclusions

Reaction kinetics of methane combustion was investigated on Co_3O_4 and Pd/Co_3O_4 (0.27 wt. % Pd) catalysts for the fuel-lean feed in the temperature range between 250 and 550 °C in the presence of 5 and 10 vol. % water in the feed and CH_4 concentrations varied between 1000 - 5000 ppmv. Significant cobalt oxide contribution to the activity of the bimetallic catalyst was observed, especially at higher water concentration. Co_3O_4 demonstrated 1st order to CH_4, 0 order to H_2O and activation energy of 69 kJ/mol. Pd/Co_3O_4 catalyst showed 1st order to CH_4, -0.37 order to H_2O and an observed activation energy of 90.7 kJ/mol, that was corrected for water adsorption to 60.6 kJ/mol. The latter is a typical activation energy for Pd/Al_2O_3 catalyst at similar conditions. The kinetic evidence was provided that the observed behaviour of Pd/Co_3O_4 catalyst is not a summation of individual activities of Co_3O_4 and Pd but the effect of strong metal-support interactions.

Acknowledgements

Financial support from Natural Sciences and Engineering Research Council of Canada (NSERC Strategic grant STPGP 478979-15) is appreciated. We thank Dr. Jing Shen for performing the TEM and CO chemisorption analyses.

3.5 References

1. Li, Z., Hoflund, G.B.: Catalytic oxidation of methane over Pd/Co_3O_4. React. Kinet. Catal. Lett. 66, 367–374 (1999)

2. Zasada, F., Janas, J., Piskorz, W., Gorczyńska, M., Sojka, Z.: Total oxidation of lean methane over cobalt spinel nanocubes controlled by the self-adjusted redox state of the catalyst: experimental and theoretical account for interplay between the Langmuir-Hinshelwood and Mars-Van Krevelen mechanisms. ACS Catal. 7, 2853–2867 (2017).

3. Sokolovskii, V.D.: Principles of oxidative catalysis on solid oxides. Catal. Rev. 32, 1–49 (1990).

4. Piskorz, W., Gryboś, J., Sojka, Z., Indyka, P., Zasada, F., Janas, J.: Reactive oxygen species on the (100) facet of cobalt spinel nanocatalyst and their relevance in $^{16}O_2$ / $^{18}O_2$ isotopic exchange, *de* N_2O, and *de* CH_4 processes—A theoretical and experimental account . ACS Catal. 5, 6879–6892 (2015).

5. Setiawan, A., Kennedy, E.M., Dlugogorski, B.Z., Adesina, A.A., Stockenhuber, M.: The stability of Co_3O_4, Fe_2O_3, Au/Co_3O_4 and Au/Fe_2O_3 catalysts in the catalytic combustion of lean methane mixtures in the presence of water.

6. Hu, L., Peng, Q., Li, Y.: Selective synthesis of Co_3O_4 nanocrystal with different shape and crystal plane effect on catalytic property for methane combustion. J. Am. Chem. Soc. 130, 16136–16137 (2008).

7. Hu, W., Lan, J., Guo, Y., Cao, X.-M., Hu, P.: Origin of efficient catalytic combustion of

methane over Co_3O_4(110): active low-coordination lattice oxygen and cooperation of multiple active sites. ACS Catal. 6, 5508–5519 (2016).

8. Choya, A., de Rivas, B., González-Velasco, J.R., Gutiérrez-Ortiz, J.I., López-Fonseca, R.: Oxidation of residual methane from VNG vehicles over Co_3O_4-based catalysts: comparison among bulk, Al_2O_3-supported and Ce-doped catalysts. Appl. Catal. B Environ. 237, 844–854 (2018).

9. Teng, F., Chen, M., Li, G., Teng, Y., Xu, T., Hang, Y., Yao, W., Santhanagopalan, S., Meng, D.D., Zhu, Y.: High combustion activity of CH_4 and catalluminescence properties of CO oxidation over porous Co_3O_4 nanorods. Appl. Catal. B Environ. 110, 133–140 (2011).

10. Willis, J.J., Goodman, E.D., Wu, L., Riscoe, A.R., Martins, P., Tassone, C.J., Cargnello, M.: Systematic identification of promoters for methane oxidation catalysts using size- and composition-controlled Pd-based bimetallic nanocrystals. J. Am. Chem. Soc. 139, 11989–11997 (2017).

11. Stefanov, P., Todorova, S., Naydenov, A., Tzaneva, B., Kolev, H., Atanasova, G., Stoyanova, D., Karakirova, Y., Aleksieva, K.: On the development of active and stable Pd-Co/γ-Al_2O_3 catalyst for complete oxidation of methane. Chem. Eng. J. 266, 329–338 (2015).

12. Chlebda, D., Gierada, M., Łojewska, J., Jędrzejczyk, R.J., Jodłowski, P.J.: In situ spectroscopic studies of methane catalytic combustion over Co, Ce, and Pd mixed oxides deposited on a steel surface. J. Catal. 350, 1–12 (2017).

13. Ercolino, G., Grzybek, G., Stelmachowski, P., Specchia, S., Kotarba, A., Specchia, V.: Pd/Co_3O_4-based catalysts prepared by solution combustion synthesis for residual methane oxidation in lean conditions.

14. Zhao, C., Zhao, Y., Li, S., Sun, Y.: Effect of Pd doping on CH_4 reactivity over Co_3O_4 catalysts from density-functional theory calculations. Cuihua Xuebao/Chinese J. Catal. 38, 813–820 (2017).

15. Hu, L., Peng, Q., Li, Y.: Low-temperature CH_4 catalytic combustion over Pd catalyst

supported on Co_3O_4 nanocrystals with well-defined crystal planes. ChemCatChem. 3, 868–874 (2011).

16. Ercolino, G., Stelmachowski, P., Grzybek, G., Kotarba, A., Specchia, S.: Optimization of Pd catalysts supported on Co_3O_4 for low-temperature lean combustion of residual methane. Appl. Catal. B Environ. 206, 712–725 (2017).

17. Boreskov, G.K., Muzykantov, V.S.: Investigation of oxide-type oxidation catalysts by reactions of oxygen isotopic exchange. Ann. N. Y. Acad. Sci. 213, 137–170 (1973).

18. Schwartz, W.R., Pfefferle, L.D.: Combustion of methane over palladium-based catalysts: support interactions. J. Phys. Chem. C. 116, 8571–8578 (2012).

19. Schwartz, W.R., Ciuparu, D., Pfefferle, L.D.: Combustion of methane over palladium-based catalysts: catalytic deactivation and role of the support. J. Phys. Chem. C. 116, 8587–8593 (2012).

20. Nassiri, H., Lee, K.-E., Hu, Y., Hayes, R.E., Scott, R.W.J., Semagina, N.: Water shifts PdO-catalyzed lean methane combustion to Pt-catalyzed rich combustion in Pd-Pt catalysts: In situ X-ray absorption spectroscopy. J. Catal. 352, 649–656 (2017).

21. Patterson, A.: The Scherrer formula for X-Ray particle size determination. Phys. Rev. 56, 978-982 (1939).

22. Thommes, M., Kaneko, K., Neimark, A.V., Olivier, J.P., Rodriquez-Reinoso, F., Rouquerol, J., Sing, K.S.W.: Physisorption of gases, with special reference to the evaluation of surface area and pore size distribution (IUPAC Technical Report). Pure Appl. Chem.; aop (2015). doi: 10.1515/pac-2014-117.

23. Abbasi, R., Wu, L., Wanke, S.E., Hayes, R.E.: Kinetics of methane combustion over Pt and Pt-Pd catalysts. Chem. Eng. Res. Des. 90, 1930–1942 (2012).

24. Zhu, G., Han, J., Zemlyanov, D.Y., Ribeiro, F.H.: The turnover rate for the catalytic combustion of methane over palladium is not sensitive to the structure of the catalyst. J. Am.

Chem. Soc. 126, 9896–9897 (2004).

25. Ribeiro, F.H., Chow, M., Dalla Betta, R.A.: Kinetics of the complete oxidation of methane over supported palladium catalysts. J. Catal. 146, 537–544 (1994).

26. Lewis, F.B., Saunders, N.H.: The thermal conductivity of NiO and CoO at the Neel temperature 6, 2525-2532 (1973).

27. Gierman, H.: Design of laboratory hydrotreating reactors. Scaling down of trickle-flow reactors. Appl. Catal. 43, 277-286 (1998).

28. Zasada, F., Piskorz, W., Cristol, S., Paul, J.-F., Kotarba, A., Sojka, Z.: Periodic density functional theory and atomistic thermodynamic studies of cobalt spinel nanocrystals in wet environment: molecular interpretation of water adsorption equilibria. J. Phys. Chem. C. 114, 22245–22253 (2010).

29. Fujimoto, K.-I., Ribeiro, F.H., Avalos-Borja, M., Iglesia, E.: Structure and reactivity of $PdOx/ZrO_2$ catalysts for methane oxidation at low temperatures. J. Catal. 179, 431–442 (1998).

30. Alyani, M., Smith, K.J.: kinetic analysis of the inhibition of CH_4 oxidation by H_2O on PdO/Al_2O_3 and $CeO_2/PdO/Al_2O_3$ catalysts. Ind. Eng. Chem. Res. 55, 8309–8318 (2016).

3.6 Electronic Supplementary Material

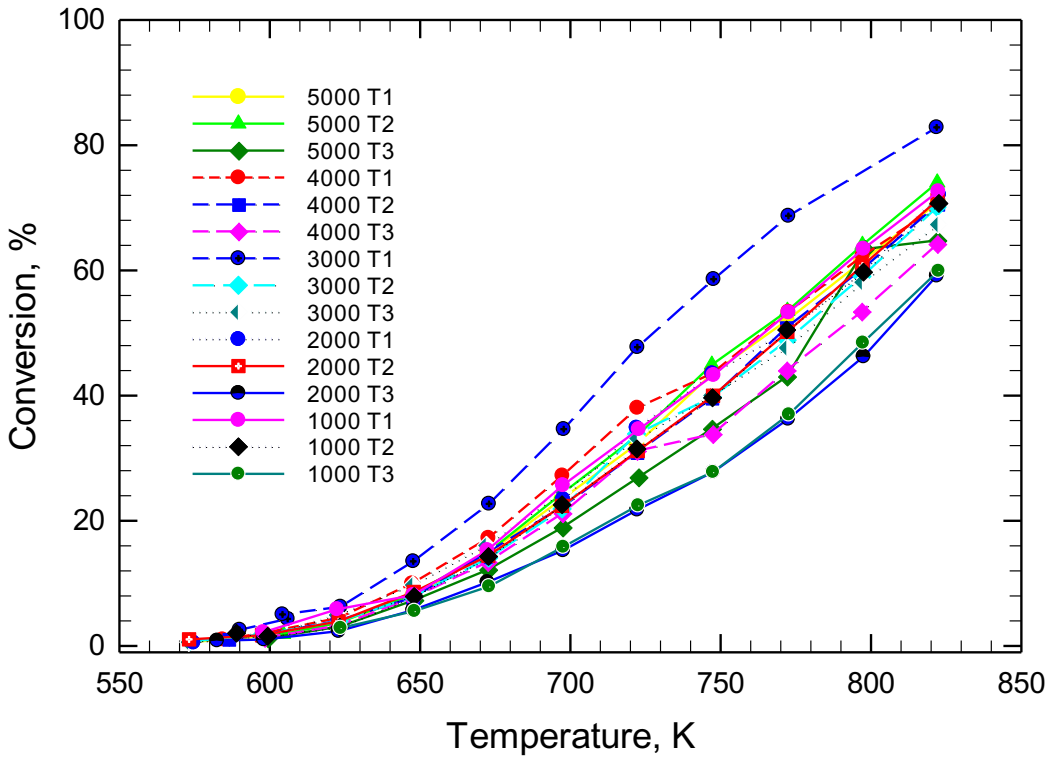

Figure 3.8 Ignition curves for Co_3O_4 catalyst for three trials (T1-T3) at different CH_4 concentrations (ppmv), 10 vol.% H_2O, 0.6 g, 210 mL_{STP}/min, 19.5 vol.% O_2, GHSV = 21,000 $L_{(STP)}/(kg_{cat} \cdot h)$. The exceptional 3000 T1 run was the first run in the series with 10% water. The order of the trials is shown in Table 1 in the main text.

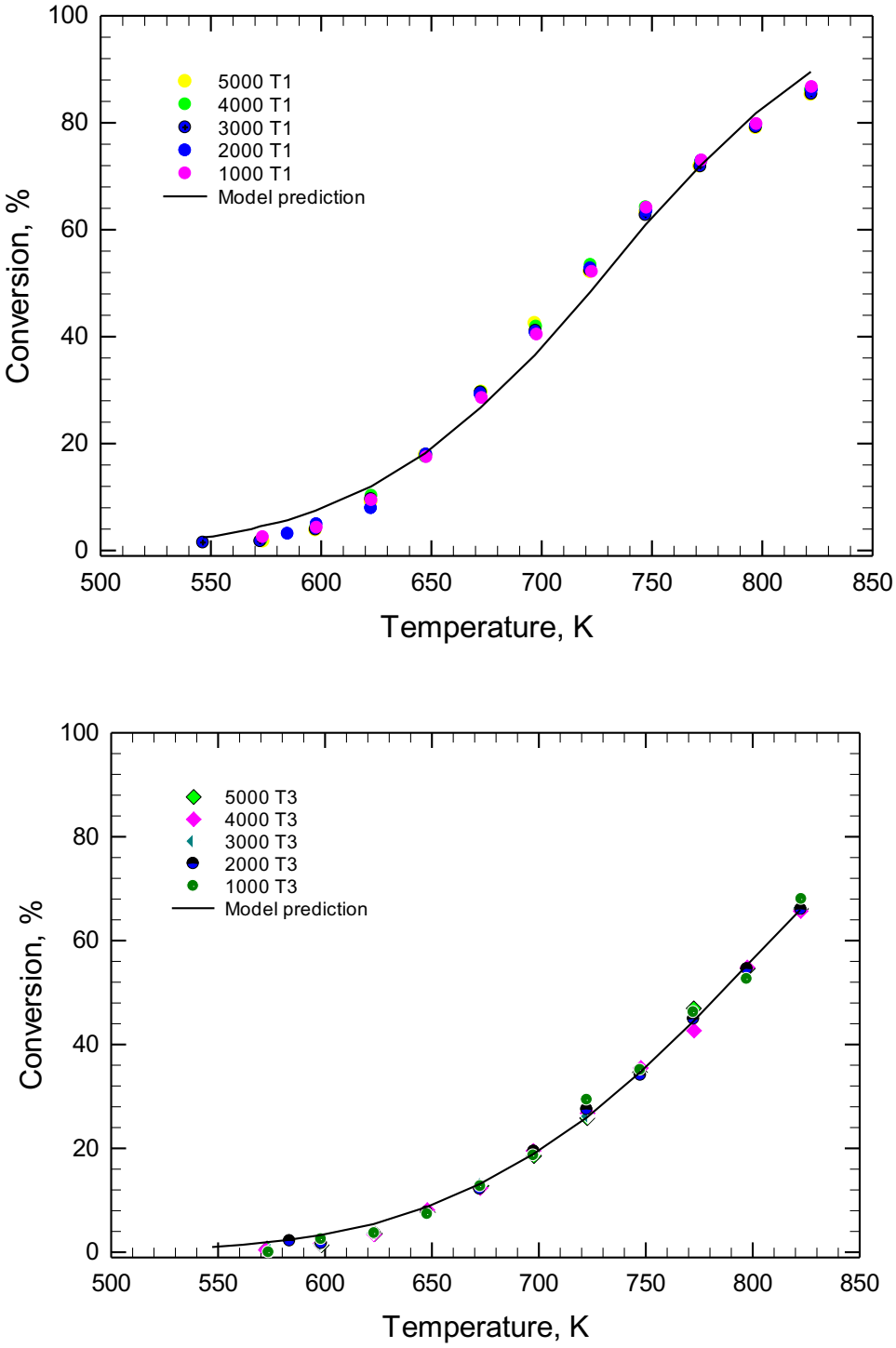

Figure 3.9 Model prediction (first order in CH_4) for the ignition curves on Co_3O_4 with 5 % water in the feed for trials (top) T1 and (bottom) T3. See Figure 3.8 caption for the reaction conditions.

3.6.1 Basis of calculations of simulation curves in Figure 3.10 10% H_2O

The simulation curves in Figure 3.10 were calculated as below:

Reactor pressure: 17 psia; Room pressure: 13.5 psia; Room temperature: 21 °C; Volumetric flow rate at lab conditions: 212 mL/min.

$$Q_2 = Q_{lab}\frac{13.5}{17}\frac{T}{294.15} = Q_{lab}(2.7 \times 10^{-3})T \quad (3\text{-}4)$$

$$X_{A_{predicted}} = 1 - \exp\left(-\frac{kw}{Q}\right) \quad (3\text{-}5)$$

$$k = A_0 \exp\left(-\frac{E_a}{RT}\right) \quad (3\text{-}6)$$

Table 3-3 Arrhenius parameters for each trial

Trial #	Pre-exponential factor, L/(g·s)	Activation energy, J/mol
T1	426.84	68965
T2	462.34	70387
T3	214.58	67092

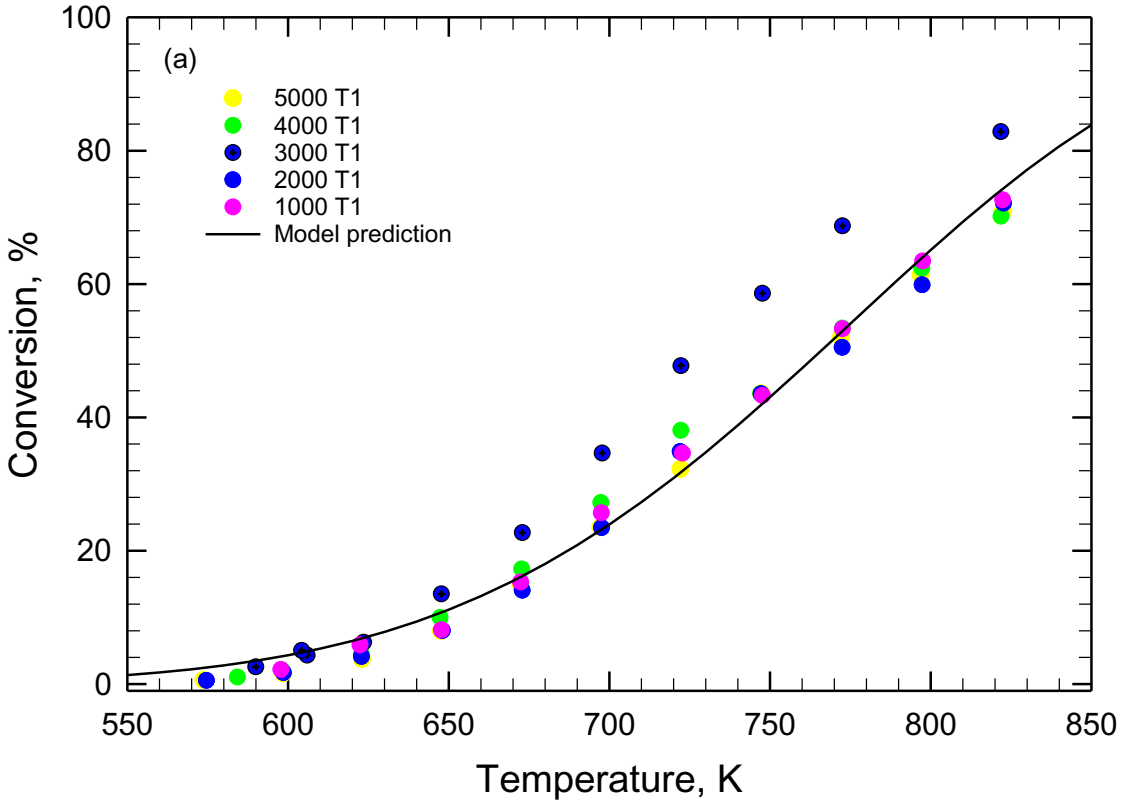
(a)
5000 T1
4000 T1
3000 T1
2000 T1
1000 T1
Model prediction
Conversion, %
Temperature, K
0
20
40
60
80
100
550
600
650
700
750
800
850

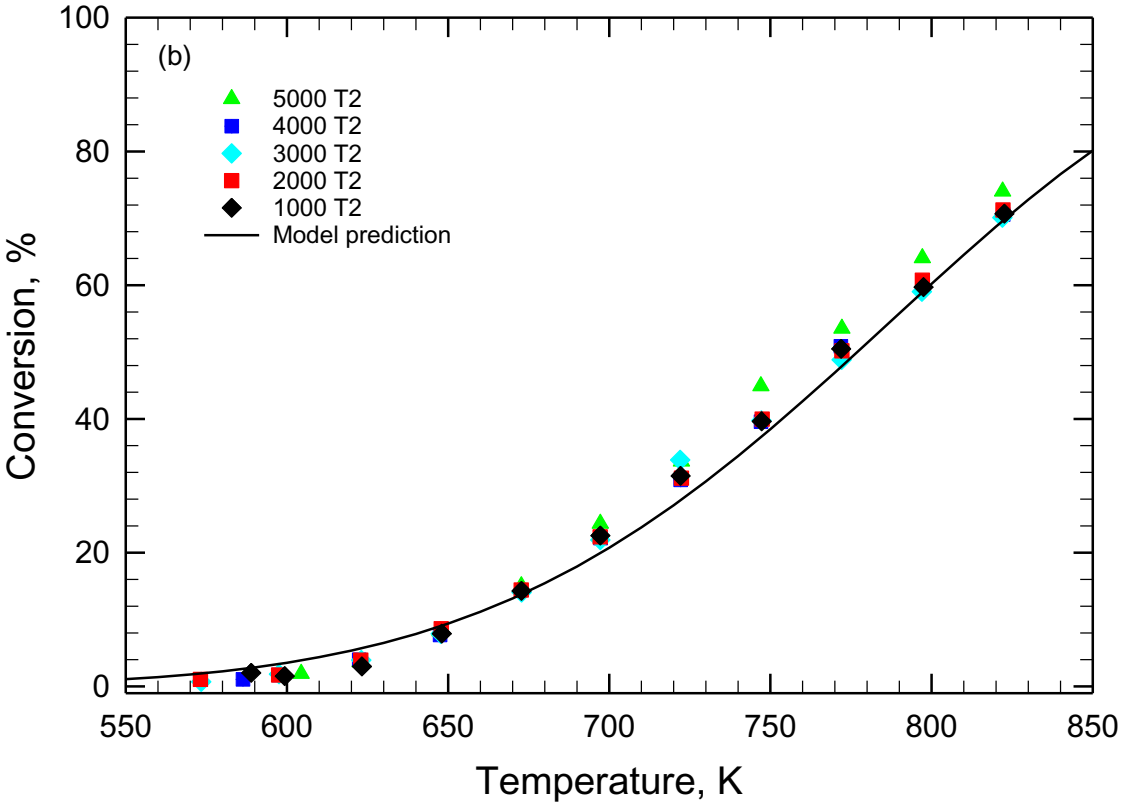
(b)
5000 T2
4000 T2
3000 T2
2000 T2
1000 T2
Model prediction
Conversion, %
Temperature, K
0
20
40
60
80
100
550
600
650
700
750
800
850

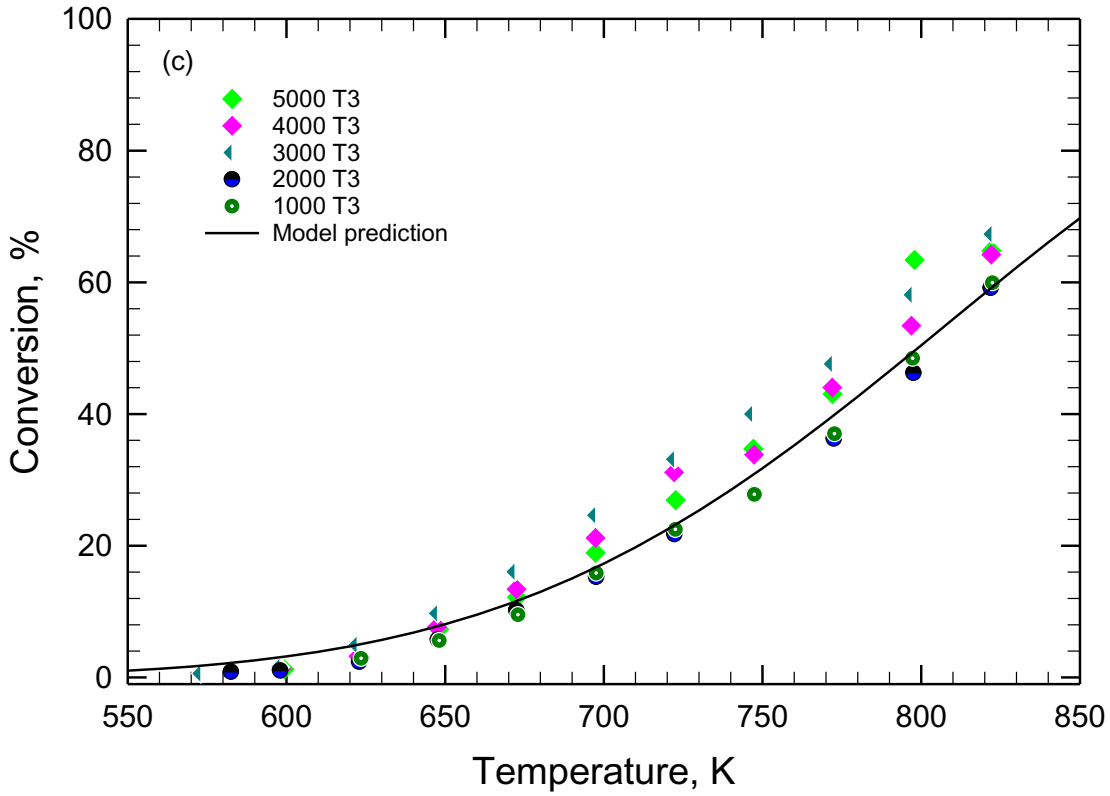

Figure 3.10 Model prediction (first order to CH_4) for the ignition curves on Co_3O_4 with 10% water in the feed for trials (a) T1, (b) T2 and (c) T3. See Figure 3.8 for the reaction conditions.

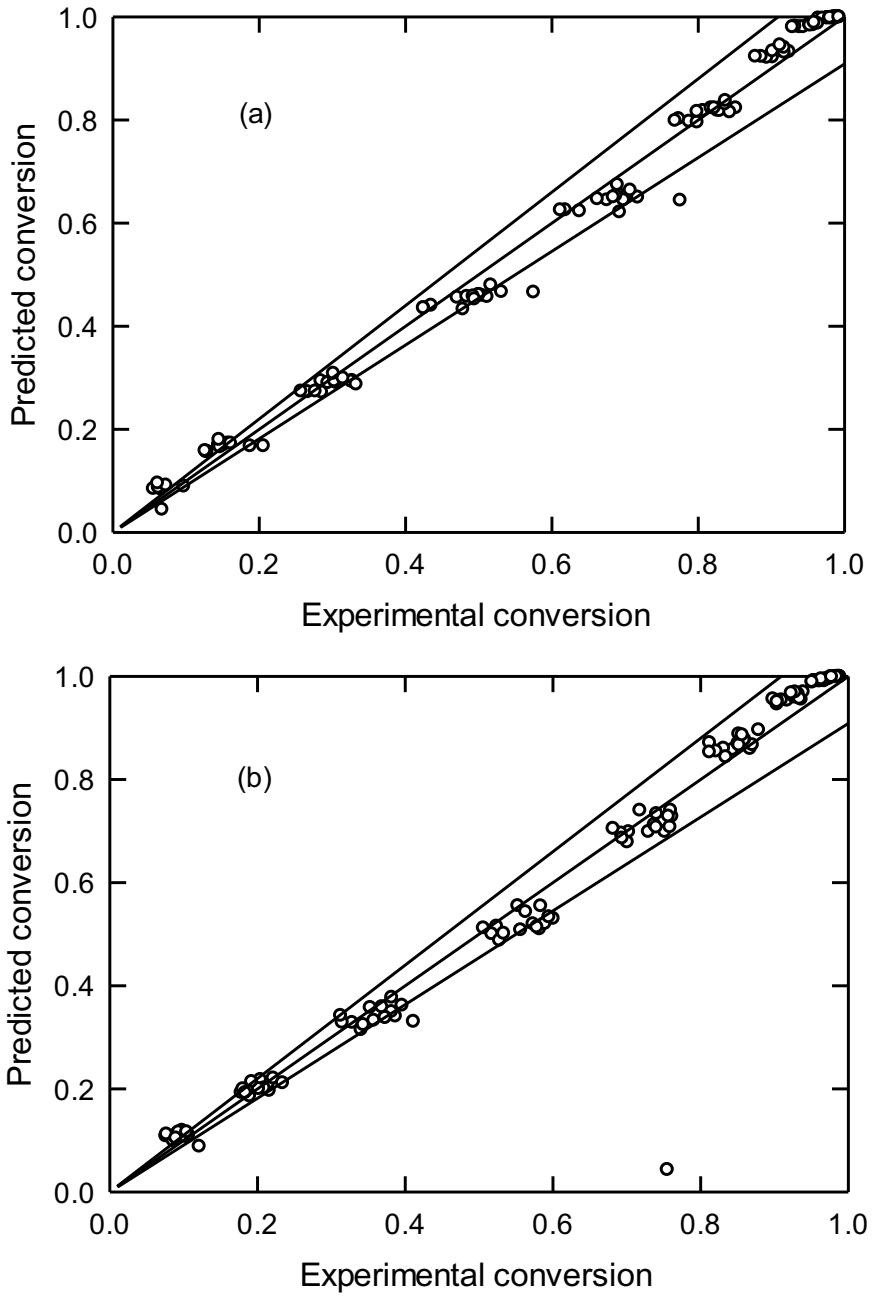

Figure 3.11 . Parity plots with plus and minus 10 % error range for the Pd/Co_3O_4 catalyst with the conversions predicted using 1st order to methane and Arrhenius law parameters from Table 1. (a) 5% water and (b) 10 % water. Reaction conditions are the same as given in Figure 3.8.

4 Strong metal-support interactions in Pd/Co_3O_4 catalyst in wet methane combustion: *in situ* X-ray absorption study[2]

4.1 Introduction

In the ongoing quest for efficient low-temperature methane combustion catalysts, preferably with reduced loadings of Pt-group metals, cobalt-containing materials have attracted increasing attention in the past decade [1-19]. In contrast to the majority of other studied promoters, cobalt oxide itself possesses a relatively high activity in methane activation [10,12,15,20]. Several studies of Sojka and colleagues reported mechanistic insights into the active sites of CoOx-catalyzed methane combustion [21-23]. Below 450°C, a suprafacial Langmuir-Hinshelwood mechanism dominates with adoxygen species activated on tetrahedral Co^T. The Mars van Krevelen mechanism on intrafacial $Co\text{-}O_{surface}$ sites does not reveal itself until at least 450-600 °C, as demonstrated by isotopic exchange experiments [21] and calculations of the relatively high activation barrier [22]. The cobalt oxide catalyst stoichiometry is thus preserved up to 450 °C, with facile suprafacial $O\text{-}Co^T$ formation, decarboxylation and dehydroxylation [22]. The first C-H bond activation is a rate-determining step [22], which is similar to Pd-catalyzed methane combustion. The oxo-cobalt active site speciation changes with temperature and oxygen partial pressure, and the activity is also structure-sensitive [21]. For selected crystal structures of Co_3O_4, Sojka and colleagues computed that the activation barriers of surface oxygen diffusion, methane activation on suprafacial $Co\text{-}O_{adsorbed}$ sites, and intrafacial $Co\text{-}O_{surface}$ sites are 0.75 eV (i.e., 72 kJ/mol), 0.83 eV (80 kJ/mol), and 1.11 eV (107 kJ/mol), respectively[21,22]. When doped with Pd, an *in situ* infrared spectroscopy study of Pd-Co catalysts used for methane combustion

[2] A version of Chapter 4 of the thesis has been published in Catalysis Science & Technology journal as "Strong metal-support interactions in Pd/Co_3O_4 catalyst in wet methane combustion: in situ X-ray absorption study" William Barrett, Somaye Nasr, Jing Shen, Yongfeng Hu, Robert E. Hayes, Robert W.J. Scott, and Natalia Semagin(2020). The in situ XAS was performed by William Barrett under the supervision of Dr. Robert W.J. Scott at the at Canadian Light Source, Saskatoon. H_2-TPR was performed by Dr. Jing Shen. All the methane combustion experiments, and characterization conducted by Somaye Nasr. Manuscript draft preparation and writing were conducted by the authors William Barrett and Somaye Nasr under the supervision of Dr. Robert W.J. Scott and Dr. Natalia Semagina. Dr. Natalia Semagina performed the final manuscript writing and she addressed all the comments of the reviewers. The work is conducted under the supervision and final approval of Dr. Natalia Semagina, Robert W.J. Scott and Dr. Robert E. Hayes.

postulated the importance of adsorbed O* species rather than the bulk O atoms and the requirement of oxidized active sites [6].

Another feature of cobalt oxide, which makes it attractive for methane combustion application, is its relatively high tolerance to water poisoning, as opposed to conventional Pd. A phase diagram of $Co(OH)_2$-CoO system shows that dehydroxylation occurs below 300 °C at a water pressure up to 2000 bar[24]. DFT calculations of dissociative water adsorption showed, for example, that at 0.1 atm H_2O and at a temperature as low as 250 °C, the surface is only 20% and 33% hydroxylated for (100) and (111) cobalt spinel planes, respectively[25]. Computational studies exclude (111) surfaces as having a primary role in catalytic processes with wet feeds [21], since they have higher affinity to water coverage as compared to (100) and (110) surfaces [25].

A recent kinetic study of Co_3O_4 and Pd/Co_3O_4 for lean methane combustion with 5 and 10% water in the feed with variable methane concentrations demonstrated that the cobalt oxide contribution to the Pd catalyst activity can reach up to 70% and is more pronounced at lower temperatures. Both catalysts showed 1st order kinetics with respect to CH_4, and 0 and -0.37 order kinetics with respect to water for Co_3O_4 and Pd/Co_3O_4 catalysts, respectively, at temperatures between 250 and 550 °C. The activation energy on the Pd-free sample was only 69 kJ/mol vs. 91 kJ/mol for the Pd/Co_3O_4 catalyst, but the former had a much lower amount of active sites (by two orders of magnitude). What was puzzling, is that the kinetic parameters of the Pd/Co_3O_4 – catalyzed reaction were not additive, based on the kinetic evidence, but synergetic ones [26].

Several studies reported the characterization of Co_3O_4, and Pd-Co materials as related to methane combustion [7,17-19]. The stability of speciation of Co_3O_4 alone was demonstrated by X-ray photoelectron spectroscopy [18]. Cobalt oxide was hypothesized to remove hydroxyls from PdO and provide its lattice oxygen to recreate PdO sites[7], while in another study Pd doping of Co_3O_4 resulted in the formation of some reduced CoO_x even in the fresh calcined materials[19]. The hypotheses were based on the *ex situ* characterization and they hinted at the existence of the strong metal-support interactions in Pd/Co_3O_4 catalysts, as also suggested in the kinetic study above [26].

The objective of the current work was to investigate the Pd and Co speciation in cobalt oxide and Pd/CoO_x catalysts during lean methane combustion in wet feeds at temperatures below 450 ºC, which are of the most interest to natural-gas vehicle exhaust aftertreatment, and which the poisoning effect of water on Pd is known[27]. The analyses were performed by *in situ* X-ray absorption spectroscopy (XAS) and were aimed to obtain the distribution of Pd and Co species, including their hydroxides, as a function of reaction temperature.

4.2 Experimental

4.2.1 Catalyst synthesis and characterization

$CoCl_2 \cdot 6H_2O$ (98%, Sigma-Aldrich), urea (Sigma-Aldrich), K60 polyvinylpyrrolidone solution (PVP, Sigma-Aldrich, 45% in aqueous solution), $Pd(AcO)_2$ (Sigma-Aldrich), 1,4-dioxane (>99.9%Sigma-Aldrich), ethylene glycol(>99.9%, Fisher Scientific) were used as received. Gas mixtures were from Praxair. Cobalt oxide was synthesized by a hydrothermal method as described earlier [26]. 2-nm PVP-stabilized Pd nanoparticles were synthesized in a colloidal solution [28], followed by deposition on cobalt oxide by acetone precipitation method. The catalysts were calcined at 550 °C for 16 h under static air ("calcined" or "fresh" catalysts). Final Pd loading was determined to be 0.3 wt.% Pd/Co_3O_4 by neutron activation analysis (Becquerel Laboratories, Maxxam Analytics, Canada). BET surface area of the samples as found earlier by N_2 adsorption 10 and 13 m^2/g, respectively [26].

X-ray photoelectron spectroscopy analyses (XPS) were performed with a Kratos Axis Ultra using a mono Al Kα source that operates at 14 kV and 15 mA. The acquired spectra were corrected for C 1s at 284.8 eV. Temperature-programmed reduction (TPR) analyses were performed with a Micromeritics AutoChem 2950 HP instrument equipped with an online Pfeiffer Vacuum Thermostat GSD 320 spectrometer calibrated for hydrogen. Detailed experimental procedures for catalyst pretreatment and TPR analysis were described earlier [29]. 0.0025 g of calcined Co_3O_4 was diluted in 0.05 g silica. Prior to TPR analysis, *in situ* reduction-oxidation treatment at 700 °C was performed to eliminate adsorbed impurities on Co_3O_4 surface. TPR analysis was then performed by heating the Co_3O_4 sample in 5% H_2/He at 20 mL/min to 700 °C,

at six different ramping rates (1, 2, 5, 7, 10, 15 °C/min) with random orders. Cobalt catalyst was re-oxidized in 10% O_2/He at 700 °C between different reduction ramping rates.

Palladium dispersion was measured by performing CO chemisorption experiments in a Micromeritics AutoChem 2920 instrument. Pd catalysts were calcined at 550 °C for 16 h in a furnace. 0.5 g of a supported Pd catalyst was packed into a quartz U-tube with quartz wool placed on both sides of the catalyst bed. Prior to CO chemisorption, supported Pd catalyst was reduced in 10% H_2/Ar (20 mL/min) at 150 °C for 1 h with a ramping rate of 10 °C/min. The reduced Pd sample was then purged by He for 30 min at 150 °C, and cooled to room temperature in He. A dynamic CO pulse chemisorption experiment was performed by dosing 3% CO/He gas at room temperate. The flow rates of the 3% CO/He loop gas and He carrier gas were 25 mL/min and 50 mL/min, respectively. Pd dispersion was calculated by assuming Pd/CO stoichiometry of 1/1.

4.2.2 Methane combustion activity

The methane combustion tests were performed in a packed-bed reactor with 0.3 g of catalysts. To mimic the same operating conditions as in the XAS experiments, the catalysts were reduced *in situ* using 5% H_2/Ar (heating from room temperature to 300 °C at ramping rate of 10 °C/min, followed by a 10-min hold. After cooling to 100 °C, the reactor was flushed with N_2 for 20 min at 100°C to remove any remaining H_2. After the reduction step, the catalyst was ready for methane combustion reactions. Methane combined with dry air (ultra-zero-level, <2 ppm H_2O) was fed to the reactor for tests at "dry" conditions. For the "wet" conditions, water was added using a pump which corresponds to 1 vol.% H_2O. Flow rates of methane and air were 0.9 mL/min (10 % CH_4/N_2) and 150 mL/min, respectively. For the methane combustion reaction, the catalyst was incrementally heated from 200 to 550°C (ramping rate of 50°C/min) and kept at each temperature for 15 min, under both wet and dry conditions. The composition of effluent gas was analyzed by using an online gas chromatograph (Agilent 7890A) equipped with a thermal conductivity and a flame-ionization detector.

4.2.3 *In Situ* X-ray Absorption Spectroscopy

The *in-situ* X-ray absorption spectroscopy (XAS) work was done using procedures that were detailed in a previous publication [30]. Briefly, an *in-situ* XAS fluorescence cell was used on the Hard X-ray Micro-Analysis (HXMA) and Soft X-ray Microcharacterization Beamline (SXRMB) beamlines which allows catalysts to be immersed in the targeted gaseous environment and the temperature to be controlled by microheaters. For the reactions under wet environment, 1 mol% water was added to the feed. L_3 edge Pd and K edge Co measurements were performed on SXRMB beamline at the Canadian Light Source, while K edge Pd measurements were performed on the HXMA beamline. Fluorescence data was collected and fit to standards using linear combination fitting using the Demeter software package [31]. For Pd speciation, similar standards were used as in a previous publication. Co standards were cobalt powder (spherical -100+325 mesh 99.8% purity Alfa Aesar) for Co(0), cobalt(II) oxide (95% Alfa Aeser) for Co(II), and lithium cobalt(III) oxide (97% Alfa Aesar) for Co(III).

4.3 Results and Discussion

4.3.1 Cobalt oxide catalyst

A conventional Co_3O_4 catalyst for methane combustion was used in its calcined form and was composed of 33 at.% of Co^{2+} and 67 at.% Co^{3+} species (as per $CoO{\cdot}Co_2O_3$ stoichiometry). The Co_3O_4 crystal structure was confirmed by X-ray diffraction (XRD) [26]. XPS analysis of the calcined catalyst shows the expected cobalt speciation as 23% of Co^{2+} and 73% of Co^{3+} species (Figure 4.1 and Table 4-4-1 in the Supporting Information), the small differences likely being due to the surface enrichment with oxygen. The composition did not change after continuous one-week methane combustion reactions in the wet feed (maximum temperature of 550 ^oC), which is in line with reported observations [18].

During methane combustion, oxygen exchange with gas phase species, oxygen diffusion, and methane activation on suprafacial or intrafacial Co-O species is expected [21-23]. To follow the reoxidation of the methane-reduced sites, we subjected the Co_3O_4 catalyst to a reductive treatment prior to the *in situ* XAS measurements (10 ^oC/min heating in 5% H_2 95% He mix to

300 ºC held at 300 ºC for 10 mins until cooled, in H_2/He mix to 100 ºC at 10 ºC/min). Figure 4.2 shows the Co_3O_4 H_2-TPR profiles at different heating rates monitored by a calibrated on-line mass spectrometer. For all the heating rates, 1.1 mol H_2/mol $_{Co}$ consumption was achieved indicating near-complete Co_3O_4 reduction to Co(0), which requires 1.3 mol H_2/mol $_{Co}$ stoichiometry. The reduction activation energy, as determined from the slope $\ln(\beta/T_{max}^2)$ vs. 1/T, is 73 kJ/mol, which is similar to previously reported values [32].

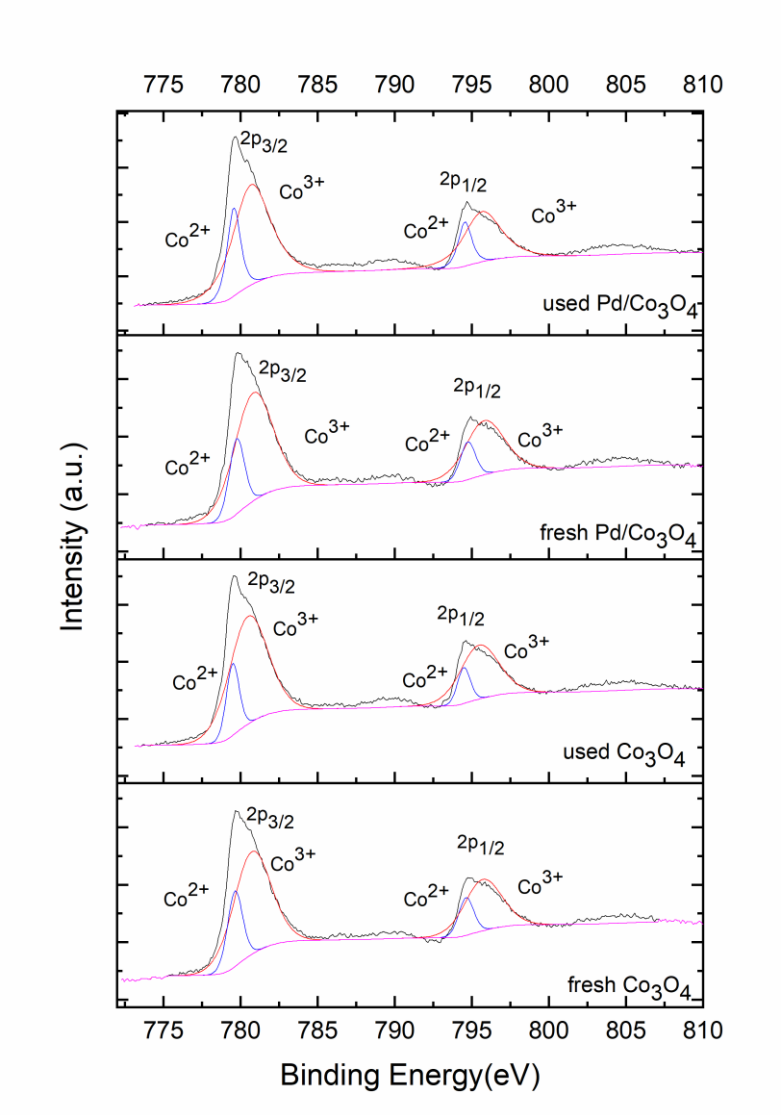

Figure 4.1 XPS profiles of Co_3O_4 and Pd/Co_3O_4 catalysts: fresh (calcined) and used in wet methane combustion for one week on stream. The quantitative analysis can be found in Table 4-4-1 in the Supporting Information.

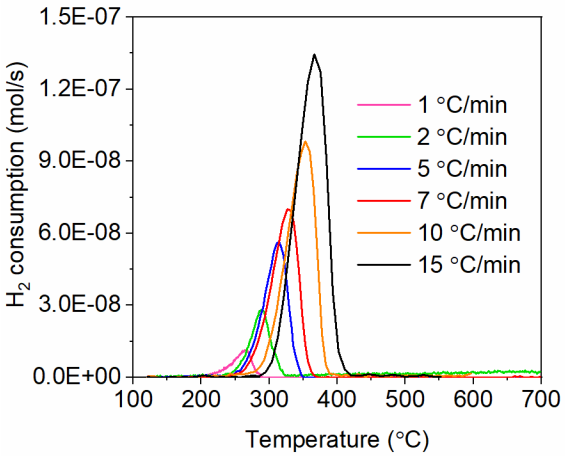

Figure 4.2 TPR profile of Co_3O_4 (0.0026 g) in H_2. The H_2 consumption is monitored by a calibrated on-line mass spectrometer.

Thus, the 10-min heating of Co_3O_4 in H_2 at 300 °C prior to the *in situ* XAS analysis, resulted only in the partial reduction, as seen from Figure 4.3 and Figure 4.5. When the pre-reduced CoO_x catalyst was subjected to an *in situ* XAS study, the presence of water did not affect the relative fraction of Co^{3+} (ca. 35-40% levels), but decreased the Co^{2+}/Co^0 ratio from 4 to 2 (Figure 4.5). The $Co(OH)_2$ contribution was checked using a standard and was found negligible, in accordance with no hydroxide detection by the XRD after the reaction[26]. Given that the water inhibits the methane combustion activity on CoO_x (Figure 4.4), as also noticed by others[10], it is apparent that water impedes the oxygen exchange and/or reoxidation of reduced cobalt sites, which is similar to the water effect on Pd-catalyzed methane combustion, although not to such a large extent as for Pd catalysts[30,33-35]. DFT calculations showed facile surface dehydroxylation at 300 – 450 °C range [22]. Pd hydroxides are measurable in this experiment and Co hydroxides are not due to the relative sizes of the species; in nanoparticle Pd the surface atoms are much more of a significant proportion of the overall atoms than is seen in the larger cobalt particles.

What is distinctively different from Pd in a conventional Pd/Al_2O_3 catalyst (as was seen in [30,35] and will be shown below), is that the oxidation degree of Co^{x+} does not increase with temperature and even at 400 °C in the presence of air the Co^{3+} fraction is only 40% as opposed to the expected 67% from the stoichiometry of Co_3O_4. Moreover, in the presence of water the Co^{2+}/Co^0 ratio slightly decreased as the reaction progressed from 100 to 400 °C (Figure 4.5b).

Note that cobalt oxidation is thermodynamically favourable at the oxygen partial pressure and temperature used according to reactions R1 and R2 (van't Hoff equation was assumed with a constant heat of reaction, the thermodynamic properties of CoO and Co_3O_4 at 298.15 K are from[36]):

R1) $Co + ½ O_2 \rightarrow CoO$ $\Delta H^o_{273\text{-}573K} = -476$ kJ/molO_2; $\Delta G^o_{573K} = -384$ kJ/molO_2

R2) $3CoO + ½ O_2 \rightarrow Co_3O_4$ $\Delta H^o_{273\text{-}573K} = -354$ kJ/molO_2; $\Delta G^o_{573K} = -178$ kJ/molO_2

The observed stability of the partially reduced cobalt oxide indicates kinetic limitations in the oxidation process. Co_3O_4 provides a low activation barrier for oxygen exchange with gas phase oxygen (67 kJ/mol [37,38]) and a relatively low methane activation energy on the suprafacial active sites of 80 kJ/mol [22]. The activation energy of CoO to Co_3O_4 oxidation (R2) is 100 kJ/mol [39]. Apparently, the rate of oxygen consumption for CoO oxidation is negligible as compared to the oxygen activation and consumption in the methane combustion.

4.3.1 Pd-doped cobalt oxide

As one can see from Figure 4.4, up to 300 °C, the activities of Co_3O_4 and Pd/Co_3O_4 catalysts in each of the dry and wet feeds are nearly identical and are mostly governed by the Co activity; indeed, at such low temperatures and low Pd dispersion of 12%, significant Pd activity is not expected, but should increase as the temperature increases. The *in situ* XAS study was performed only for the wet feed for Pd/Co_3O_4 catalyst, as is relevant for exhaust aftertreatment for natural gas vehicles. The cobalt oxide speciation changes dramatically once Pd is incorporated to increase the combustion activity. As in the case of Co_3O_4 catalyst, the Pd/Co_3O_4 catalyst was pre-reduced at 300 °C at a heating rate 10 ºC/min. As seen from the TPR profile (Figure 4.6), the Co_3O_4 reduction occurs at lower temperatures as compared to the Pd-free sample (Figure 4.2). This is likely due to the reduction of Pd, followed by hydride formation, and the hydride then spills over to the Co_3O_4 support to reduce the support. As a result of Pd-catalyzed Co_3O_4 reduction, a higher Co reduction degree is observed by *in situ* XAS for the pre-reduced sample at low temperatures (Figure 4.7); unlike in the Co_3O_4 system, the Pd/CoO_x system has no Co(III) is present at all at the beginning of the methane oxidation reaction, and 50% of the Co is present as

Co(0). During the methane combustion reaction, between 200 and 400 °C, this metallic Co is oxidized with the formation of Co^{2+} and Co^{3+}. The activation energies of both Co → CoO (reaction R1) and CoO → Co_3O_4 (reaction R2) are similar, 96-100 kJ/mol respectively [39]. Thus, it is likely that the enhanced oxidation in the presence of Pd occurs because of preliminary oxygen activation on Pd, and the activated atomic oxygen on the Pd surface allows for the reduced activation energy of cobalt oxidation.

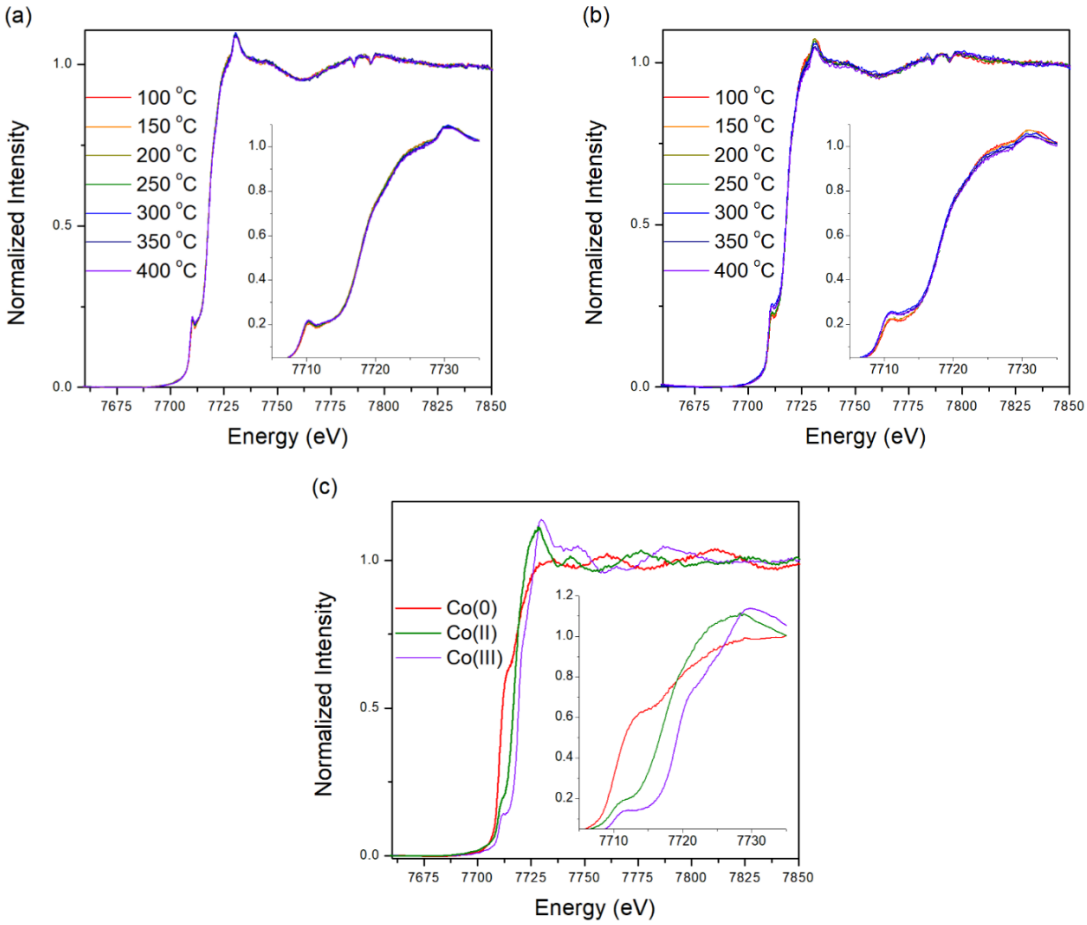

Figure 4.3 Co K edge *in situ* XAS data of the Pd-free cobalt oxide catalyst under a) dry, b) wet methane combustion conditions and c) cobalt standards.

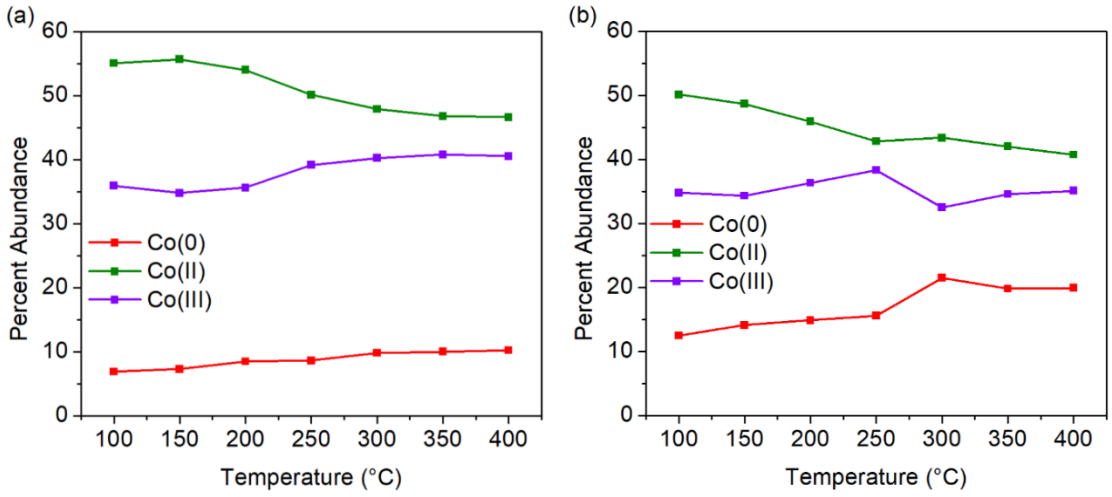

Figure 4.5 Linear combination fitting of the Co K edge *in situ* XAS data for the Pd-free cobalt oxide catalyst during a) dry, and b) wet methane combustion conditions.

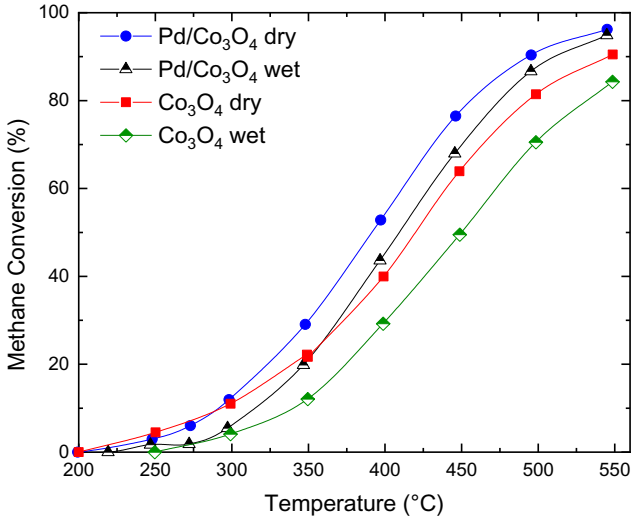

Figure 4.4 Methane combustion activity of the reduced catalysts in the dry and wet feed. 600 ppmv CH_4, 1 mol.% H_2O, 0.3 g of catalysts, Pd dispersion is 12%.

The *in situ* XAS spectra at the Pd K and L_3 edges are shown in Figure 4.8, along with Pd standards. The Pd K edge data (Figure 4.8a) demonstrates that there is very little change to the Pd K edge XAS spectra as a function of temperature. Compared to the Pd K edge data for this system, the Pd L_3 edge (Figure 4.8c) shows greater changes with respect to temperature. The white line at the Pd L_3 edge is due to $2p_{3/2}$ to 4d transitions in Pd, and an increasing white line intensity is consistent with increased vacancies in the Pd 4d band. This increase is essentially vertical, which indicates that presence of electron-withdrawing species, and not oxidation state changes, may be causing the intensity increase (similar Pd L_3 edge spectra for Pd/Al_2O_3 systems in which Pd oxidation was seen show both white lines increase and the edge shifts as expected for Pd oxidation)[30]. The Pd K edge stability also indicates the lack of oxidation state changes of the Pd catalyst. These electron withdrawing species are removing electron density from 4d orbitals. Such species could be formate intermediates, which are known methane combustion intermediates [40], including on Pd-Co systems [6]. The Pd K edge, which is not sensitive to vacancies in the 4d orbitals, does not exhibit this change, and is therefore used for linear combination fitting analyses to determine the speciation of the Pd catalyst.

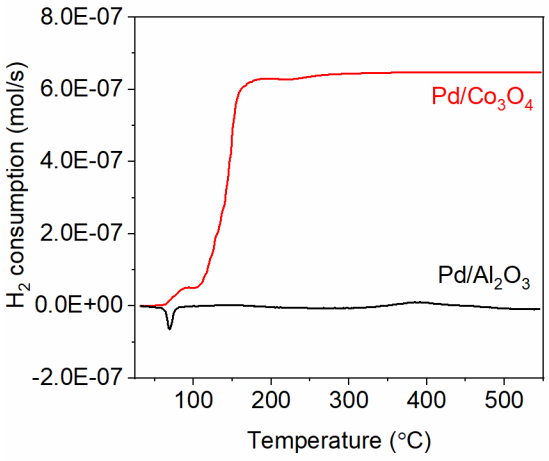

Figure 4.6 TPR in H_2 at 10 °C/min heating rate (0.5 g of each sample). A Pd/Al_2O_3 catalyst is shown for comparison to demonstrate that Co reduction is the primary cause of H_2 consumption, presumably by spillover of activated hydrogen from β-Hydride of Pd. Reproduced with permission from [109], copyright 2019, Elsevier.

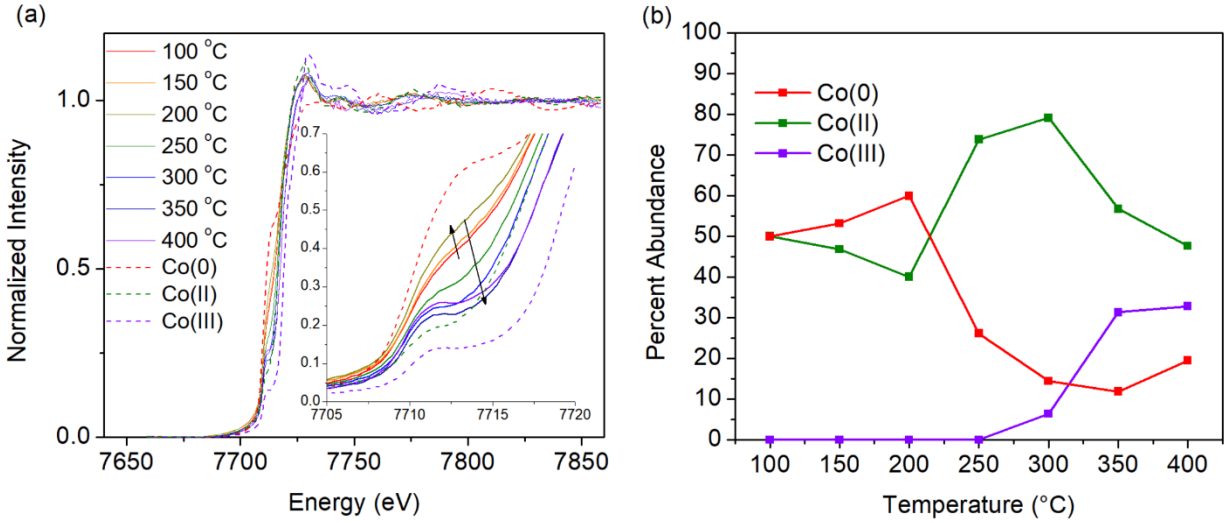

Figure 4.7 . Co K edge XAS spectra of Pd/CoO_x a) during in situ wet combustion and b) with linear combination fitting.

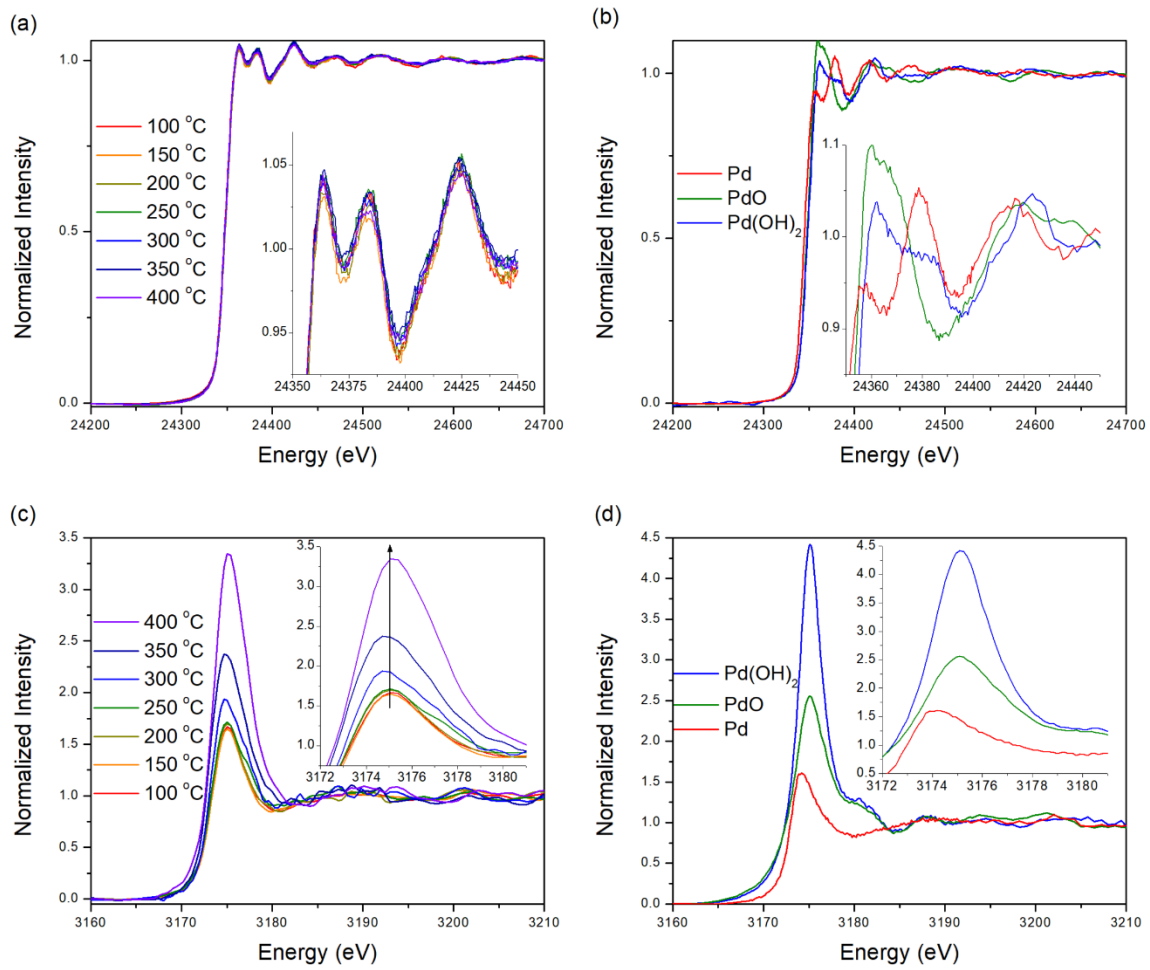

Figure 4.8 (a) Pd K edge XAS spectra of Pd/CoO_x catalyst under *in situ* wet methane oxidation conditions and (b) Pd K edge standards; (c) Pd L_3 edge of the Pd/Co_3O_4 catalyst *in situ* and (d) Pd L_3 edge standards.

Figure 4.9 presents linear combination fittings for Pd species on Co_3O_4 support and also on Al_2O_3 from our previous work in the same *in situ* XAS conditions during wet methane combustion [30,35]. Pd/Al_2O_3 is a conventional benchmark material in methane combustion catalysis; the methane combustion performance of this systems can be found in Figure 4.10 in the Supporting Information, with combustion activity starting at 300 °C. The striking difference between the two catalysts is that approximately 80% of Pd remains in its reduced form on the Co_3O_4 support, while it progressively oxidizes in Pd/Al_2O_3 system. At this temperature and

partial oxygen pressure, the oxidation of Pd is thermodynamically favourable [35,41], but its oxidation is kinetically limited [42,43]:

R3) $Pd + ½\ O_2 \rightarrow PdO$ $\Delta H^o_{273\text{-}573K} = -226\ kJ/mol_{Pd}$; $\Delta G^o_{573K} = -55\ kJ/\ mol_{Pd}$

The presence of a PdO shell (even incomplete) has been proven as a requirement for methane combustion catalysis [43]. Below 450 °C, both catalysts indeed show the PdO formation in the amounts near or below their dispersions, in agreement with the PdO active site requirements. However, the metallic Pd core progressively oxidizes on Al_2O_3 support, but not on the CoO_x.

As was shown above for the Co state on Pd/CoO_x catalyst (Figure 4.7), the enhanced cobalt oxidation in the presence of Pd could occur because of preliminary oxygen activation on Pd. This is supported by the lack of oxidized Pd (Figure 4.9). The oxygen transfer from the oxidized Pd shell to the reduced cobalt oxide is thermodynamically favourable (the thermodynamic properties at 298.15 K for PdO and CoO are from [44] and [36], respectively):

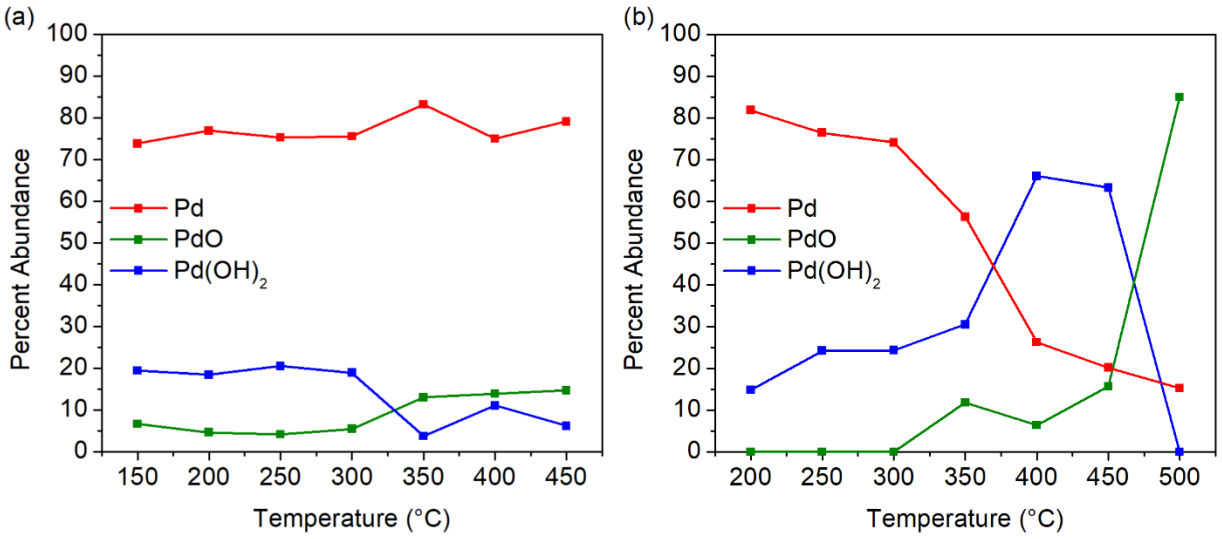

Figure 4.9 Pd speciation from *in situ* XAS during wet methane combustion starting with the reduced catalysts: (a) Pd/Co_3O_4 with Pd dispersion of 12% and (b) Pd/Al_2O_3 with Pd dispersion of 40%. reprinted from [30] with permission, copyright John Wiley and Sons, 2019.

R4) $PdO + Co \rightarrow Pd + CoO$ $\Delta H^{o}_{273\text{-}573K} = -125$ kJ/mol$_{Pd}$; $\Delta G^{o}_{573K} = -137$ kJ/mol$_{Pd}$

R5) $PdO + 3CoO \rightarrow Pd + Co_3O_4$ $\Delta H^{o}_{273\text{-}573K} = -64$ kJ/mol$_{Pd}$; $\Delta G^{o}_{573K} = -35$ kJ/mol$_{Pd}$

Thus, the observed speciation *in situ* during the methane combustion on Pd/CoO_x catalyst signifies that strong metal-support interactions occur via oxygen activation on Pd and its transfer to cobalt oxide for its oxidation and also oxygen use in Co-catalyzed methane oxidation.

In terms of the oxygen activation kinetics, heat of oxygen chemisorption on Pd is actually lower than on cobalt oxide, which is - 150 kJ/mol for Pd [45] vs. -63 kJ/mol for Co [37,38]. According to the Brønsted-Polyani principle, the activation energy of oxygen activation on Pd is higher than on Co (86 kJ/mol for Pd [37] vs. 63-67 kJ/mol for Co [37,38] and a lower rate of oxygen binding on Pd may be expected. The seemingly puzzling contradiction in the methane oxidation catalysis is typically explained by the number of available active sites. Indeed, as deduced from the kinetics of methane combustion on Co_3O_4 and Pd/Co_3O_4, the number of active sites in the latter catalyst is two orders of magnitude higher than in the former, so oxygen activation on Pd occurs faster than on Co[46]. Thus, the thermodynamic driving force for Co oxidation by PdO (R4 and R5) is complemented by the fast kinetics of PdO formation on the Pd nanoparticle surfaces. The bulk PdO oxidation is thermodynamically unfavorable in the presence of reduced Co (R3-R5), and the stand-alone bulk Pd oxidation needs to overcome the activation barrier of 111-116 kJ/mol [7]. In the case of the Pd/Al_2O_3 catalyst, Pd progressively oxidizes (Figure 4.9) because Pd is the only possible donor for the excess oxygen species, while reduced CoO_x extracts those oxygen species and prevents Pd bulk oxidation.

Another observation of Pd speciation under wet methane combustion is that on Pd/CoO_x system the formation of methane combustion-inactive $Pd(OH)_2$ seems to be suppressed as compared to the Al_2O_3 system (Figure 4.9). It is suggested that when temperature increases T>450°C the hydroxyls desorb from the catalyst surface as water molecules. The following dehydroxylations may occur (the thermodynamic properties at 298.15 K for $Al(OH)_3$ are from [48], $Pd(OH)_2$ are from [44,49], and $Co(OH)_2$ are from[36]:

R5) $2/3Al(OH)_3 \rightarrow 1/3\ Al_2O_3 + H_2O$, $\Delta H^{o}_{273\text{-}573K} = 61$ kJ/mol$_{H2O}$; $\Delta G^{o}_{573K} = -36$ kJ/mol$_{H2O}$

R6) $Co(OH)_2 \rightarrow CoO + H_2O$, $\Delta H^o_{273\text{-}573K} = 55$ kJ/mol$_{H2O}$; $\Delta G^o_{573K} = -33$ kJ/mol$_{H2O}$

R7) $Pd(OH)_2 \rightarrow PdO + H_2O$, $\Delta H^o_{273\text{-}573K} = 30$ kJ/mol$_{H2O}$; $\Delta G^o_{573K} = -25$ kJ/mol$_{H2O}$

It is, thus, not thermodynamically feasible that hydroxyl species from $Pd(OH)_2$ could be accepted by CoO.

A detailed examination of Figure 4.9 actually suggests that CoO_x does not affect the degree of hydroxylation of the Pd surface. Up to 350 ^oC, for both Pd/CoO_x and Pd/Al_2O_3 catalyst the hydroxylated fraction is within the Pd dispersion values (12% and 40%, respectively), the deviations being due to the particle polydispersity. Above that temperature up to 450 ^oC, Pd on alumina is hydroxylated almost completely because of small particle size and overall easy oxidation. Pd on CoO_x is not getting oxidized, as discussed above, so the stoichiometry of $Pd + ½O_2 + H_2O \rightarrow Pd(OH)_2$ reaction cannot be satisfied in the bulk of larger Pd particles. The trends for $Pd(OH)_2$ vs. PdO on both supports are rather similar: the increase in catalytically-relevant PdO fraction occurs starting at 300 ^oC. The reason that we do not see a significant PdO on Al_2O_3 before 300 ^oC is most likely due to hydroxylation of oxidized small Pd particles [35].

This explains the kinetic result obtained earlier for the Pd/Co_3O_4 catalyst for wet methane combustion: the methane combustion activation energy on Pd/Co_3O_4 is 91 kJ/mol, including water adsorption enthalpy, or 61 kJ/mol corrected for water [26]. This latter value is a typical water-corrected activation energy for Pd/Al_2O_3 catalyst [50]. It appears that in the Pd/Co_3O_4 catalyst, it is not Pd performance which is affected by CoO_x (i.e., the kinetic order with respect to water is improved to -0.37 for the Pd/Co_3O_4 catalyst instead of -1 for Co_3O_4)[26], but Pd activates and supplies oxygen to Co-O suprafacial active sites and thus enhances the Co-catalyzed methane combustion performance. As the cobalt oxide surface is more resistant to poisoning by water than PdO, the reaction order with respect to water is affected in a positive way, as Co sites contribute to methane combustion because of Pd feeding activated oxygen to them.

4.4 Conclusions

Co_3O_4 and Pd/Co_3O_4 catalysts were analyzed for Pd and Co speciation during wet lean methane combustion at temperature range of 150 – 450 ^oC by means of *in situ* X-ray absorption spectroscopy. The contributions from metallic Pd, PdO, and $Pd(OH)_2$ and metallic Co, Co(II), and Co(III) oxides were quantified as a function of temperature. The Pd-free sample showed a remarkable stability of its species regardless of temperature and water addition to the feed. In a partially pre-reduced Pd/CoO_x catalyst, cobalt oxide served as an acceptor for the activated oxygen, supplied by surface PdO, while Pd remained largely unoxidized below the surface. The presence of the cobalt oxide did not affect the hydroxylation degree of the exposed Pd surface. We considered bulk thermodynamics of the involved processes, as well as their reported activation energies and kinetic data from a previous study on methane combustion [26]. In combination with the results from the *in situ* XAS experiments, we suggest that the kinetically relevant strong metal-support interactions in the Pd/CoO_x system are due to Pd supplying activated oxygen to Co suprafacial active sites, and not the opposite. In this system, thus, Pd has a double role: as a promoter for Co-catalyzed methane combustion and as an active catalyst itself, which is not affected by the presence of CoO_x.

Acknowledgements

We thank Dr. Danielle Covelli at the University of Saskatchewan's Saskatchewan Structural Sciences Centre (SSSC) for assistance with XPS acquisition. We thank Dr. Ning Chen and Weifeng Chen on the HXMA beamline for assistance with high energy XAS measurements. The XAS work was performed at the Canadian Light Source, which is supported by the Canadian Foundation for Innovation, Natural Sciences and Engineering Research Council of Canada, the University of Saskatchewan, the Government of Saskatchewan, Western Economic Diversification Canada, the National Research Council Canada, and the Canadian Institutes of Health Research. Financial support from Natural Sciences and Engineering Research Council of Canada (NSERC Strategic grant STPGP 478979-15) is appreciated.

4.5 References

1. Z. Li and G. B. Hoflund, React. Kinet. Catal. Lett., 1999, 66, 367–374.

2. T. C. Xiao, S. F. Ji, H. T. Wang, K. S. Coleman and M. L. H. Green, J. Mol. Catal. A Chem., 2001, 175, 111–123.

3. W. Hu, J. Lan, Y. Guo, X. M. Cao and P. Hu, ACS Catal., 2016, 6, 5508–5519.

4. H. A. Doan, M. K. Sharma, W. S. Epling and L. C. Grabow, ChemCatChem, 2017, 9, 1520.

5. J. J. Willis, E. D. Goodman, L. Wu, A. R. Riscoe, P. Martins, C. J. Tassone and M. Cargnello, J. Am. Chem. Soc., 2017, 139, 11989–11997.

6. P. J. Jodłowski, R. J. Jędrzejczyk, D. Chlebda, M. Gierada and J. Łojewska, J. Catal., 2017, 350, 1–12.

7. G. Ercolino, P. Stelmachowski, G. Grzybek, A. Kotarba and S. Specchia, Appl. Catal. B Environ., 2017, 206, 712–725.

8. C. Zhao, Y. Zhao, S. Li and Y. Sun, Cuihua Xuebao/Chinese J. Catal., 2017, 38, 813–820.

9. J. Dou, Y. Tang, L. Nie, C. M. Andolina, X. Zhang, S. House, Y. Li, J. Yang and F. Tao, Catal. Today, 2018, 311, 48–55.

10. A. Choya, B. de Rivas, J. R. González-Velasco, J. I. Gutiérrez-Ortiz and R. López-Fonseca, Appl. Catal. B Environ., 2018, 237, 844–854.

11. D. Zagoraios, A. Athanasiadi, I. Kalaitzidou, S. Ntais, A. Katsaounis, A. Caravaca, P. Vernoux and C. G. Vayenas, Catal. Today, , DOI:10.1016/j.cattod.2019.02.030.

12. G. B. Hoflund and Z. Li, Appl. Surf. Sci., 2006, 253, 2830–2834.

13. L. F. Liotta, G. Di Carlo, G. Pantaleo, G. Deganello, E. M. Borla and M. Pidria, Catal. Commun., 2007, 8, 299–304.

14. L. Hu, Q. Peng and Y. Li, ChemCatChem, 2011, 3, 868–874.

15. F. Wang, L. Zhang, L. Xu, Z. Deng and W. Shi, Fuel, 2017, 203, 419–429.

16. P. J. Jodłowski, R. J. Jedrzejszyk, A. Rogulska, A. Wach, P. Kustrowski, M. Sitarz, T. Lojewski, A. Kolodziej and J. Lojewska, Spectrochim. Acta Part A Mol. Biomol. Spectrosc., 2014, 131, 696–701.

17. P. Stefanov, S. Todorova, A. Naydenov, B. Tzaneva, H. Kolev, G. Atanasova, D. Stoyanova, Y. Karakirova and K. Aleksieva, Chem. Eng. J., 2015, 266, 329–338.

18. A. Setiawan, E. M. Kennedy, B. Z. Dlugogorski, A. A. Adesina and M. Stockenhuber, Catal. Today, 2015, 258, 276–283.

19. G. Ercolino, G. Grzybek, P. Stelmachowski, S. Specchia, A. Kotarba and V. Specchia, Catal. Today, 2015, 257, 66–71.

20. L. Hu, Q. Peng and Y. Li, J. Am. Chem. Soc., 2008, 130, 16136–16137.

21. F. Zasada, W. Piskorz, J. Janas, J. Gryboš, P. Indyka and Z. Sojka, ACS Catal., 2015, 5, 6879–6892.

22. F. Zasada, J. Janas, W. Piskorz, M. Gorczyńska and Z. Sojka, ACS Catal., 2017, 7, 2853–2867.

23. F. Zasada, J. Gryboś, C. Hudy, J. Janas and Z. Sojka, Catal. Today, , DOI:10.1016/j.cattod.2019.03.061.

24. B. Basavalingu, J. A. K. Tareen and G. T. Bhandage, J. Mater. Sci. Lett., 1986, 5, 1227–1229.

25. F. Zasada, W. Piskorz, S. Cristol and A. Kotarba, Langmuir, 2010, 22245–22253.

26. S. Nasr, N. Semagina and R. E. Hayes, Emiss. Control Sci. Technol., 2019, https://doi.org/10.1007/s40825-019-00143-0.

27. W. Huang, E. D. Goodman, P. Losch and M. Cargnello, Ind. Eng. Chem. Res., 2018, 57, 10261–10268.

28. H. Nassiri, K.-E. Lee, Y. Hu, R. E. Hayes, R. W. J. Scott and N. Semagina, ChemPhysChem, 2017, 18, 238–244.

29. J. Shen, R. E. Hayes and N. Semagina, Catal. Today, , DOI:10.1016/j.cattod.2019.12.041.

30. W. Barrett, J. Shen, Y. Hu, R. E. Hayes, R. W. J. Scott and N. Semagina, ChemCatChem, 2020, 12, 944–952.

31. B. Ravel and M. Newville, J. Synchrotron Radiat., 2005, 12, 537–541.

32. B. Tomic-Tucakovic, D. Majstorovic, D. Jelic and S. Mentus, Thermochim. Acta, 2012, 541, 15–24.

33. W. R. Schwartz, D. Ciuparu and L. D. Pfefferle, J. Phys. Chem. C, 2012, 116, 8587–8593.

34. W. R. Schwartz and L. D. Pfefferle, J. Phys. Chem. C, 2012, 116, 8571–8578.

35. H. Nassiri, K.-E. Lee, Y. Hu, R. E. Hayes, R. W. J. Scott and N. Semagina, J. Catal., 2017, 352, 649–656.

36. D. Wagman, W. Evans, V. Parker, R. Schumm, I. Halow, S. Bailey, K. Churney and R. Nuttal, J. Phys. Chem. Ref. Data, 1982, 11, 1–407.

37. G. K. Boreskov and V. S. Muzykantov, Ann. N. Y. Acad. Sci., 1973, 213, 137–170.

38. G. I. Panov, M. V. Parfenov and V. N. Parmon, Catal. Rev. - Sci. Eng., 2015, 57, 436–477.

39. E. A. Gulbransen and K. F. Andrew, J. Electrochem. Soc., 1951, 98, 241.

40. H. Stotz, L. Maier, A. Boubnov, A. T. Gremminger, J. D. Grunwaldt and O. Deutschmann, J. Catal., 2019, 370, 152–175.

41. R. E. Hayes and S. T. Kolaczkowski, Introduction to catalytic combustion, Gordon and

Breach Science Publishers, 1997.

42. H. Xiong, K. Lester, T. Ressler, R. Schlögl, L. F. Allard and A. K. Datye, Catal. Letters, 2017, 147, 1095–1103.

43. E. D. Goodman, A. A. Ye, A. Aitbekova, O. Mueller, A. R. Riscoe, T. Nguyen, A. S. Hoffman, A. Boubnov, K. C. Bustillo, M. Nachtegaal, S. R. Bare and M. Cargnello, J. Chem. Phys., 2019, 151, 154703-1-154703–12.

44. N. N. Smirnova, T. A. Bykova, N. A. Polotnyanko, N. D. Shikina and I. L. Khodakovskii, Russ. J. Phys. Chem. A, 2010, 84, 1851–1855.

45. J. M. Christensen, J. D. Grunwaldt and A. D. Jensen, Appl. Catal. B Environ., 2016, 188, 235–244.

46. V. D. Sokolovskii, Catal. Rev., 1990, 32, 1–49.

47. J. Han, D. Y. Zemlyanov and F. H. Ribeiro, Surf. Sci., 2006, 600, 2752–2761.

48. G. Verdes, R. Gout and S. Castet, Eur. J. Mineral., 2014, 4, 767–792.

49. C. F. Cullis, T. G. Nevell and D. L. Trimm, J. Chem. Soc. Faraday Trans. 1 Phys. Chem. Condens. Phases, 1972, 68, 1406–1412.

50. M. Alyani and K. J. Smith, Ind. Eng. Chem. Res., 2016, 55, 8309–8318.

4.6 Electronic Supplementary Information

Table 4-4-1 Co 2p XPS parameters for the fresh and used Co_3O_4 and Pd/Co_3O_4 catalysts.

Catalyst	Fresh Co_3O_4	Used Co_3O_4	Fresh Pd/Co_3O_4	Used Pd/Co_3O_4
BE of Co^{3+} $2p_{3/2}$, eV	780.7	780.4	780.8	780.6
BE of Co^{3+} $2p_{1/2}$, eV	795.7	795.4	795.8	795.6
DBE of Co^{3+} 2p, eV	15	15	15	15
FWHM of Co^{3+} 2p, eV	2.8	2.9	2.9	3
Area of Co^{3+} $2p_{3/2}$	8368	6673.6	9140.3	7431.2
Area of Co^{3+} $2p_{1/2}$	4184	3336.8	4570.2	3715.6
BE of Co^{2+} $2p_{3/2}$, eV	779.6	779.4	779.7	779.5
BE of Co^{2+} $2p_{1/2}$, eV	794.6	794.4	794.7	794.5
DBE of Co^{2+} 2p, eV	15	15	15	15
FWHM of Co^{2+} 2p, eV	1.1	0.9	1.1	1
Area of Co^{2+} $2p_{3/2}$	2460.3	1472	2477.2	2075.7
Area of Co^{2+} $2p_{1/2}$	1230.2	736	1238.6	1037.9
Residual STD	3.7	3.8	3.5	4.6
Fraction of Co^{3+}, at%	77.2	81.9	78.6	78.1
Fraction of Co^{2+}, at%	22.7	18	21.3	21.8

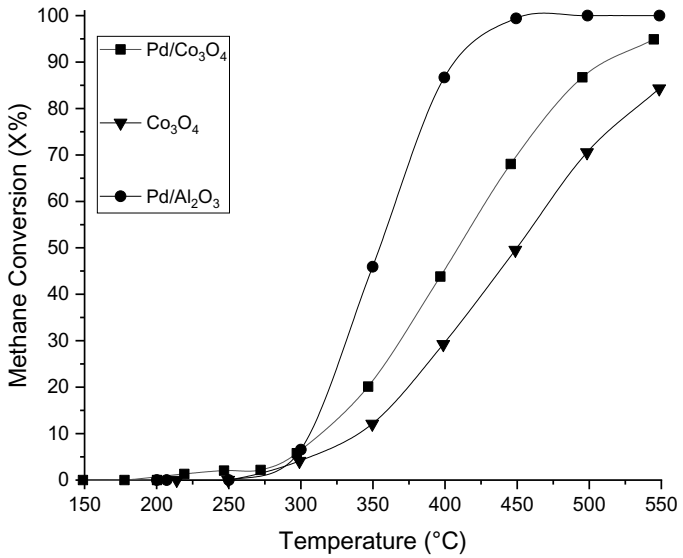

Figure 4.10 Methane combustion activity of the prereduced catalysts (300 ^{o}C, in H_2) in the wet feed. 0.3 g catalyst loading, with 0.3 wt.% Pd in each of Co_3O_4 and Al_2O_3. Pd dispersion is 12% in Pd/Co_3O_4 and 40% in Pd/Al_2O_3.

5 Stable ceria-supported cobalt catalyst for methane combustion[3]

5.1 Introduction

In a search for a Pt-group-metal-free methane combustion catalyst, cobalt oxide-containing materials attract the most interest because of their ability to activate and oxidize methane [1-15]. For stoichiometric engines, CoO_x may increase the operational window of air-to-fuel ratio (lambda) by supplying its lattice oxygen for complete combustion [6]. For CH_4-lean feeds, the oxide is active at relatively low temperatures with the combustion activation energies in the range of 60-80 kJ/mol [1,16]. Moreover, CoO_x is not poisoned by water in the wet feeds to the same extent as the conventional PdO/Al_2O_3, which exhibits negative first order to water in methane combustion [17]. The thermodynamic analysis predicts only partial water coverage of cobalt oxide surface at combustion-relevant temperatures and water content [18].

Our recent kinetic study of Co_3O_4 catalyst in methane-lean combustion in the presence of 5 and 10% water in the feed showed zero-order to water and first order to methane at the used conditions and an activation energy of 69 kJ/mol[16]. However, we observed progressive catalyst deactivation, which manifested itself in the decrease of preexponential factor of the Arrhenius equation (i.e., number of active sites) and a loss of specific surface area. Co_3O_4 crystal size in its fresh state was in the range from 20 to 300 nm.

In view of such promising combustion properties but insufficient amount of active sites and sintering of the pure Co_3O_4 catalyst, in this work, we aimed to address the former two disadvantages by cobalt deposition on a solid support, which is a typical strategy in heterogeneous catalyst preparation for an increased dispersion and stability. We avoided the use of Al_2O_3 because of the possible formation of cobalt aluminate spinel [1] but selected CeO_2 as a

[3] Chapter 5 of the thesis has been submitted to the Canadian Journal of Chemical Engineering as "Remarkable stability of kinetic parameters of Co_3O_4/CeO_2 catalyzed methane combustion" Somaye Nasr, Robert E. Hayes, Natalia Semagina (2020). All the experiments, characterizations, analyses and manuscript draft preparation and writing were conducted by Somaye Nasr under the supervision of Dr. Natalia Semagina and Dr. Robert E. Hayes.

viable support because it is already added in the formulations of exhaust treatment catalysts as an oxygen-storage component. Different supports for Co have been addressed in the literature for a variety of catalytic applications, including CeO_2 [1,19-22]. A recent report from 2020 [2] addresses Co/CeO_2 and Co/Al_2O_3-CeO_2 catalysts performance in wet and dry methane combustion; however, the stability of the Co/CeO_2 catalyst and effect of water concentration were not evaluated. In this contribution, we focus on the effect of water and hydrothermal ageing on alumina-free Co/CeO_2 catalyst while comparing with Co_3O_4-only catalyst and show the stability of kinetic parameters during 100 hours on stream.

5.2 Experimental details

5.2.1 Catalyst synthesis and characterization

Commercial CeO_2 support was impregnated with cobalt precursor via incipient wetness impregnation method. Cerium (IV) oxide (powder, <5 μm, 99.9% metal basis, Sigma Aldrich) was calcined at 500 ºC for 3 h prior to the impregnation. $Co(NO_3)_2{\cdot}6H_2O$ (Aldrich, 99.999%) precursor was dissolved in ethanol (>99.9%, Fisher Scientific). The resulting catalyst was dried overnight at 95 °C in a furnace, followed by calcination in static air at 550 °C for 16 h ("fresh" or "calcined" catalyst).

The cobalt loading of 8.6 wt.% was confirmed by neutron active analysis at Becquerel Laboratories (Maxxam Analytics, Canada). Surface area and porosity analysis were performed using Autosorb SI, Quantachrome USA; the samples were degassed at 300 ºC for 3 prior to analysis. X-ray powder diffraction (XRD) analyses were performed on D/Max-rA diffractometer with a step of 0.06º 2θ. The scanning electron microscopy (SEM) coupled with energy-dispersive X-ray spectroscopy (EDX) mapping was performed using a JEL JEM-ARM200cF microscope.

5.2.2 Catalytic activity measurements

The methane combustion reactions were performed in a packed-bed tubular reactor of 0.95 cm internal diameter equipped with an online gas chromatographic (GC) analysis, as described previously [23]. The reactor was packed with 2 g of catalyst. 8.5 mL_{STP}/min of with 10% CH_4/N_2

(Praxair) were mixed with dry air to achieve 4000 ppmv methane concentration. A peristaltic pump was used for water addition, which is preheated prior to the injection to the reactor. A total gas flow of 206±5 mL_{STP}/min was used, which corresponded to a space velocity of 6,180 $L_{STP}/(kg_{cat} \cdot h)$. Initially, the ignition (IG) and extinction (EX) were performed in the dry and wet (5 vol. % H_2O) feed by heating and cooling between 250 °C to 550 °C at the rate of 50 °C/min, with 50 °C steps held for 33 min for three GC measurements. The procedure was followed by a hydrothermal ageing (HTA) *in situ* for ~68 h in the feed with 4000 ppmv CH_4 and 5 vol. % H_2O by performing one-hour long cycles between 475 °C and 550 °C. After 47-hour ageing cycles, the temperature was held at 475 °C for 21 h. Finally, three sets of ignition and extinction tests were performed, using and 5 vol. % H_2O, 10 vol. % H_2O and dry feed. The support (CeO_2) was tested in a similar condition as the catalyst. The absence of mass and heat transfer limitations was verified as in our previous work [16].

5.3 Results and discussion

5.3.1 Catalyst characterization

X-ray diffraction profiles of the fresh (calcined) and used (after 100 hours on stream, as described in Section 5.2) Co_3O_4/CeO_2 (8.6 wt.% Co) catalysts are near-identical (Figure 5.1) and show no changes in the crystalline structure of the material after hydrothermal ageing. Cobalt oxide is present as Co_3O_4 phase. Scherrer equation was applied to calculate the Co_3O_4 crystal size using the strongest peak at 2θ of 43.096°, with a shape factor of 0.94, which resulted in the particle size of 44 nm. The BET surface area of the calcined catalyst was found to be 2 m^2/g; the N_2 physisorption isotherms are shown in Figure 5.2. They correspond to the Type II isotherm for nonporous supports with minor contributions from mesopores. The Co_3O_4 size of 44 nm may be expected for such high loadings and low-area support. Cobalt distribution on the ceria surface was relatively uniform, as seen from Figure 5.3.

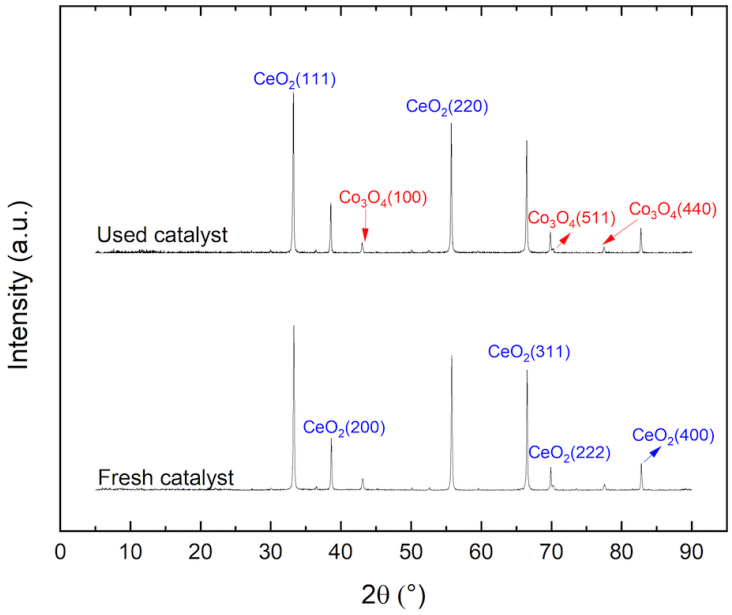

Figure 5.1 XRD profiles of the fresh and used Co_3O_4/CeO_2 (8.6 wt.% Co) catalysts.

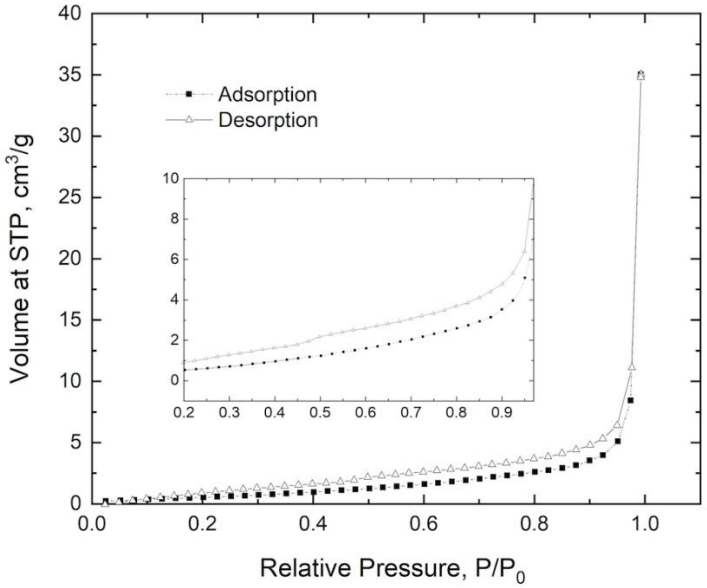

Figure 5.2 N_2 adsorption-desorption isotherms for the fresh (calcined) Co_3O_4/CeO_2 catalyst.

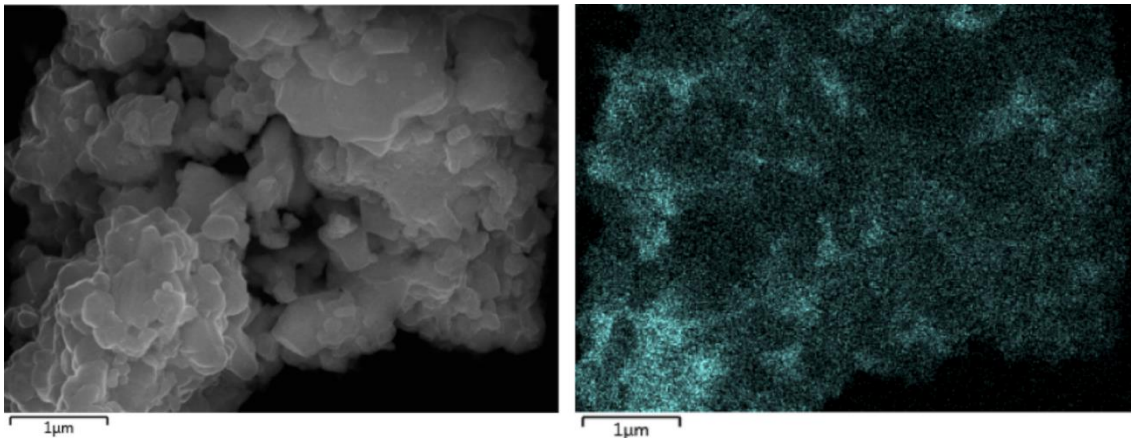

Figure 5.3 Scanning electron micrograph (left) and cobalt distribution (right) for the used Co_3O_4/CeO_2 catalyst.

5.3.2 Catalytic performance

The catalyst was tested in methane combustion overall for over 100 hours on stream in the following order: ignition and extinction were performed for the dry feed, feed with 5 vol.% water, followed by hydrothermal ageing (HTA) for 68 h at 475 °C and 550 °C, as described in Section 5.2.2.The HTA was followed by ignition and extinction experiments with 5%, 10%, and 0% water in the feed. The obtained ignition-extinction curves are shown in Figure 5.4. Except for the first experiment, the catalyst does not show hysteresis between ignition and extinction. 5% water addition to the dry feed decreases conversion, for example, from ~50% to ~30% at 450 °C, as expected for cobalt catalysts. However, further water addition at 10% has a statistically negligible impact on the activity. This finding is in line with our previous report on unsupported Co_3O_4 catalyst [16], as well as with known oxide resistance to water coverage at applicable temperatures and partial water pressure [18].

The remarkable feature, which distinguishes the supported Co_3O_4/CeO_2 catalyst from the unsupported one, is that regardless of the order of experiments within 100 hours on stream, the catalyst demonstrated identical performance at the same conditions, and fully restored its activity to the original level of the first experiment at dry conditions. This indicates a superior catalyst hydrothermal stability and constancy of active sites, as opposed to the bulk Co_3O_4, which

progressively lost the number of active sites as demonstrated by the preexponential factor of the Arrhenius equation [16].

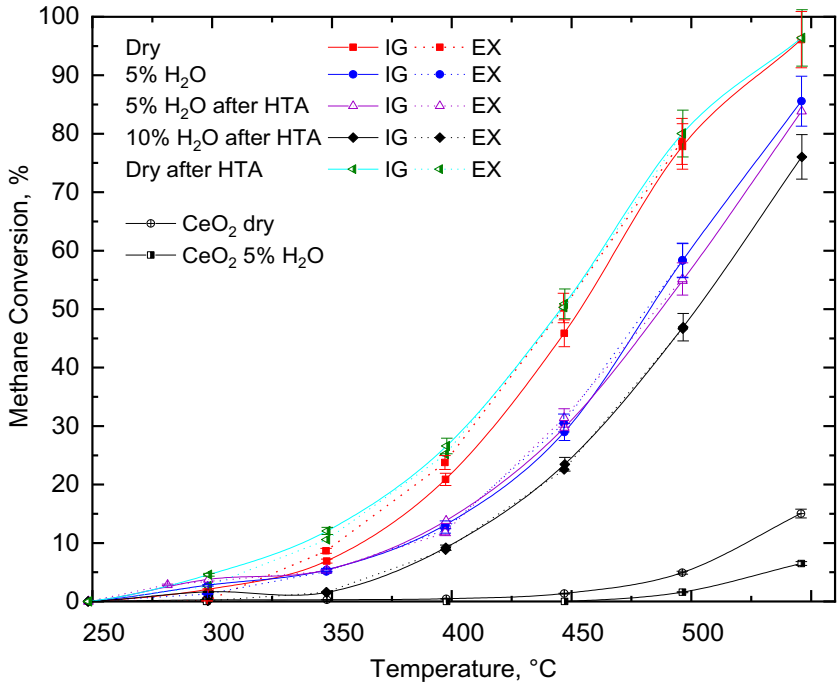

Figure 5.4 Ignition (IG) and extinction (EX) curves on Co_3O_4/CeO_2 catalyst in the dry and wet feeds before and after 68 hours of hydrothermal ageing (HTA) with 5% water.

In Figure 5.5 only two Arrhenius plots are presented but each of them includes several experiments (5 sets of experiments) from Fig. 5.4, such as the "dry" feed plot includes data for the first and the last experiments, while the "wet" feed plot includes three experiments: with 5% water before and after HTA and with 10% water. For the rate constant calculation, we used first order to methane and zero order to water, as found in our previous work for Co_3O_4 catalyst [16]. Only data between 10 and 90% conversion were used. Table 5-1 lists the obtained kinetic parameters. A similar activation energy of 71-74 kJ/mol was reported by other authors as well [1].

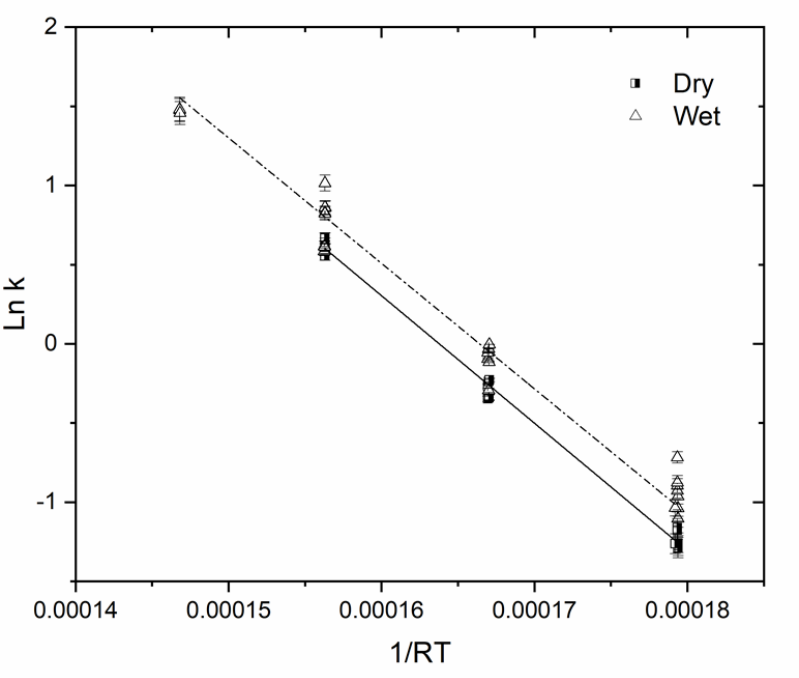

Figure 5.5 Arrhenius plot obtained for combined data at dry and wet conditions.

Table 5-1 Kinetic parameters of the Arrhenius equation for the lumped data at all dry and all wet conditions from Figure 5.4 R^2 is above 0.97.

Conditions	**Activation energy, kJ/mol**	**Pre-exponential factor,**	**Mean rate constant at 700 K**	
		L/(g_{Co3O4}·s)	**L/(kg_{Co3O4}·s)**	**L/(kg_{cat}·s)**
Dry	73.4 ± 1.0	3540 ± 706	11.7	1.4
Wet (5 and 10% water)	75.3 ± 2.4	2323 ± 1133	5.6	0.7
Data for bulk Co_3O_4 at 5 and 10% water [16]	69.3	410	2.8	

The obtained results (Table 5-1) indicate cobalt deposition on ceria indeed increases the number of active sites as expected for a supported vs. bulk catalyst but it does not affect the reaction activation energy. Indeed, with the large size of Co_3O_4 crystals (44 nm), metal-support interactions are unlikely. Water presence did not affect the activation energy but reduced the

number of available sites. As the catalyst displayed the same preexponential factor at dry conditions before and after HTA, water did not lead to the particle sintering but only to the partial blockage of the oxide surface. Between 5 and 10% water in the feed, there was no statistically significant difference between the amount of active sites, indicating that the oxide surface is only partially susceptible to the water coverage and was blocked already by 5% water in the feed with other sites remaining tolerant to the water presence. Overall, the cobalt deposition resulted in approximately twice more efficient cobalt utilization on its mass basis, but the total catalyst activity reduced 4-fold because of 11% loading of Co_3O_4 on CeO_2. However, the deposition resulted in the constancy of active sites and stable catalyst performance.

5.4 Conclusions

Deposition of 8.6 wt.% of cobalt on ceria produced a sintering-resistant methane combustion catalyst for the application in the methane-lean wet feed up to 550 ^oC. Cobalt deposition did not affect the activation energy as compared to the bulk catalyst (69-73 kJ/mol) but expectedly increase the number of active sites. Water addition did not affect the activation energy but only reduced the number of available active sites when water was added to the dry feed as 5 mol%. The effect of further water increase to 10% in the feed was negligible. The catalyst demonstrated the same performance after 100 hours on stream. Ceria role was only to stabilize the Co_3O_4 nanoparticles against sintering. The introduction of cobalt oxide in the exhaust treatment catalysts is also beneficial for N_2O decomposition [22, 24–26] and CO oxidation [6, 21, 27, 28]. The material represents a viable alternative to Pt-group metal catalysts from the viewpoint of the catalyst price, abundance, and water tolerance; however, larger converter size will be required to accommodate the required amounts of the catalyst.

Acknowledgments

The work was supported by the Natural Sciences and Engineering Research Council of Canada (Strategic Project grant STPGP 478979-15). We thank Dr. Shihong Xu (nanoFAB Fabrication & Characterization Center at University of Alberta) for SEM-EDX analyses and Kate Nichols for the XRD analyses.

5.5 References

1. Choya A, de Rivas B, González-Velasco JR, Gutiérrez-Ortiz JI, López-Fonseca R (2018) Oxidation of residual methane from VNG vehicles over Co_3O_4-based catalysts: Comparison among bulk, Al_2O_3-supported and Ce-doped catalysts. Appl Catal B Environ 237:844–854. https://doi.org/10.1016/j.apcatb.2018.06.050

2. Choya A, de Rivas B, González-Velasco JR, Gutiérrez-Ortiz JI, López-Fonseca R (2020) Oxidation of lean methane over cobalt catalysts supported on ceria/alumina. Appl Catal A Gen 591:117381. https://doi.org/10.1016/j.apcata.2019.117381

3. Jodłowski PJ, Jędrzejczyk RJ, Chlebda D, Gierada M, Łojewska J (2017) In situ spectroscopic studies of methane catalytic combustion over Co, Ce, and Pd mixed oxides deposited on a steel surface. J Catal 350:1–12. https://doi.org/10.1016/j.jcat.2017.03.022

4. Zasada F, Janas J, Piskorz W, Gorczyńska M, Sojka Z (2017) Total oxidation of lean methane over cobalt spinel nanocubes controlled by the self-adjusted redox state of the catalyst: experimental and theoretical account for interplay between the Langmuir-Hinshelwood and Mars-van Krevelen mechanisms. ACS Catal 7:2853–2867. https://doi.org/10.1021/acscatal.6b03139

5. Setiawan A, Kennedy EM, Dlugogorski BZ, Adesina AA, Stockenhuber M (2015) The stability of Co_3O_4, Fe_2O_3, Au/Co_3O_4 and Au/Fe_2O_3 catalysts in the catalytic combustion of lean methane mixtures in the presence of water. Catal Today 258:276–283. https://doi.org/10.1016/j.cattod.2014.11.031

6. Shen J, Hayes RE, Semagina N (2019) On the contribution of oxygen from Co_3O_4 to the Pd-catalyzed methane combustion. Catal Today. https://doi.org/10.1016/j.cattod.2019.12.041

7. Todorova S, Naydenov A, Velinova R, Kolev H., Larin AV, Stoyanova D, Shopska M, Tenchev K, Stefanov P (2019) $Pd–MeO_x/Al_2O_3$ (Me = Co, La, Ce) catalysts for methane combustion. React Kinet Mech Catal 126:663–678. https://doi.org/10.1007/s11144-018-1523-9

8. Wang Q, Peng Y, Fu J, Kyzas GZ, Billah SMR, An S (2015) Synthesis, characterization, and catalytic evaluation of Co_3O_4/γ-Al_2O_3 as methane combustion catalysts: Significance of Co species and the redox cycle. Appl Catal B Environ 168–169:42–50. https://doi.org/10.1016/j.apcatb.2014.12.016

9. Huang Q, Li W, Lei Y, Guan S, Zheng X, Pan Y, Wen W, Zhu J, Zhang H, Lin Q (2018) Catalytic performance of novel hierarchical porous flower-like $NiCo_2O_4$ supported Pd in lean methane oxidation. Catal Letters 148:2799–2811. https://doi.org/10.1007/s10562-018-2397-1

10. Zasada F, Gryboś J, Hudy C, Janas J, Sojka Z (2019) Total oxidation of lean methane over cobalt spinel nanocubes—Mechanistic vistas gained from DFT modeling and catalytic isotopic investigations. Catal Today. https://doi.org/10.1016/j.cattod.2019.03.061

11. Dou J, Tang Y, Nie L, Andolina CM, Zhang X, House S, Li Y, Yang J, Tao F (2018) Complete oxidation of methane on Co_3O_4/CeO_2 nanocomposite: a synergetic effect. Catal Today 311:48–55. https://doi.org/10.1016/j.cattod.2017.12.027

12. Liotta LF, Di Carlo G, Pantaleo G, Deganello G, Borla EM, Pidria M (2007) Honeycomb supported Co_3O_4/CeO_2 catalyst for CO/CH_4 emissions abatement: Effect of low Pd-Pt content on the catalytic activity. Catal Commun 8:299–304. https://doi.org/10.1016/j.catcom.2006.06.027

13. Wang F, Zhang L, Xu L, Deng Z, Shi W (2017) Low temperature CO oxidation and CH_4 combustion over Co_3O_4 nanosheets. Fuel 203:419–429. https://doi.org/10.1016/j.fuel.2017.04.140

14. Xiao TC, Ji SF, Wang HT, Coleman KS, Green MLH (2001) Methane combustion over supported cobalt catalysts. J Mol Catal A Chem 175:111–123. https://doi.org/10.1016/S1381-1169(01)00205-9

15. Hu W, Lan J, Guo Y, Cao XM, Hu P (2016) Origin of efficient catalytic combustion of methane over Co_3O_4 (110): Active low-coordination lattice oxygen and cooperation of multiple active Sites. ACS Catal 6:5508–5519. https://doi.org/10.1021/acscatal.6b01080

16. Nasr S, Semagina N, Hayes RE (2019) Kinetic modeling of Co_3O_4 and Pd/Co_3O_4-catalyzed

wet lean methane combustion. Emiss Control Sci Technol https://doi.org/10.1007/s40825-019-00143-0

17. Zhu G, Han J, Zemlyanov DY, Ribeiro FH (2004) The turnover rate for the catalytic combustion of methane over palladium is not sensitive to the structure of the catalyst. J Am Chem Soc 126:9896–9897. https://doi.org/10.1021/ja049406s

18. Zasada F, Piskorz W, Cristol S, Kotarba A (2010) Periodic density functional theory and atomistic thermodynamic studies of cobalt spinel nanocrystals in wet environment : Molecular interpretation of water adsorption. Langmuir 22245–22253

19. Greluk M, Rotko M, Machocki A (2016) Conversion of ethanol over Co/CeO_2 and KCo/CeO_2 catalysts for hydrogen production. Catal Letters 146:163–173. https://doi.org/10.1007/s10562-015-1628-y

20. Guerrero-Caballero J, Kane T, Haidar N, Jalowiecki-Duhamel L, Löfberg A (2019) Ni, Co, Fe supported on ceria and Zr doped ceria as oxygen carriers for chemical looping dry reforming of methane. Catal Today 333:251–258. https://doi.org/10.1016/j.cattod.2018.11.064

21. Gu C, Li Y, Mo Y, Lan J, Jiang Y, Feng S (2020) Rod-like and mushroom-like Co_3O_4–CeO_2 catalysts derived from Ce-1,3,5-benzene tricarboxylic acid for CO preferential oxidation: effects of compositions and morphology. React Kinet Mech Catal 129:135–151. https://doi.org/10.1007/s11144-019-01693-8

22. Jirátová K, Kovanda F, Balabánová J, Kolousˇek D, Klegová A, Pacultová K, Obalová L (2017) Cobalt oxide catalysts supported on CeO_2–TiO_2 for ethanol oxidation and N_2O decomposition. React Kinet Mech Catal 121:121–139. https://doi.org/10.1007/s11144-017-1142-x

23. Nassiri H, Lee K-E, Hu Y, Hayes RE, Scott RWJ, Semagina N (2017) Water shifts PdO-catalyzed lean methane combustion to Pt-catalyzed rich combustion in Pd–Pt catalysts: In situ X-ray absorption spectroscopy. J Catal 352:649–656. https://doi.org/10.1016/j.jcat.2017.06.008

24. Li Y, Wang X (2019) MgO modifying Al_2O_3 to load cobalt oxide for catalytic N_2O

decomposition. Catal Letters 149:1856–1863. https://doi.org/10.1007/s10562-019-02789-5

25. Xu J, Lu G, Guo Y, Guo Y, Gong XQ (2017) A highly effective catalyst of Co-CeO_2 for the oxidation of diesel soot: The excellent NO oxidation activity and NO_x storage capacity. Appl Catal A Gen 535:1–8. https://doi.org/10.1016/j.apcata.2017.02.005

26. Pietrogiacomi D, Campa MC, Ardemani L, Occhiuzzi M (2019) Operando FTIR study of Fe-MOR, Co-MOR, and Ni-MOR as catalysts for simultaneous abatement of NO_x and N_2O with CH_4 in the presence of O_2. An insight on reaction pathway. Catal Today 336:131–138. https://doi.org/10.1016/j.cattod.2018.12.053

27. Woods MP, Gawade P, Tan B, Ozkan US (2010) Preferential oxidation of carbon monoxide on Co/CeO_2 nanoparticles. Appl Catal B Environ 97:28–35. https://doi.org/10.1016/j.apcatb.2010.03.015

28. Todorova S, Blin JL, Naydenov A, Lebeau B, Kolev H, Gaudin P, Dotzeva A, Velinova R, Filkova D, Ivanova I, Vidal L, Michelin L, Josien L, Tenchev K (2019) Co_3O_4 -MnO_x oxides supported on SBA-15 for CO and VOCs oxidation. Catal Today 10.1016/j.cattod.2019.05.018. https://doi.org/10.1016/j.cattod.2019.05.018

6 Conclusions and future work

6.1 Conclusions

Due to high cost of noble metals there is a growing demand to design a catalyst which has lower amount of platinum-group metal (PGM) in its formulation. This thesis focused on using non-PGM transition metals as a promoter and as a support for Pd catalysts used for lean methane combustion reaction under wet condition. Cobalt was chosen because of its lowest oxygen bonding energy and its relatively high activity in oxygen and methane activation among 3d elements. The first step was to investigate the kinetics of the reaction over Pd/Co_3O_4 catalyst and on bare Co_3O_4. Additionally, the hydrothermal ageing behaviour of the catalysts was also assessed. The experiments were performed with both dry and wet feed (5 and 10 vol. %) in the temperature range between 250-550°C. The Pd/Co_3O_4 catalyst showed first order reaction kinetics to methane and negative 0.37 order to H_2O. The results showed a significant contribution of cobalt oxide to the activity of the bimetallic catalyst. The bare Co_3O_4 catalyst exhibited first order reaction kinetics to methane and zero order to water. It is concluded that the Pd/Co_3O_4 catalyst behavior is impacted by strong metal-support interactions (SMSI) but not a summation of the individual activities of cobalt oxide and palladium.

To further understand the specifics of SMSI in Pd/Co_3O_4, the next step was to investigate the Pd and Co speciation in cobalt oxide and Pd/CoO_x catalysts during lean methane combustion in wet feed at temperatures between 150-450 ^oC. To achieve this objective, *in situ* X-ray absorption spectroscopy (XAS) were performed for the reactions over Co_3O_4 and Pd/Co_3O_4. The aim of this analysis was to obtain the distribution of Pd and Co species, including their hydroxides, as a function of reaction temperature. It appears that Pd activates and supplies oxygen to Co-O suprafacial active sites, thus enhancing the Co-catalyzed methane combustion performance. As the cobalt oxide surface is more resistant to poisoning by water than PdO, the reaction order with respect to water is affected positively, as Co sites contribute to methane combustion because of Pd feeding activated oxygen to them. The contributions from metallic Pd, PdO, and $Pd(OH)_2$ and metallic Co, Co(II), and Co(III) oxides were quantified as a function of temperature. The Pd-free sample showed a remarkable stability of its species regardless of temperature and water addition

to the feed. As mentioned, the kinetically relevant strong metal-support interactions in the Pd/CoO_x system are due to Pd supplying activated oxygen to Co suprafacial active sites, and not the opposite. Consequently, Pd has a double role: as a promoter for Co-catalyzed methane combustion and as an active catalyst itself, which is not affected by the presence of CoO_x.

After clarification on the Pd and Co speciation in cobalt oxide and Pd/CoO_x catalysts during lean methane combustion, the next goal was to design a practical catalyst that is relatively cheap while exhibiting high activity under wet condition. To do so it was hypothesized that by using ceria oxide in the cobalt oxide system would enhance the low dispersion of cobalt, hence improving the catalyst activity. Ceria was chosen since it is well known for its high oxygen storage capacity and is used in converter formulations. The reaction kinetics of lean methane combustion was studied under wet and dry conditions. The results revealed that metal-support interactions are unlikely due to the relatively large Co_3O_4 particle size (44 nm). Hydrothermal ageing (100 h on stream) of the catalyst did not impact its performance, indicating that ceria's role was to stabilize the Co_3O_4 nanoparticles against sintering. Water presence did not affect the activation energy but did reduce the number of available sites. Since the catalyst displayed the same pre-exponential factor at dry conditions before and after HTA, water did not lead to the particle sintering but only to the partial blockage of the oxide surface. Overall, the cobalt deposition caused approximately doubled the efficiency of cobalt utilization on a mass basis, but the total catalyst activity reduced 4-fold because of the 11% loading of Co_3O_4 on CeO_2. Nonetheless, the deposition did not impact the number of active sites and stability of the catalyst performance.

6.2 Future work

- Optimizing the Pd: Co metal ratio in the catalyst which has governing impact on the catalyst activity and therefore, the catalyst price.
- Reducing the particle size of the cobalt oxide in Co_3O_4/CeO_2 formulations by developing a different synthesis method to enhance the catalyst activity.
- Prepare lower cobalt loading Co_3O_4/CeO_2 catalyst.
- Prepare washcoat material and test the proposed optimal catalyst in a real feed.

7 Bibliography

Abbasi, R., Wu, L., Wanke, S. E., & Hayes, R. E. (2012). Kinetics of methane combustion over Pt and Pt-Pd catalysts. *Chemical Engineering Research and Design*, *90*(11), 1930–1942. https://doi.org/10.1016/j.cherd.2012.03.003

Alyani, M., & Smith, K. J. (2016). Kinetic Analysis of the Inhibition of CH_4 Oxidation by H_2O on PdO/Al_2O_3 and $CeO_2/PdO/Al_2O_3$ Catalysts. *Industrial and Engineering Chemistry Research*, *55*(30), 8309–8318. https://doi.org/10.1021/acs.iecr.6b01881

Arai, H., & Machida, M. (1991). Recent progress in high-temperature catalytic combustion. *Catalysis Today*, *10*(1), 81–94. https://doi.org/10.1016/0920-5861(91)80076-L

Au-Yeung, J., Chen, K., Bell, A. T., & Iglesia, E. (1999). Isotopic studies of methane oxidation pathways on PdO catalysts. *Journal of Catalysis*, *188*(1), 132–139. https://doi.org/10.1006/jcat.1999.2643

Bahlawane, N.: Kinetics of methane combustion over CVD-made cobalt oxide catalysts. Appl. Catal. B Environ. 67, 168–176 (2006). doi:10.1016/j.apcatb.2006.03.024

Barrett, W., Shen, J., Hu, Y., Hayes, R. E., Scott, R. W. J., & Semagina, N. (2020). Understanding the Role of SnO_2 Support in Water-Tolerant Methane Combustion: In situ Observation of $Pd(OH)_2$ and Comparison with Pd/Al_2O_3. *ChemCatChem*, *12*, 944–952. https://doi.org/10.1002/cctc.201901744

Basavalingu, B., Tareen, J. A. K., & Bhandage, G. T. (1986). Thermodynamic properties of $Co(OH)_2$ from hydrothermal equilibria in cobalt oxide systems. *Journal of Materials Science Letters*, *5*(12), 1227–1229. https://doi.org/10.1007/bf01729373

Boreskov, G. K., & Muzykantov, V. S. (1973). Investigation of Oxide-Type Oxidation Catalysts By Reactions of Oxygen Isotopic Exchange. *Annals of the New York Academy of Sciences*, *213*(1), 137–170. https://doi.org/10.1111/j.1749-6632.1973.tb51065.x

Burch, R. Low NO_x options in catalytic combustion and emission control, 35 Catalysis Today §

(1997). Elsevier. https://doi.org/10.1016/S0920-5861(96)00131-9

Burch, R., Crittle, D. J., & Hayes, M. J. (1999). C-H bond activation in hydrocarbon oxidation on heterogeneous catalysts. *Catalysis Today*, *47*(1–4), 229–234. https://doi.org/10.1016/S0920-5861(98)00303-4

Bychkov, V.Y., Tulenin, Y.P., Slinko, M.M., Khudorozhkov, A.K., Bukhtiyarov, V.I., Sokolov, S., Korchak, V.N.: Self-oscillations during methane oxidation over Pd/Al_2O_3: Variations of Pd oxidation state and their effect on Pd catalytic activity. Appl. Catal. A Gen. 522, 40–44 (2016). doi:10.1016/J.APCATA.2016.04.024

Cargnello, M., Delgado Jan, J.J., Hernndez Garrido, J.C., Bakhmutsky, K., Montini, T., Calvino Gmez, J.J., Gorte, R.J., Fornasiero, P.: Exceptional activity for methane combustion over modular Pd@CeO_2 subunits on functionalized Al_2O_3. Science (80-.). 337, 713–717 (2012). doi:10.1126/science.1222887

Chen, J., Arandiyan, H., Gao, X., & Li, J. (2015). Recent Advances in Catalysts for Methane Combustion. *Catalysis Surveys from Asia*, *19*(3), 140–171. https://doi.org/10.1007/s10563-015-9191-5

Chin, Y.-H., Buda, C., Neurock, M., Iglesia, E.: Consequences of metal-oxide interconversion for C-H bond activation during CH_4 reactions on Pd catalysts. J. Am. Chem. Soc. 135, 15425–15442 (2013). doi:10.1021/ja405004m

Chlebda, D., Gierada, M., Łojewska, J., Jędrzejczyk, R. J., & Jodłowski, P. J. (2017). In situ spectroscopic studies of methane catalytic combustion over Co, Ce, and Pd mixed oxides deposited on a steel surface. *Journal of Catalysis*, *350*, 1–12. https://doi.org/10.1016/j.jcat.2017.03.022

Choya, Andoni, de Rivas, B., González-Velasco, J. R., Gutiérrez-Ortiz, J. I., & López-Fonseca, R. (2018). Oxidation of residual methane from VNG vehicles over Co_3O_4-based catalysts: Comparison among bulk, Al_2O_3-supported and Ce-doped catalysts. *Applied Catalysis B: Environmental*, *237*, 844–854. https://doi.org/10.1016/J.APCATB.2018.06.050

Choya, Andoni, de Rivas, B., González-Velasco, J. R., Gutiérrez-Ortiz, J. I., & López-Fonseca, R. (2020). Oxidation of lean methane over cobalt catalysts supported on ceria/alumina. *Applied Catalysis A: General*, *591*(December 2019), 117381. https://doi.org/10.1016/j.apcata.2019.117381

Christensen, J. M., Grunwaldt, J. D., & Jensen, A. D. (2016). Importance of the oxygen bond strength for catalytic activity in soot oxidation. *Applied Catalysis B: Environmental*, *188*, 235–244. https://doi.org/10.1016/j.apcatb.2016.01.068

Ciuparu, D, Altman, E., & Pfefferle, L. (2001). Contributions of lattice oxygen in methane combustion over PdO-based catalysts. *Journal of Catalysis*, *203*(1), 64–74. https://doi.org/10.1006/jcat.2001.3331

Ciuparu, D, Bozon-Verduraz, F., & Pfefferle, L. (2002). Oxygen exchange between palladium and oxide supports in combustion catalysts. *Journal of Physical Chemistry B*, *106*(13), 3434–3442. https://doi.org/10.1021/jp013577r

Ciuparu, D, Lyubovsky, M. R., Altman, E., Pfefferle, L. D., & Datye, A. (2002). Catalytic combustion of methane over palladium-based catalysts. *Catalysis Reviews - Science and Engineering*, *44*(4), 593–649. https://doi.org/10.1081/CR-120015482

Ciuparu, D, Perkins, E., & Pfefferle, L. (2004). In situ DR-FTIR investigation of surface hydroxyls on γ-Al_2O_3 supported PdO catalysts during methane combustion. *Applied Catalysis A: General*, *263*(2), 145–153. https://doi.org/10.1016/j.apcata.2003.12.006

Colussi, S., Trovarelli, A., Vesselli, E., Baraldi, A., Comelli, G., Groppi, G., Llorca, J.: Structure and morphology of Pd/Al_2O_3 and Pd/CeO_2/Al_2O_3 combustion catalysts in Pd-PdO transformation hysteresis. Appl. Catal. A Gen. 390, 1–10 (2010). doi:10.1016/j.apcata.2010.09.033

Cullis, C. F., Nevell, T. G., & Trimm, D. L. (1972). Role of the catalyst support in the oxidation of methane over palladium. *Journal of the Chemical Society, Faraday Transactions 1: Physical Chemistry in Condensed Phases*, *68*(0), 1406–1412. https://doi.org/10.1039/F19726801406

Doan, H. A., Sharma, M. K., Epling, W. S., & Grabow, L. C. (2017). From Active-Site Models

to Real Catalysts: Importance of the Material Gap in the Design of Pd Catalysts for Methane Oxidation. *ChemCatChem*, *9*(9), 1520. https://doi.org/10.1002/cctc.201700660

Dou, J., Tang, Y., Nie, L., Andolina, C. M., Zhang, X., House, S., … Tao, F. (2018). Complete oxidation of methane on Co_3O_4/CeO_2 nanocomposite: a synergetic effect. *Catalysis Today*, *311*, 48–55. https://doi.org/10.1016/j.cattod.2017.12.027

Ercolino, G., Grzybek, G., Stelmachowski, P., Specchia, S., Kotarba, A., & Specchia, V. (2015). Pd/Co_3O_4-based catalysts prepared by solution combustion synthesis for residual methane oxidation in lean conditions. *Catalysis Today*, *257*(P1), 66–71. https://doi.org/10.1016/j.cattod.2015.03.006

Ercolino, G., Stelmachowski, P., Grzybek, G., Kotarba, A., & Specchia, S. (2017). Optimization of Pd catalysts supported on Co_3O_4 for low-temperature lean combustion of residual methane. *Applied Catalysis B: Environmental*, *206*, 712–725

Ercolino, G., Karimi, S., Stelmachowski, P., Specchia, S.: Catalytic combustion of residual methane on alumina monoliths and open cell foams coated with Pd/Co_3O_4, (2017)

Escandón, L. S., Niño, D., Díaz, E., Ordóñez, S., & Díez, F. V. (2008). Effect of hydrothermal ageing on the performance of Ce-promoted PdO/ZrO_2 for methane combustion. *Catalysis Communications*, *9*(13), 2291–2296. https://doi.org/10.1016/j.catcom.2008.05.026

Farrauto, R.J., Lampert, J.K., Hobson, M.C., Waterman, E.M.: Thermal decomposition and reformation of PdO catalysts; support effects. Appl. Catal. B, Environ. 6, 263–270 (1995). doi:10.1016/0926-3373(95)00015-1

Forzatti, P., & Lietti, L. (1999). Catalyst deactivation. *Catalysis Today*, *52*(2–3), 165–181. https://doi.org/10.1016/S0920-5861(99)00074-7

Fuller, Edward N, Paul D Schettler, and J Calvin. Giddings. 1966. New Method for Prediction of Binary Gas-Phase Diffusion Coefficients. *Industrial & Engineering Chemistry* 58 (5): 18–27. https://doi.org/10.1021/ie50677a007

Fujimoto, K., Ribeiro, F. H., Avalos-Borja, M., & Iglesia, E. (1998). Structure and Reactivity of PdO_x/ZrO_2Catalysts for Methane Oxidation at Low Temperatures. *Journal of Catalysis*, *179*(2), 431–442. https://doi.org/https://doi.org/10.1006/jcat.1998.2178

Fujimoto, K.-I., Ribeiro, F.H., Bell, A.T., Iglesia, E.: Reaction pathways and structural requirements in the catalytic oxidation of methane at low temperatures. In: ACS Division of Petroleum Chemistry, Inc. Preprints. pp. 110–113 (1996)

Garbowski, E., Feumi-Jantou, C., Mouaddib, N., Primet, M.: Catalytic combustion of methane over palladium supported on alumina catalysts: Evidence for reconstruction of particles. Appl. Catal. A, Gen. 109, 277–291 (1994). doi:10.1016/0926-860X(94)80124-X

Gélin, P., Primet, M.: Complete oxidation of methane at low temperature over noble metal based catalysts: a review, (2002)

Gélin, P., Urfels, L., Primet, M., Tena, E.: Complete oxidation of methane at low temperature over Pt and Pd catalysts for the abatement of lean-burn natural gas fuelled vehicles emissions: influence of water and sulphur containing compounds. Catal. Today. 83, 45–57 (2003). doi:10.1016/S0920-5861(03)00215-3

Gholami, R., Alyani, M., & Smith, K. J. (2015). Deactivation of Pd catalysts by water during low temperature methane oxidation relevant to natural gas vehicle converters. *Catalysts*, *5*(2), 561–594. https://doi.org/10.3390/catal5020561

Gierman, H. (1988). Design of laboratory hydrotreating reactors: Scaling Down of Trickle-flow Reactors. *Applied Catalysis*, *43*(2), 277–286. https://doi.org/https://doi.org/10.1016/S0166-9834(00)82732-3

Goodman, E. D., Ye, A. A., Aitbekova, A., Mueller, O., Riscoe, A. R., Nguyen, T., … Cargnello, M. (2019). Palladium oxidation leads to methane combustion activity : Effects of particle size and alloying with platinum. *Journal of Chemical Physics*, *151*, 154703-1-154703–154712. https://doi.org/10.1063/1.5126219

Greluk, M., Rotko, M., & Machocki, A. (2016). Conversion of Ethanol over Co/CeO_2 and

KCo/CeO_2 Catalysts for Hydrogen Production. *Catalysis Letters*, *146*(1), 163–173. https://doi.org/10.1007/s10562-015-1628-y

Groppi, G., Cristiani, C., Lietti, L., Forzatti, P.: Study of PdO/Pd transformation over alumina supported catalysts for natural gas combustion. Stud. Surf. Sci. Catal. 130, 3801–3806 (2000). doi:10.1016/S0167-2991(00)80615-1

Gu, C., Li, Y., Mo, Y., Lan, J., Jiang, Y., & Feng, S. (2020). Rod-like and mushroom-like Co_3O_4–CeO_2 catalysts derived from Ce-1,3,5-benzene tricarboxylic acid for CO preferential oxidation: effects of compositions and morphology. *Reaction Kinetics, Mechanisms and Catalysis*, *129*(1), 135–151. https://doi.org/10.1007/s11144-019-01693-8

Guerrero-Caballero, J., Kane, T., Haidar, N., Jalowiecki-Duhamel, L., & Löfberg, A. (2019). Ni, Co, Fe supported on Ceria and Zr doped Ceria as oxygen carriers for chemical looping dry reforming of methane. *Catalysis Today*, *333*(September), 251–258. https://doi.org/10.1016/j.cattod.2018.11.064

Gulbransen, E. A., & Andrew, K. F. (1951). The Kinetics of the Oxidation of Cobalt. *Journal of The Electrochemical Society*, *98*(6), 241. https://doi.org/10.1149/1.2778139

H.S. Fogler. (2005). Elements of chemical reaction engineering, 4th Ed., Prentice Hall.

Han, J., Zemlyanov, D. Y., & Ribeiro, F. H. (2006). Interaction of O_2 with Pd single crystals in the range 1-150 Torr: Oxygen dissolution and reaction. *Surface Science*, *600*(13), 2752–2761. https://doi.org/10.1016/j.susc.2006.04.042

Hayes, R., Mmbaga, J. (2013). Introduction to Chemical Reactor Analysis, 2nd Ed., Boca Raton.

Hayes, R. E., & Kolaczkowski, S. T. (1997). *Introduction to catalytic combustion*. Australia: Gordon and Breach.

Hoflund, G. B., & Li, Z. (2006). Surface characterization study of a Pd/Co_3O_4 methane oxidation catalyst. *Applied Surface Science*, *253*(5), 2830–2834. https://doi.org/10.1016/j.apsusc.2006.05.115

Hu, L, Peng, Q., & Li, Y. (2011). Low-temperature CH_4 Catalytic Combustion over Pd Catalyst Supported on Co_3O_4 Nanocrystals with Well-Defined Crystal Planes. *ChemCatChem*, *3*(5), 868–874. https://doi.org/10.1002/cctc.201000407

Hu, Linhua, Peng, Q., & Li, Y. (2008). Selective Synthesis of Co_3O_4 Nanocrystal with Different Shape and Crystal. *Journal of the American Chemical Society*, *130*(48), 16136–16137. https://doi.org/10.1021/ja806400e

Hu, Linhua, Peng, Q., & Li, Y. (2011). Low-temperature CH_4 Catalytic Combustion over Pd Catalyst Supported on Co_3O_4 Nanocrystals with Well-Defined Crystal Planes. *ChemCatChem*, *3*(5), 868–874. https://doi.org/10.1002/cctc.201000407

Hu, W., Lan, J., Guo, Y., Cao, X. M., & Hu, P. (2016). Origin of Efficient Catalytic Combustion of Methane over Co_3O_4 (110): Active Low-Coordination Lattice Oxygen and Cooperation of Multiple Active Sites. *ACS Catalysis*, *6*(8), 5508–5519. https://doi.org/10.1021/acscatal.6b01080

Huang, Q., Li, W., Lin, Q., Zheng, X., Pan, H., Pi, D., … Zhang, H. (2018). Catalytic performance of Pd–$NiCo_2O_4/SiO_2$ in lean methane combustion at low temperature. *Journal of the Energy Institute*, *91*(5), 733–742. https://doi.org/https://doi.org/10.1016/j.joei.2017.05.008

Huang, W., Goodman, E. D., Losch, P., & Cargnello, M. (2018). Deconvoluting Transient Water Effects on the Activity of Pd Methane Combustion Catalysts. *Industrial and Engineering Chemistry Research*, *57*(31), 10261–10268. research-article. https://doi.org/10.1021/acs.iecr.8b01915

Huang, F., Chen, J., Hu, W., Li, G., Wu, Y., Yuan, S., Zhong, L., Chen, Y.: Pd or PdO: Catalytic active site of methane oxidation operated close to stoichiometric air-to-fuel for natural gas vehicles. Appl. Catal. B Environ. 219, 73–81 (2017). doi:10.1016/j.apcatb.2017.07.037

Impacts des normes antipollution sur la demande mondiale en platinoïdes : cas du platine, du palladium et du rhodium | Minéralinfo. (n.d.). Retrieved February 28, 2020, from http://www.mineralinfo.fr/ecomine/impacts-normes-antipollution-demande-mondiale-en-platinoides-cas-platine-palladium-rhodium

Irandoust, S., Andersson, B.: Monolithic Catalysts for Nonautomobile Applications. Catal. Rev. 30, 341–392 (1988). doi:10.1080/01614948808080809

Jirátová, K., Kovanda, F., Balabánová, J., Koloušek, D., Klegová, A., Pacultová, K., & Obalová, L. (2017). Cobalt oxide catalysts supported on CeO_2–TiO_2 for ethanol oxidation and N_2O decomposition. *Reaction Kinetics, Mechanisms and Catalysis*, *121*(1), 121–139. https://doi.org/10.1007/s11144-017-1142-x

Jodłowski, P. J., Jędrzejczyk, R. J., Rogulska, A., Wach, A., Kuśtrowski, P., Sitarz, M., … Łojewska, J. (2014). Spectroscopic characterization of Co_3O_4 catalyst doped with CeO_2 and PdO for methane catalytic combustion. *Spectrochimica Acta Part A: Molecular and Biomolecular Spectroscopy*. https://doi.org///doi.org/10.1016/j.saa.2014.05.027

Kubaschewski, O., & Alcock, C. B. (1979). *Metallurgical thermochemistry*. Oxford ; New York : Pergamon Press, c1979; 5th ed., rev. and enl.

Le Page, J. F. (1987). Applied heterogeneous catalysis: design, manufacture, use of solid ctalysts. Paris: Technip

Li, Y., & Wang, X. (2019). MgO Modifying Al_2O_3 to Load Cobalt Oxide for Catalytic N_2O Decomposition. *Catalysis Letters*, *149*(7), 1856–1863. https://doi.org/10.1007/s10562-019-02789-5

Li, Z., & Hoflund, G. B. (1999). Catalytic oxidation of methane over Pd/Co_3O_4. *Reaction Kinetics and Catalysis Letters*, *66*(2), 367–374

Lichtenberg, F., & Kleinsorgen, K. (1996). Stability enhancement of the CoOOH conductive network of nickel hydroxide electrodes. *Journal of Power Sources*, *62*(2), 207–211. https://doi.org/10.1016/S0378-7753(96)02431-7

Lin, H.-K., Chiu, H.-C., Tsai, H.-C., Chien, S.-H., & Wang, C.-B. (2003). Synthesis, characterization and catalytic oxidation of carbon monoxide overcobalt oxide. *Catalysis Letters*, *88*(3–4), 169–174. https://doi.org/1024013822986

Lin, J., Chen, Y., Liu, X., Chen, X., Zheng, Y., Huang, F., … Jiang, L. (2020). Microstructural property regulation and performance in methane combustion reaction of ordered mesoporous alumina supported palladium-cobalt bimetallic catalysts. *Applied Catalysis B: Environmental*, *263*. https://doi.org/10.1016/j.apcatb.2019.118269

Liotta, L. F., Di Carlo, G., Pantaleo, G., Deganello, G., Borla, E. M., & Pidria, M. (2007). Honeycomb supported Co_3O_4/CeO_2 catalyst for CO/CH_4 emissions abatement: Effect of low Pd–Pt content on the catalytic activity. *Catalysis Communications*, *8*(3), 299–304. https://doi.org/10.1016/j.catcom.2006.06.027

Long, E., Zhang, X., Li, Y., Liu, Z., Wang, Y., Gong, M., & Chen, Y. (2010). Effect of cobalt oxide on performance of Pd catalysts for lean-burn natural gas vehicles in the presence and absence of water vapor. *Journal of Natural Gas Chemistry*, *19*(2), 134–138. https://doi.org/10.1016/S1003-9953(09)60044-X

Liu, B., Checkel, M.D., Hayes, R.E.: Experimental study of a reverse flow catalytic converter for a dual fuel engine. Can. J. Chem. Eng. 79, 491–506 (2001). doi:10.1002/cjce.5450790405

Machin, N.E., Karakaya, C., Celepci, A.: Catalytic combustion of methane on La-, Ce-, and Co-based mixed oxides. Energy and Fuels. 22, 2166–2171 (2008). doi:10.1021/ef8000983

Makhlouf, S. A. (2002). Magnetic properties of Co_3O_4 nanoparticles. *Journal of Magnetism and Magnetic Materials*, *246*(1–2), 184–190. https://doi.org/10.1016/S0304-8853(02)00050-1

Mears, D E. 1971. Tests for Transport Limitations in Experimental Catalytic Reactors. *Industrial & Engineering Chemistry Process Design and Development* 10 (4): 541–47. https://doi.org/10.1021/i260040a020

Müller, C.A., Maciejewski, M., Koeppel, R.A., Baiker, A.: Combustion of methane over palladium/zirconia derived from a glassy Pd-Zr alloy: Effect of Pd particle size on catalytic behavior. J. Catal. 166, 36–43 (1997). doi:10.1006/jcat.1997.1501.

Müller, C.A., Maciejewski, M., Koeppel, R.A., Baiker, A.: Combustion of methane over palladium/zirconia: Effect of Pd-particle size and role of lattice oxygen. Catal. Today. 47, 245–

252 (1999). doi:10.1016/S0920-5861(98)00305-8

N. Frössling.(1938),Uber die Verdunstung fallender Tropfen. *Gerlands, Beitr.Geophys.,* 52, 170-178

Nasr, S., Semagina, N., & Hayes, R. E. (2019). Kinetic Modeling of Co_3O_4 and Pd/Co_3O_4-Catalyzed Wet Lean Methane Combustion. *Emission Control Science and Technology*, https://doi.org/10.1007/s40825-019-00143-0. https://doi.org/10.1007/s40825-019-00143-0

Nassiri, H., Lee, K.-E., Hu, Y., Hayes, R. E., Scott, R. W. J., & Semagina, N. (2017a). Platinum Inhibits Low-Temperature Dry Lean Methane Combustion through Palladium Reduction in Pd-Pt/Al_2O_3: An In Situ X-ray Absorption Study. *ChemPhysChem*, *18*(2), 238–244. https://doi.org/10.1002/cphc.201600993

Nassiri, H., Lee, K.-E., Hu, Y., Hayes, R. E., Scott, R. W. J., & Semagina, N. (2017b). Water shifts PdO-catalyzed lean methane combustion to Pt-catalyzed rich combustion in PdPt catalysts: In situ X-ray absorption spectroscopy. *Journal of Catalysis*, *352*, 649–656. https://doi.org/10.1016/j.jcat.2017.06.008

Panov, G. I., Parfenov, M. V., & Parmon, V. N. (2015). The Brønsted-Evans-Polanyi Correlations in Oxidation Catalysis. *Catalysis Reviews - Science and Engineering*, *57*(4), 436–477. https://doi.org/10.1080/01614940.2015.1074487

Patterson, A. L. (1939). The Scherrer Formula for X-Ray Particle Size Determination. *Physical Review*, *56*(10), 978–982. https://doi.org/10.1103/PhysRev.56.978

Pérez-Ramírez, J, R J Berger, G Mul, F Kapteijn, and J A Moulijn. 2000. “Six-Flow Reactor Technology a Review on Fast Catalyst Screening and Kinetic Studies.” *Catalysis Today* 60 (1): 93–109. https://doi.org/10.1016/S0920-5861(00)00321-7

Persson, K., Pfefferle, L. D., Schwartz, W., Ersson, A., & Jrs, S. G. (2007). Stability of palladium-based catalysts during catalytic combustion of methane: The influence of water. *Applied Catalysis B: Environmental*, *74*(3–4), 242–250. https://doi.org/10.1016/j.apcatb.2007.02.015

Pietrogiacomi, D., Campa, M. C., Ardemani, L., & Occhiuzzi, M. (2019). Operando FTIR study of Fe-MOR, Co-MOR, and Ni-MOR as catalysts for simultaneous abatement of NO_x and N_2O with CH_4 in the presence of O_2. An insight on reaction pathway. *Catalysis Today*, *336*(September 2018), 131–138. https://doi.org/10.1016/j.cattod.2018.12.053

Piskorz, W., Gryboś, J., Sojka, Z., Indyka, P., Zasada, F., & Janas, J. (2015). Reactive Oxygen Species on the (100) Facet of Cobalt Spinel Nanocatalyst and their Relevance in $^{16}O_2$ /$^{18}O_2$ Isotopic Exchange, de N_2O, and de CH_4 Processes—A Theoretical and Experimental Account . *ACS Catalysis*, *5*(11), 6879–6892. https://doi.org/10.1021/acscatal.5b01900

Pitchai, R., Klier, K.: Partial Oxidation of Methane. Catal. Rev. 28, 13–88 (1986). doi:10.1080/03602458608068085

Pu, Z., Liu, Y., Zhou, H., Huang, W., Zheng, Y., Li, X. (2017) Catalytic combustion of lean methane at low temperature over ZrO_2-modified Co_3O_4 catalysts

Qi, W., Ran, J., Wang, R., Du, X., Shi, J., Niu, J., Zhang, P., Ran, M.: Kinetic consequences of methane combustion on Pd, Pt and Pd-Pt catalysts. RSC Adv. 6, 109834–109845 (2016). doi:10.1039/c6ra21150j

Rassoul, M., Gaillard, F., Garbowski, E., & Primet, M. (2001). Synthesis and Characterisation of Bimetallic Pd–Rh/Alumina Combustion Catalysts. *Journal of Catalysis*. https://doi.org/10.1006/jcat.2001.3328

Ravel, B., & Newville, M. (2005). ATHENA, ARTEMIS, HEPHAESTUS: data analysis for X-ray absorption spectroscopy using IFEFFIT. *Journal of Synchrotron Radiation*, *12*, 537–541

Ribeiro, F. H., Chow, M., & Dalla Betta, R. A. (1994). Kinetics of the complete oxidation of methane over supported palladium catalysts. *Journal of Catalysis*, *146*(2), 537–544. https://doi.org/10.1006/jcat.1994.1092

Satsuma, A., Tojo, T., Okuda, K., Yamamoto, Y., Arai, S., & Oyama, J. (2015). Effect of preparation method of Co-promoted Pd/alumina for methane combustion. *Catalysis Today*, *242*(PB), 308–314. https://doi.org/10.1016/j.cattod.2014.05.046

Schwartz, W R, & Pfefferle, L. D. (2012). Combustion of methane over palladium-based catalysts: Support interactions. *Journal of Physical Chemistry C*, *116*(15), 8571–8578. https://doi.org/10.1021/jp2119668

Seimanides, S., Stoukides, M.: Catalytic oxidation of methane on polycrystalline palladium supported on stabilized zirconia. J. Catal. 98, 540–549 (1986). doi:10.1016/0021-9517(86)90342-8

Setiawan, A., Kennedy, E. M., Dlugogorski, B. Z., Adesina, A. A., & Stockenhuber, M. (2015). The stability of Co_3O_4, Fe_2O_3, Au/Co_3O_4 and Au/Fe_2O_3 catalysts in the catalytic combustion of lean methane mixtures in the presence of water. *Catalysis Today*. https://doi.org///doi.org/10.1016/j.cattod.2014.11.031

Shen, J., Hayes, R. E., & Semagina, N. (2019). On the contribution of oxygen from Co_3O_4 to the Pd-catalyzed methane combustion. *Catalysis Today*. https://doi.org/https://doi.org/10.1016/j.cattod.2019.12.041

Smirnova, N. N., Bykova, T. A., Polotnyanko, N. A., Shikina, N. D., & Khodakovskii, I. L. (2010). Low-temperature heat capacity and standard entropy of PdO(cr.). *Russian Journal of Physical Chemistry A*, *84*(11), 1851–1855. https://doi.org/10.1134/s0036024410110051

Sokolovskii, V. D. (1990). Principles of Oxidative Catalysis on Solid Oxides. *Catalysis Reviews*, *32*(1–2), 1–49. https://doi.org/10.1080/01614949009349939

Stefanov, P., Todorova, S., Naydenov, A., Tzaneva, B., Kolev, H., Atanasova, G., … Aleksieva, K. (2015). On the development of active and stable Pd-Co/γ-Al_2O_3 catalyst for complete oxidation of methane. *Chemical Engineering Journal*, *266*, 329–338. https://doi.org/10.1016/j.cej.2014.12.099

Stotz, H., Maier, L., Boubnov, A., Gremminger, A. T., Grunwaldt, J. D., & Deutschmann, O. (2019b). Surface reaction kinetics of methane oxidation over PdO. *Journal of Catalysis*, *370*, 152–175. https://doi.org/10.1016/j.jcat.2018.12.007

Stotz, H., Maier, L., Deutschmann, O.: Methane Oxidation over Palladium: On the Mechanism

in Fuel-Rich Mixtures at High Temperatures. Top. Catal. 60, 83–109 (2017). doi:10.1007/s11244-016-0717-5

Strobel, R., Grunwaldt, J.-D., Camenzind, A., Pratsinis, S. E., & Baiker, A. (2005). Flame-made alumina supported Pd-Pt nanoparticles: Structural properties and catalytic behavior in methane combustion. *Catalysis Letters*, *104*(1–2), 9–16. https://doi.org/10.1007/s10562-005-7429-y

Tang, C.-W., Wang, C.-B., & Chien, S.-H. (2008). Characterization of cobalt oxides studied by FT-IR, Raman, TPR and TG-MS. *Thermochimica Acta*. https://doi.org///doi.org/10.1016/j.tca.2008.04.015

Tao, F.F., Shan, J.-J., Nguyen, L., Wang, Z., Zhang, S., Zhang, L., Wu, Z., Huang, W., Zeng, S., Hu, P.: Understanding complete oxidation of methane on spinel oxides at a molecular level. Nat. Commun. 6, (2015). doi:10.1038/ncomms8798

Taylor, K.C.: Automobile Catalytic Converters BT - Catalysis: Science and Technology Volume 5. Presented at the (1984)

Teng, F., Chen, M., Li, G., Teng, Y., Xu, T., Hang, Y., … Zhu, Y. (2011). High combustion activity of CH_4 and catalluminescence properties of CO oxidation over porous Co_3O_4 nanorods. *Applied Catalysis B: Environmental*, *110*, 133–140. https://doi.org/10.1016/j.apcatb.2011.08.035

Todorova, S., Blin, J. L., Naydenov, A., Lebeau, B., Kolev, H., Gaudin, P., … Tenchev, K. (2019). Co_3O_4 -MnO_x oxides supported on SBA-15 for CO and VOCs oxidation. *Catalysis Today*, (May), 10.1016/j.cattod.2019.05.018. https://doi.org/10.1016/j.cattod.2019.05.018

Todorova, S., Naydenov, A., Velinova, R., Kolev, H., Larin, A. V., Stoyanova, D., … Stefanov, P. (2019). Pd–MeO_x/Al_2O_3 (Me = Co, La, Ce) catalysts for methane combustion. *Reaction Kinetics, Mechanisms and Catalysis*, *126*(2), 663–678. https://doi.org/10.1007/s11144-018-1523-9

Tomic-Tucakovic, B., Majstorovic, D., Jelic, D., & Mentus, S. (2012). Thermogravimetric study of the kinetics of Co_3O_4 reduction by hydrogen. *Thermochimica Acta*, *541*, 15–24.

Verdes, G., Gout, R., & Castet, S. (2014). Thermodynamic properties of the aluminate ion and of bayerite, boehmite, diaspore and gibbsite. *European Journal of Mineralogy*, *4*(4), 767–792. https://doi.org/10.1127/ejm/4/4/0767

Wagman, D., Evans, W., Parker, V., Schumm, R., Halow, I., Bailey, S., … Nuttal, R. (1982). The NBS tables of chemical thermodynamic properties. Selected values for inorganic and C1 and C2 organic substances in SI units. *Journal of Physical and Chemical Reference Data*, *11*(2), 1–407.

Wang, F, Zhang, L., Xu, L., Deng, Z., & Shi, W. (2017). Low temperature CO oxidation and CH_4 combustion over Co_3O_4 nanosheets. *Fuel*, *203*, 419–429. https://doi.org/10.1016/j.fuel.2017.04.140

Wang, Qing, Peng, Y., Fu, J., Kyzas, G. Z., Billah, S. M. R., & An, S. (2015). Synthesis, characterization, and catalytic evaluation of Co_3O_4/γ-Al_2O_3 as methane combustion catalysts: Significance of Co species and the redox cycle. *Applied Catalysis B: Environmental*. https://doi.org///doi.org/10.1016/j.apcatb.2014.12.016

Watanabe, T., Kawashima, K., Tagawa, Y., Tashiro, K., Anoda, H., Ichioka, K., … Zhang, G. (2007). New DOC for light duty diesel DPF system. *SAE Technical Papers*. https://doi.org/10.4271/2007-01-1920

Willis, J J, Goodman, E. D., Wu, L., Riscoe, A. R., Martins, P., Tassone, C. J., & Cargnello, M. (2017). Systematic Identification of Promoters for Methane Oxidation Catalysts Using Size- and Composition-Controlled Pd-Based Bimetallic Nanocrystals. *Journal of the American Chemical Society*, *139*(34), 11989–11997. https://doi.org/10.1021/jacs.7b06260

Woods, M. P., Gawade, P., Tan, B., & Ozkan, U. S. (2010). Preferential oxidation of carbon monoxide on Co/CeO_2 nanoparticles. *Applied Catalysis B: Environmental*, *97*(1–2), 28–35. https://doi.org/10.1016/j.apcatb.2010.03.015

Wu, R.-J., Wu, J.-G., Tsai, T.-K., & Yeh, C.-T. (2006). Use of cobalt oxide CoOOH in a carbon monoxide sensor operating at low temperatures. *Sensors and Actuators B: Chemical*.

https://doi.org///doi.org/10.1016/j.snb.2006.01.053

Xiao, T. C., Ji, S. F., Wang, H. T., Coleman, K. S., & Green, M. L. H. (2001). Methane combustion over supported cobalt catalysts. *Journal of Molecular Catalysis A: Chemical*, *175*(1–2), 111–123. https://doi.org/10.1016/S1381-1169(01)00205-9

Xiong, H., Lester, K., Ressler, T., Schlögl, R., Allard, L. F., & Datye, A. K. (2017). Metastable Pd ⇔ PdO Structures During High Temperature Methane Oxidation. *Catalysis Letters*, *147*(5), 1095–1103. https://doi.org/10.1007/s10562-017-2023-7

Xu, J., Lu, G., Guo, Y., Guo, Y., & Gong, X. Q. (2017). A highly effective catalyst of Co-CeO_2 for the oxidation of diesel soot: The excellent NO oxidation activity and NOx storage capacity. *Applied Catalysis A: General*, *535*, 1–8. https://doi.org/10.1016/j.apcata.2017.02.005

Xu, Q., Kharas, K. C., Croley, B. J., & Datye, A. K. (2011). The Sintering of Supported Pd Automotive Catalysts. *ChemCatChem*, *3*(6), 1004–1014. https://doi.org/10.1002/cctc.201000392

Yeh, T.-F., Bi, J.-L., Lee, H.-G., Chu, K.-S., & Wang, C.-B. (2006). Phase transformation and catalytic activity of hexaaluminates upon high temperature pretreatment. *Journal of Alloys and Compounds*, *425*(1–2), 353–356. https://doi.org/10.1016/j.jallcom.2006.01.055

Zagoraios, D., Athanasiadi, A., Kalaitzidou, I., Ntais, S., Katsaounis, A., Caravaca, A., … Vayenas, C. G. (2019). Electrochemical promotion of methane oxidation over nanodispersed Pd/Co_3O_4 catalysts. *Catalysis Today*, (November 2018). https://doi.org/10.1016/j.cattod.2019.02.030

Zasada, F., Gryboś, J., Budiyanto, E., Janas, J., & Sojka, Z. (2019). Oxygen species stabilized on the cobalt spinel nano-octahedra at various reaction conditions and their role in catalytic CO and CH_4 oxidation, N_2O decomposition and oxygen isotopic exchange. *Journal of Catalysis*, *371*, 224–235. https://doi.org/10.1016/J.JCAT.2019.02.010

Zasada, F., Gryboś, J., Hudy, C., Janas, J., & Sojka, Z. (2019). Total oxidation of lean methane over cobalt spinel nanocubes—Mechanistic vistas gained from DFT modeling and catalytic isotopic investigations. *Catalysis Today*, (November 2018).

https://doi.org/10.1016/j.cattod.2019.03.061

Zasada, F., Janas, J., Piskorz, W., Gorczyńska, M., & Sojka, Z. (2017). Total Oxidation of Lean Methane over Cobalt Spinel Nanocubes Controlled by the Self-Adjusted Redox State of the Catalyst: Experimental and Theoretical Account for Interplay between the Langmuir-Hinshelwood and Mars-Van Krevelen Mechanisms. *ACS Catalysis*, *7*(4), 2853–2867. https://doi.org/10.1021/acscatal.6b03139

Zasada, F., Piskorz, W., Cristol, S., Paul, J.-F., Kotarba, A., & Sojka, Z. (2010). Periodic Density Functional Theory and Atomistic Thermodynamic Studies of Cobalt Spinel Nanocrystals in Wet Environment: Molecular Interpretation of Water Adsorption Equilibria. *The Journal of Physical Chemistry C*, *114*(50), 22245–22253. https://doi.org/10.1021/jp109264b

Zasada, F., Piskorz, W., Janas, J., Gryboš, J., Indyka, P., & Sojka, Z. (2015). Reactive Oxygen Species on the (100) Facet of Cobalt Spinel Nanocatalyst and their Relevance in $^{16}O_2/^{18}O_2$ Isotopic Exchange, deN_2O, and deCH_4 Processes-A Theoretical and Experimental Account. *ACS Catalysis*, *5*(11), 6879–6892. https://doi.org/10.1021/acscatal.5b01900

Zhao, C., Zhao, Y., Li, S., & Sun, Y. (2017). Effect of Pd doping on CH_4 reactivity over Co_3O_4 catalysts from density-functional theory calculations. *Cuihua Xuebao/Chinese Journal of Catalysis*, *38*(5), 813–820. https://doi.org/10.1016/S1872-2067(17)62817-1

Zheng, Y., Yu, Y., Zhou, H., Huang, W., & Pu, Z. (2020). Combustion of lean methane over Co_3O_4 catalysts prepared with different cobalt precursors. *RSC Advances*, *10*(8), 4490–4498. https://doi.org/10.1039/C9RA09544F

Zhu, G, Han, J., Zemlyanov, D. Y., & Ribeiro, F. H. (2004). The turnover rate for the catalytic combustion of methane over palladium is not sensitive to the structure of the catalyst. *Journal of the American Chemical Society*, *126*(32), 9896–9897. https://doi.org/10.1021/ja049406s

Zhu, G., Han, J., Zemlyanov, D.Y., Ribeiro, F.H.: Temperature dependence of the kinetics for the complete oxidation of methane on palladium and palladium oxide. J. Phys. Chem. B. 109, 2331–2337 (2005). doi:10.1021/jp0488665